UTS UNIVERSITY OF TECHNOLOGY SYDNEY

Performance of Phase Change Cementitious Composites with Self-heating Capacity

by Xiaonan Wang

Thesis submitted in fulfilment of the requirements for the degree of

Doctor of Philosophy

under the supervision of
A/Prof. Wengui Li (Principal supervisor)
Prof. Hadi Khabbaz (Co-supervisor)
Dr. Yuhan Huang (Co-supervisor)

University of Technology Sydney
Faculty of Engineering and Information Technology

December 2024

CERTIFICATE OF ORIGINAL AUTHORSHIP

I, Xiaonan Wang declare that this thesis, is submitted in fulfilment of the requirements for the award of Doctor of Philosophy, in the Faculty of Engineering and Information Technology at the University of Technology Sydney.

This thesis is wholly my own work unless otherwise referenced or acknowledged. In addition, I certify that all information sources and literature used are indicated in the thesis. This document has not been submitted for qualifications at any other academic institution.

This research is supported by the Australian Government Research Training Program.

Signature: Production Note:
Signature removed prior to publication.

Date 06/12/2024

ACKNOWLEDGEMENT

When I stepped onto the UTS campus, I could not imagine that it would be such a wonderful experience. It is close to the end of my Ph.D study and the experience is dose enjoyable and amazing. That can not be completed without the favour of others, although I dedicate myself to the study.

I am glad to express my sincere appreciation to my principal supervisor, A/Prof. Wengui Li, who spares no effort to support my research by offering valuable guidance, constructive discussion, and warm encouragement. The supervision helps me to follow the correct and productive path to complete research and explore science. At the same time, my co-supervisors, Prof. Hadi Khabbaz and Dr. Yuhan Huang, are very nice in providing effective solutions.

There are many complex problems for the Ph.D study and I enjoy the strong support of all members in UTS Tech Lab, Science Lab, CEE Research, Faculty Administration, and GRS. In particular, my group members cultivate an energetic condition for us to cooperate on the research and help each other in living. That is indispensable for an overseas student. Also, I appreciate CSC to support me to live and study financially.

My family always provide silent support, not just the last few years. I am so lucky to grow up here, where I learned how to be myself. Their support is priceless, and they ask for nothing. In addition, my wife has been accompanying me since we fell in love, even though she needs to live around 10 thousand km from the hometown. Nothing can express my gratitude but love her as long as I am alive.

Xiaonan Wang
06/12/2024
Australia, Sydney, Ultimo

LIST OF PUBLICATIONS

Journal papers:

[1] Wang, X., Li, W., Luo, Z., Wang, K. & Shah, S.P. 2022, 'A critical review on phase change materials (PCM) for sustainable and energy efficient building: Design, characteristic, performance and application', *Energy and Buildings*, vol. 260, p. 111923.

[2] Wang, X., Li, W., Huang, Y., Zhang, S. & Wang, K. 2023, 'Study on shape-stabilised paraffin-ceramsite composites with stable strength as phase change material (PCM) for energy storage', *Construction and Building Materials*, vol. 388, p. 131678.

[3] Wang, X., Li, W., Guo, Y., Kashani, A., Wang, K., Ferrara, L. & Agudelo, I. 2024, 'Concrete 3D printing technology for sustainable construction: A review on raw material, concrete type and performance', *Developments in the Built Environment*, vol. 17, p. 100378.

[4] Wang, X., Li, W., Guo, Y., Wang, K., & Huang, Y. 2024, 'Performance of Cement Mortar with Inorganic Na2SO4·10H2O-Na2HPO4·12H2O Shape-stabilization phase change material', *Journal of Materials in Civil Engineering*, Accepted.

Book chapter:

[1] Luo, Z., Guo, Y., Zhao, C., Wang, X., Zhang, X., Wu, V. & Li, W. 2024, '15 - Nano/micro characterization on interfacial transition zones in fly ash–based geopolymer concrete', in J. de Brito, F. Agrela & R.V. Silva (eds), *The Path to Green Concrete*, Woodhead Publishing, pp. 445-75.

.

Conference Presentation:

[1] Wang, X. & Li, W. 2022, 'Review and analysis of additive manufacturing in concrete for sustainable development and resource-saving', *10th International Symposium on Cement and Concrete*

[2] Wang, X. & Li, W. 2023, 'Influence of inorganic shape stable phase change material on mechanical properties of cement mortar', *4th International Symposium for Emerging Researchers in Composites for Infrastructure*

TABLE OF CONTENTS

LIST OF ACRONYMS

CA	Capric Acid	$CH_3(CH_2)_8COOH$
CB	Carbon Black	
CF	Carbon Fibre	
CLMS	Carbon Layer-Modified Mesoporous Silica	
CNT	Carbon Nano Tube	
DSC	Differential Scanning Calorimeter	
EDS	Energy Dispersive Spectroscopy	
EG	Expanded Graphite	
EGA	Expanded Glass Aggregate	
EP	Expanded Perlite	
EPC	EP/PCM composite	
EPCM	EPC-based mortar	
EPM	EP-based mortar	
FTIR	Fourier Transform Infrared Spectroscopy	
ITZ	Interfacial Transition Zone	
LA	Lauric Acid	$CH_3(CH_2)_{10}COOH$
LAL	Lauryl Alcohol	$CH_3(CH_2)_{11}OH$
LWA	Lightweight Aggregates	
MA	Myristic Acid	$CH_3(CH_2)_{12}COOH$
MacroPCM	Macroencapsulated Phase Change Material	
MicroPCM	Microencapsulated Phase Change Material	
NHP	Disodium Hydrogen Phosphate Dodecahydrate	$Na_2HPO_4 \cdot 12H_2O$
NS	Sodium Sulphate Decahydrate	$Na_2SO_4 \cdot 10H_2O$

PA	Palmitic Acid	$CH_3(CH_2)_{14}COOH$
PCM	Phase Change Material	
PEG	Polyethylene Glycol	
PET	Polyethylene Terephthalate	
PU	Polyurethane	
SA	Stearic Acid	$CH_3(CH_2)_{16}COOH$
SAT	Sodium Acetate Trihydrate	$CH_3COONa{\cdot}3H_2O$
SEM	Scanning Electron Microscopy	
SS	Silica Sand	
SSM	SS-based mortar	
SSPCM	Shape-Stabilized Phase Change Material	
STP	Sodium Thiosulfate Pentahydrate	$NaS_2O_3{\cdot}5H_2O$
TC	Thermal Conductivity	
TD	Tetradecyl Alcohol	$CH_3(CH_2)_{13}OH$
TEOS	Tetraethyl Orthosilicate	$Si(OC_2H_5)_4$
TES	Thermal Energy Storage	
TGA	Thermo-Gravimetric Analysis	
XRD	X-Ray Diffraction	

LIST OF FIGURES

LIST OF TABLES

ABSTRACT

Energy consumption remains a global challenge, with the construction sector being a significant contributor. Phase Change Materials (PCM) are introduced in construction to store heat energy and regulate temperature, reducing the reliance on air conditioners. Concrete is an ideal carrier for PCM, making PCM concrete a promising solution for energy savings and sustainable development.

This study focuses on the performance of shape-stabilised PCM composites (SSPCM). The first research emphasises the structural variation of supporting materials, ceramsite as coarse aggregate, and its impact on PCM loading, leakage prevention, and strength. Ceramsite with interconnected small pores are identified as advantageous. These structures promote a stable composite state, with PCM loss between 1% and 3%. A higher strength of SSPCM composites at room temperature indicates that weak SSPCM is not a universal cause of reduced PCM concrete strength.

Given the broader applicability of fine aggregates, expanded perlite is used as a carrier, with a eutectic inorganic hydrated salt as the core PCM. Experiments investigate the impact of these materials on concrete's physical properties. The study offers a novel explanation for mechanical changes from a thermal perspective, considering factors like the PCM's chemical properties, its role in regulating hydration heat, and its compatibility with the cement matrix. New insights emphasise the PCM's influence on concrete performance.

To improve thermal convection efficiency, multi-dimensional carbon materials are incorporated into the PCM concrete. Thermal regulation shows a temperature difference of 1.6 °C within an hour, with a time lag of 10 to 20 minutes. While PCM concrete faces challenges with weak mechanical properties, a novel carbon additive formulation

enhances strength by 24%. The synergistic effect of various carbon additives proves essential in improving both the thermal and mechanical properties of PCM concrete, highlighting the potential of optimised additive combinations.

The research also explores multifunctional concrete. While PCM concrete passively regulates temperature, combining it with active self-heating capabilities improves performance under varying temperature conditions. In experiments, the temperature of concrete increases by over 30 °C. The study also examines the electrical properties of the concrete using alternating-current impedance. Furthermore, hydrated salt-based SSPCMs improve conductivity by releasing free ions at elevated temperatures, further boosting the concrete's thermal and electrical performance.

In summary, this study enhances the functionality of PCM concrete by investigating its key capabilities. Through comprehensive analysis, the research offers valuable insights and recommendations for optimising PCM concrete's performance and expanding its potential applications.

CHAPTER 1. INTRODUCTION

1.1 Background

Modern infrastructures are required to satisfy increasing demands for enhanced sustainability, green economy, intelligent performance and extended longevity. This urges various developments in advanced and smart materials, design, manufacturing, and testing techniques. Phase Change Material (PCM) is one of such smart materials where their states can be changed between gas, liquid, and solid when they suffer heating or cooling (Razak et al. 2020). In the phase-changing period, energy is absorbed or released naturally to relieve temperature fluctuation so that the thermal properties of construction materials are modified. The PCM has attracted growing attention and it is a widely accepted way to save energy and make a green environment (da Cunha & de Aguiar 2020; Qin et al. 2023; Rathore et al. 2022). The paper publication about PCM is shown in Figure 1.1 (Wang et al. 2022).

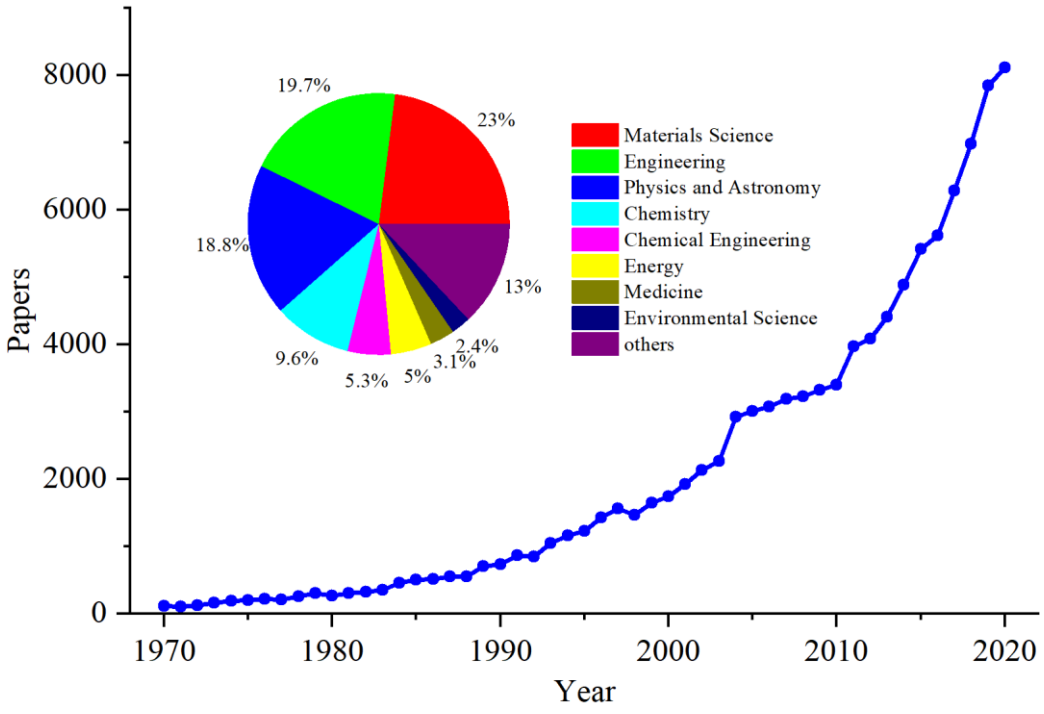

Figure 1.1 Academic publication of PCM (up to 2021) (Wang et al. 2022)

PCMs provide positive solutions for improving energy efficiency and enhancing the thermal properties of construction materials. However, they also pose some negative impacts, such as weakening mechanical properties and increasing costs, chemical instability and so on. PCM-Incorporation-Application is roughly the key structure of PCM research. Although plentiful materials have the capacity for phase change, only some of them are suitable due to the higher latent heat and favourable phase change point in construction, when eutectic PCMs present greater potential to become more optimal, but much effort is required. Current incorporation methods and applications in construction materials can meet the essential requirements, yet the effectiveness is inadequate, including low efficiency of phase changing, leading to low energy storage. Future development of PCMs, including novel PCM and efficient incorporation, as well as their application and function in construction, are expected.

1.1.1 **Significance of PCM**

Civil infrastructures, like buildings, bridges, and pavements, often undergo temperature differences during their entire service lives, including the different temperatures between interior and exterior, summer and winter, day and night, and construction and operation. These differences often pose negative effects on structural performance where extra energy-consuming ways are employed to ease the problems. Taking the building room as an example, residents use an air conditioner to defend the barely tolerable indoor temperature in the summer and warm the room in the winter resulting in a large consumption of electricity. The heat flux through the houses is the important reason causing uncomfortable indoor temperatures (Lakhdari, Chikh & Campo 2020). Heat preservation and insulation are achieved by the heat insulation layer in most buildings which is a conventional and popular method (Jia et al. 2021a). However, the heat

insulation layer is able to block the heat flow but it has little influence on Thermal Energy Storage (TES). TES can control the heat flow based on storing and relocating the redundant thermal energy in which PCMs show great capability (Al-Absi, Mohd Isa & Ismail 2020). PCMs incorporated in walls, ceilings, and indoor coatings can reallocate energy in an appropriate manner that remits heat transferring and narrows the temperature fluctuation range (Arkar & Medved 2007) promoting huge energy saving (Beiranvand & Mohaghegh 2021). In this case, the energy waste is alleviated further leading to the reduction of pollution and lower demand for electric and fossil energy (Rathore & Shukla 2020). Briefly, PCMs can restore and release thermal mass by phase change when suffering temperature fluctuation, which is useful for improving energy efficiency and reducing energy consumption (Ahangari & Maerefat 2019; Kawaguchi et al. 2020).

Other than temperature modification and energy-saving, PCMs play a critical role in controlling construction quality since they significantly influence mechanical properties, corrosion of reinforcement, and durability. Most construction materials are produced based on cement, like mortar and concrete, which are major base materials for PCMs application, where hydration reaction is the essential process to provide strong strength. Sometimes improper hydration heat leads to weak strength and shrinkage cracks. Also, the temperature differences mentioned in the last paragraph tend to decrease safety and durability. In this case, PCMs could modify hydration heat and relieve temperature differences to enhance strength and decrease cracks of cement-based materials bringing durability improvement (Šavija 2018). Also, the mix design of concrete/mortar may be changed because of the PCM addition that is a considerable factor in the quality of this production. To be more exact, there are two forms of PCM application, micro and macro composites, and this paragraph discusses the former.

1.1.2 **Requirement of PCM and limitation of present work**

From the presented results, there are many problems impeding the development and application of PCMs in construction. It is supposed to be a thermal regulator and energy saver, showing little adverse impacts on the conventional ability of construction. With the hope of good social and economic influence, PCM applications should be available for mass production with low costs. At the current stage, there is a large space to make progress on thermal ability enhancement, negative effect elimination, and economical industrial production. The critical problems are summarized as follows.

The fundamental one is the selection of optimal PCMs with specific thermal properties since there are various demands in different construction (Cao, Bui & Kjøniksen 2019; Qu et al. 2021; Rolka et al. 2021). Mostly, PCMs show different thermal properties where phase change temperature, latent heat, and thermal conductivity are the most important that determine thermal regulation and energy saving. Although ambient condition poses significant impacts on their performance, some universal requirements are concluded for the thermal properties of PCMs. 1. proper phase change point (the point should be close to the expected maintained temperature). 2. high latent heat (absorb and release high energy in limited PCM content). 3. good thermal conductivity (improve the efficiency of the whole phase change process).

Then, the optimal carrying or containing method, incorporation, is significant to bridge the gap between raw PCM and its application. The critical requirement of this stage is to boost the compatibility between PCM and matrix material; otherwise, the basic ability of building material may be broken (such as the weak strength of concrete (Ilyas et al. 2021)). Furthermore, the fabrication of construction materials is precise and the original design is changed leading to performance reduction due to the addition of micro PCM composites. PCMs have relatively lower stability compared to conventional construction

materials that is prone to decrease the durability. This process has shown progress to achieve moderate compatibility but the reduced effectiveness of phase change brings important concentration. In another word, there are two crucial objectives for ideal incorporation. Firstly, ensure the integrity of PCM/incorporation/building material. Secondly, eliminate the adverse effects of incorporation on PCM thermal performance.

What is presented at the last two paragraphs focuses on the performance of PCM building material before universal application. There are also two problems that need solutions. 1. Mass production meets various requirements based on service conditions. The impacts of ambient conditions on PCM have been proven as very serious although the regulation is far from comprehensive. Therefore, available methods to modify design are necessary for mass production that is an indispensable condition for universal application. Generally, mass production should be economic, adjustable and high-quality. 2. Affordable price of PCM composites to control the cost of construction. The surcharge be attributed to raw material and production process. In many research plans, the price of raw materials is more expensive than that of conventional building materials, such as graphene (Chi et al. 2021) and copper nanoparticles (Nitsas & Koronaki 2021). In addition, to get optimal ability the modification process may be complex and need huge of time leading the cost to rise steadily. Taking the adjustment for practical application in consideration, the budget increases further.

If superiorities are brought into full play and inferiorities are controlled, PCMs can improve the comprehensive properties of the construction. Now available achievements complete a major step towards success. Unfortunately, it is obvious that the currently finished research is not strong enough to support the widespread use of PCMs introduced in constructs.

1.2 Research objectives and scope

1.2.1 **Novel PCM composites with enhanced properties**

PCMs play a pivotal role in determining the relevance of research in this field. However, no PCM to date can be considered perfect. A novel PCM has the potential to address many of the challenges present in current applications. In addition to core PCMs, several critical factors must be considered for PCM composites, including corrosion resistance, thermal conductivity (TC), and structural integrity. Although some methods have been proven reliable, they often involve complex processes that are time-consuming and costly. These challenges must be overcome before PCM composites can be widely produced and applied.

The present study aims to investigate the key properties of PCM composites using various pure PCMs and supporting materials. The research progresses from coarse to fine composite materials, with a clear focus on specific objectives and carefully selected investigative methods. Coarse PCM composites offer greater flexibility in terms of performance enhancement, with suggested improvements focusing on raw material production. In contrast, fine PCM composites are more susceptible to the influence of their intrinsic properties, and the research addresses potential issues and possible modifications to optimize their performance.

1.2.2 **Features of PCM building material**

The effectiveness of PCMs in buildings is largely determined by their total heat storage capacity. Given the limitations of energy absorption density, increasing the amount of PCM can enhance thermal regulation more effectively. Concrete constitutes the majority of building materials in most structures, providing significant potential for PCM integration. As a result, concrete is the primary medium in which PCM composites are

incorporated. However, the addition of PCM to concrete can significantly alter its workability and physical properties, which may have a profound impact on its practical applications (Richardson, Heniegal & Tindall 2017). These changes are influenced not only by the inherent characteristics of the PCM composites but also by the method and parameters of their incorporation. To achieve meaningful advancements, additional data and research are required. Numerous factors must be carefully considered, particularly with regard to the mechanical properties of the concrete, such as strength, shrinkage, and microstructure, alongside the thermal properties. Throughout this study, the analysis is guided by the impact of PCM on these various properties.

1.2.3 **Thermal performance and influence on temperature**

The primary advantage of PCMs lies in their impact on thermal regulation. The enhancement of energy storage and temperature control is not solely determined by the properties of the PCM, but also by its synergistic interaction with concrete and the overall integration of concrete in buildings. This interaction is significant and warrants attention from multiple perspectives. Various proposals for improving PCM-concrete systems have been introduced. The use of PCM requires specific adjustments to the thermal conductivity of concrete, which differs from traditional methods aimed at energy savings. Consequently, this thesis treats PCM and concrete as distinct components for modification, while also considering them as a cohesive system that functions synergistically. Notably, the thermal performance of PCM-integrated concrete is examined at both macro and micro levels, under conditions that replicate real-world applications.

1.2.4 **Multifunctional building material**

In recent decades, numerous innovative types of concrete have been developed, demonstrating significant potential and promising prospects. One approach to creating

multifunctional concrete is through the integration of different functional properties. Several studies have demonstrated the feasibility of this approach. For instance, Uthaichotirat et al. (2020) introduced recycled aggregate concrete impregnated with PCMs, where the PCM significantly improved the thermal properties of the composite. The PCM and recycled aggregates exhibited good compatibility. Similarly, Ren et al. (2020) explored the use of PCMs in ultra-high-performance concrete, demonstrating that PCMs have the potential to further enhance the capabilities of such concrete, while also ensuring satisfactory chemical stability. Hunger et al. (2009) investigated encapsulated PCMs, which were able to maintain the self-compacting ability of the concrete while also improving its thermal properties in self-compacting concrete.

One particular aspect of interest is self-heating, which can arise from two distinct mechanisms. Self-heating concrete represents an active technology that adjusts temperature, while PCM concrete uses a passive method for temperature regulation. Combining these technologies could enable concrete to better address the various temperature-related challenges it may face. In addition, carbon materials have gained popularity in the modification of PCM concrete, serving as critical components for generating electrical conductivity pathways necessary for self-heating. This combination provides a promising solution for multifunctional concrete with both energy storage and self-heating capabilities. The successful results of such innovations offer significant benefits for the development of advanced concrete materials.

CHAPTER 2. LITERATURE REVIEW

PCMs have a huge potential ability to enhance energy-saving and improve buildings as friendlier to the environment while there is mass energy demand leading to pollution generation at this stage. Unfortunately, there is still a huge gap between ideal and practical performance that is far from mass production and common application. After decades of development, many valuable conclusions can be drawn up, offering meaningful research direction for the future.

2.1 PCM properties

Most materials have the phase change feature in nature. For instance, the water turns into water vapour above the boiling point and into ice under the freezing point. These materials can be defined as PCMs but only some of them are able to become PCMs in constructs as thermal performance enhancers. Most PCMs can be classified into 3 kinds (organic, inorganic, and eutectic) based on constitution. Due to the different molecular structures, obvious characteristics can be seen from the classification.

2.1.1 **Organic PCM**

Organic PCMs have a wide range of thermal properties due to their various molecular structures, mostly hydrocarbon molecules. Paraffin is the most typical organic PCM attracting much attention (Qu et al. 2020; Razak et al. 2020; Sun et al. 2020), which consists of a mixture of alkanes containing between twenty and forty carbon atoms. The pure alkanes have an obvious phase change phenomenon at room temperature that endows them to become PCMs. Some of them with the general chemical formula C_nH_{2n+2}, like hexadecane (Chriaa et al. 2021), cetane (Jia et al. 2021b), heptadecane (Konuklu et al. 2020) and n-eicosane (Do et al. 2021), have been demonstrated that they have positive

impacts as PCMs. Generally, the melting temperatures of alkanes increase with relative molecular mass or the number of carbon atoms. Hexadecane (Chriaa et al. 2021) has the chemical formula $C_{16}H_{34}$ with a phase change point of 18-20 °C and enthalpy of 224 kJ/kg, a saturated hydrocarbon of the alkane's family with good compatibility and no chemical reaction with supporting materials. With the increase of relative molecular mass, the melting temperature of heptadecane ($C_{17}H_{36}$) (Konuklu et al. 2020) and n-eicosane ($C_{20}H_{42}$) (Do et al. 2021) were 22.91 °C and 37.27 °C respectively but the enthalpy of n-eicosane was lower. These materials also presented good incorporation operability and no chemical interaction with supporting materials.

Paraffin is a mixture of various alkanes so it showed different properties in experiments (Sun et al. 2020; Uthaichotirat et al. 2020; Yang et al. 2016). Meng et al. (2020a) believed the paraffin-based PCM showed the advantages of suitable phase change temperature and enthalpy, good thermal stability and reliability, and effective temperature regulation performance. For the suitable phase change temperature and enthalpy, paraffin showed various melting points and could be modified to the design value. Qu et al. (2020) selected paraffin with a melting temperature of around 44 °C that can be modified to 35-44 °C with a beneficial latent of 260 kJ/kg, which was appropriate to prevent hot flow in summer. The good thermal stability was proved widely. Ramakrishnan et al. (2015) selected paraffin RT21 consisting of saturated hydrocarbons produced by Rubitherm company to fabricate a novel PCM composite. After 100 thermal cycles from 15-35 °C, a common variation range of temperature in Australian summer, the paraffin RT21 still had stable energy storage capability with negligible reduction. Tt got common acceptance for effective temperature regulation performance (Kao et al. 2012; Yu et al. 2020). For instance, Khan, Bhuiyan & Ahmed (2020) used paraffin wax type P56-58 produced by Merck. The PCM reduced the heat flux by up to 17.2% between hot and cold water baths

leading to fewer temperature fluctuations and a significant time delay (up to 40 min) to reach the given temperature.

In general, paraffin has been one of the most prevailing PCM and has been used in various research (Al-Yasiri & Szabó 2021; Shi et al. 2021a). After decades of development, some commercial PCM products were produced by companies like BASF. The paraffin was preferred PCM in some products like Micronal PCM DS 5001 X (Joulin et al. 2014) and Micronal DS 5040X (Shi et al. 2020), Mikrathermic D24 (Snoeck et al. 2016). These products are well-encapsulated PCM components based on polymer shells.

Apart from a pure and mixed alkane (paraffin), other organic PCMs mainly are organic acid (Chen et al. 2010; Ren, Liu & Gao 2020; Zhang et al. 2021) and organic alcohol (Chi et al. 2021). The fatty acid is an important organic acid that is a carboxylic acid with a long aliphatic chain including saturated fatty acids (caprylic acid, capric acid, lauric acid, etc.) and unsaturated fatty acids (myristoleic acid, palmitoleic acid, sapienic acid, etc.). The lauric acid (LA) attracted much attention with a melting temperature higher than 40 °C and good latent heat (Chen et al. 2021a). Stearic acid (SA) had a higher phase change temperature of around 50 °C and high enthalpy (Zhang et al. 2021). The tetradecanol, saturated fatty alcohol, had great latent over 230 kJ/kg and a moderate phase change point (Chi et al. 2021).

Macromolecule materials have been widely used in the incorporation and a few polymers like polyethylene glycol (PEG) also showed the capability as core PCM. Some researchers have explored the application of polymers in PCM. Fan et al. (2021) took the modified polyurethane (PU) as a solid-solid PCM. They used PEG to synthesize different molecular weights of PU. Tang et al. (2016) made dye-linked PU as additional PCM. Karaman et al. used PEG (Karaman et al. 2011) to fabricate a novel SSPCM with suitable

melting and freezing temperatures and moderate latent heat. In other research, PEG played a positive role as core PCM and its thermal properties were improved (Chen et al. 2021c; Feng et al. 2021). The important properties of many popular organic PCMs are shown in Table 2.1.

Table 2.1 Main properties of sample organic PCMs

PCM	Phase change temperature (°C)	Density (kg/m^3)	Enthalpy (kJ/kg)	Refs.
Hexadecane	T_p: 18-20	–	H_p: 224	(Chriaa et al. 2021)
Cetane	T_p: 18	880 at solid 770 at liquid	H_p: 231	(Jia et al. 2021b)
Heptadecane	T_m: 22.91 T_s: 21.75	–	H_m: 182.36 H_s: 209.62	(Konuklu et al. 2020)
n-eicosane	T_m: 37.27 T_s: 28.87	–	H_p: 250.41	(Do et al. 2021)
Paraffin ZDJN-28	T_p: 26-28	850 at solid 765 at liquid	H_p: 231.2	(Sun et al. 2020)
Paraffin	T_p: 44-46	–	H_m: 259 H_s: 260	(Qu et al. 2020)
Paraffin	T_p: 48.2-60.5	–	H_p: 136.4	(Yang et al. 2016)
Paraffin6035	T_p: 57.2-59.9	–	–	(Uthaichotirat et al. 2020)
Paraffin	T_m: 49.8	–	H_m: 208.4	(Shi et al. 2021a)

	T_s: 52.9		H_s: 198.2	
Paraffin	T_m: 60.3 (tested)	900 at 20 °C	H_m: 212.5 H_s: 212.5	(Shi et al. 2021b)
Paraffin	T_m: 21	–	H_m: 212.7	(Meng et al. 2020a)
Paraffin wax P56-58	T_p: 42-72	900	H_p: 250	(Khan, Bhuiyan & Ahmed 2020)
Paraffin RT21	T_m: 24.5 (peak) T_s: 20.2 (peak)	–	H_m: 133.3 H_s: 132.1	(Ramakrishnan et al. 2015)
Paraffin	T_p: 56-58	–	H_m: 246.74 H_s: 238.14	(Yu et al. 2020)
Paraffin	T_p: 41-44	–	H_p: 128.5	(Kao et al. 2012)
Paraffin	T_m: 58.52 (peak) T_s: 56.18 (peak)	–	H_m: 151.56 H_s: 144.62	(Li, Fang & Liu 2010)
Paraffin wax	T_p: 18	880	H_p: 236.81	(Li et al. 2021b)
Paraffin wax	T_m: 44	930 at solid 830 at liquid	H_m: 190	(Al-Yasiri & Szabó 2021)
Lauric Acid	T_m: 37.026 (tested)		H_m: 145.998	(Chen et al. 2010)
Lauric Acid	T_m: 43.5-48.2	940 at solid 885 at liquid	H_m: 187.21	(Chen et al. 2021a)
Stearic Acid	T_m: 53.1 (peak) T_s: 49.3 (peak)	–	H_m: 194.0 H_s: 193.4	(Zhang et al. 2021)

Hexadecanol	T_m: 42.1	–	H_m: 232.6	(Tang et al. 2016)
Tetradecanol	T_m: 36.2 T_s: 33.1	–	H_m: 234.7 H_s: 231.8	(Chi et al. 2021)
dye-linked PU	T_p: 54.7 (peak)	–	H_p: 128.2	(Tang et al. 2016)
PU-5	T_m: 59.08 (peak) T_s: 28.46 (peak)	–	H_m: 129.59 H_s: 105.45	(Fan et al. 2021)
PEG 1000	T_m: 33.32 (peak) T_s: 29.67 (peak)	–	H_m: 143.16 H_s: 166.71	(Karaman et al. 2011)
PEG	T_m: 62 (peak) T_s: 35.1 (peak)	–	H_m: 198.5 H_s: 176.9	(Chen et al. 2021c)
PEG	T_m: 52.48 T_s: 19.18	–	H_m: 153 H_s: 151.46	(Feng et al. 2021)
Pentaglycerine	T_m: 86.06 (peak) T_s: 75.12 (peak)		H_m: 166.0 H_s: 159.1	(Zhang et al. 2018)

2.1.2 **Inorganic PCM**

Inorganic PCMs also are an important part showing different features compared with organic ones and inorganic salts are typical examples. Bauer, Laing & Tamme (2012) investigated and compared experiment results focusing on important properties of sodium nitrate ($NaNO_3$) as a PCM. Besides nitrite formation in molten $NaNO_3$ was extended to relatively lower temperatures, thermo-physical property data presented its reliability as a PCM. Although the enthalpy was good, it was noticeable that the average melting point was higher than 300 °C. Similar features were shown by Laing et al. (2009) in the

application of solar thermal power plants. A preferred kind was the hydrated inorganic salt with a low melting point. Sodium sulfate (Na_2SO_4) had a high melting temperature of 884 °C but sodium sulfate decahydrate ($Na_2SO_4 \cdot 10H_2O$) counterpart was only 32.4 °C due to the water of crystallization (Islam & Ahmed 2021). In this experiment, the $Na_2SO_4 \cdot 10H_2O$ layer successfully reduced the maximum mean temperature by 3 °C (Islam & Ahmed 2021). Fang et al. (2021) introduced calcium chloride hexahydrate ($CaCl_2 \cdot 6H_2O$) as PCM for room temperature regulation. This $CaCl_2 \cdot 6H_2O$ had a melting point of 28.84 °C and latent heat of 170.2 J/g and was changed by 6% $CO(NH_2)_2$ to 24.18 °C and 149.2 J/g respectively. This change enhanced the thermal performance according to the condition in the experiment. There was also commercial inorganic PCM with low phase change temperature, like SavE® OM37 (Rathore & Shukla 2020) with a melting point of 35 - 40 °C and latent heat of 218 J/g, but the examples were rare. The important properties of many popular inorganic PCMs are shown in Table 2.2.

Table 2.2 Main properties of sample inorganic PCMs

PCM	Phase change temperature (°C)	Density (kg/m^3)	Enthalpy (kJ/kg)	Refs.
SavE® OM37	T_m: 35-40	860 at 40 °C 960 at 30 °C	H_m: 218	(Rathore & Shukla 2020)
$NaNO_3$	T_m: 306	2260	H_m: 170-190	(Bauer, Laing & Tamme 2012)
$NaNO_3$	T_m: 305	2110 at 304 °C 1908 at 306 °C	H_m: 178	(Laing et al. 2009)

$Na_2SO_4 \cdot H_2O$	T_m: 32.4	1464	H_m: 252	(Islam & Ahmed 2021)
$CaCl_2 \cdot 6H_2O$	T_m: 28.84		H_m: 170.2	(Fang et al. 2021)
$CaCl_2 \cdot 6H_2O$-$CO(NH_2)_2$	T_m: 24.18		H_m: 149.2	(Fang et al. 2021)

2.1.3 **Eutectic PCM**

Eutectic is a homogeneous mixture of substances that melts or solidifies at a single temperature that is lower than the melting point of any of the constituents (Guthrie 1884). Eutectic PCMs mean that two or more PCMs are mixed to get a novel PCM with specific properties. A eutectic alloy is common in some industries, improving our daily life, and it may be a eutectic PCM thanks to the phase change of metal. Kawaguchi et al. (2020) took Zn-30 wt% Al alloy as the eutectic PCM coated by ZnO and Al_2O_3. It exhibited good potential as a heat storage material over 400 °C but it is not suitable for building materials. Other eutectic alloy and inorganic-inorganic eutectic PCMs met the same problem (Miliozzi, Chieruzzi & Torre 2019) including ternary hybrid molten salt (Li_2CO_3-K_2CO_3-Na_2CO_3). Miliozzi, Chieruzzi & Torre (2019) investigated the properties of solar salts consisting of 40% potassium nitrate (KNO_3) and 60% sodium nitrate ($NaNO_3$) as PCMs in cement mortars, at an operative temperature higher than the melting temperature, under different incorporation methods and morphological kinds.

On the contrary, organic-organic eutectic PCMs embraced building materials efficiently and demonstrated prosperous developments. Meng & Wang (2020) designed a capric and lauric fatty acid (CA-LA with a mass fraction of 66:34) eutectic form-stable PCM. Xiao, He & Wang (2021) produced LA-SA with different melting temperatures of 42 °C, 50 °C,

and 58 °C by changing the proportion. Ren, Liu & Gao (2020) designed PCMs based on ternary fatty acids consisting of LA, myristic acid (MA) and palmitic acid (PA). The results demonstrated its good performance of compatibility and energy regulation. myristic acid and tetradecyl alcohol (MA-TD) were melted well together with a mass ratio of 9:16 (Dong et al. 2020a). This PCM showed good latent heat and a suitable phase change point for regulating room temperature. Yang et al. (2020) designed a PCM comprising lauryl alcohol (LAL), SA and aluminium oxide nanoparticles (LAL-SA/Al_2O_3). Based on thermal properties obtained from experiments, the optimal proportion is proposed, and Al_2O_3 was not responsible for phase change. Its properties were kept with only 2.4% and 2.2% difference after 200 times cycles from -10 °C to 80 °C.

The other eutectic PCMs consist of organic and inorganic PCMs which have the potential to narrow the obvious gap between organic and inorganic with ideal properties. Chen et al. (2021b) introduced sodium acetate trihydrate (SAT) and sodium thiosulfate pentahydrate (STP) to prepare a SAT-STP eutectic hydrated salt PCM. The favourable mass fraction of SAT and STP is 28:72 that have high enthalpy and good phase transition temperature. The differences among eutectic PCMs were obvious. The merging of organic and inorganic PCMs has the possibility for perfect properties but the current research is lacking. The important properties of many popular inorganic PCMs are shown in Table 2.3.

Table 2.3 Main properties of sample eutectic PCMs

PCM	Phase change temperature (°C)	Density (kg/m^3)	Enthalpy (kJ/kg)	Refs.

Zn-Al	T_p: 429.8-508.5	–	H_p: 166	(Kawaguchi et al. 2020)
KNO_3:$NaNO_3$ (4:6)	T_m: 225.7	2290	H_m: 110	(Miliozzi, Chieruzzi & Torre 2019)
KNO_3:$NaNO_3$ (5:5)	T_m: 220	–	–	(Li et al. 2015)
Li_2CO_3:K_2CO_3:Na_2CO_3 (32:35:33)	T_m: 395.1 T_s: 377.9	2310	H_m: 273 H_s: 228.2	(Li et al. 2018)
Binary Fatty Acids (CA, LA)	T_m: 19.79	–	H_m: 154.16	(Meng & Wang 2020)
Ternary Fatty Acids (LA, MA, PA)	T_m: 33.5	–	H_m: 143	(Ren, Liu & Gao 2020)
LA-SA/Al_2O_3 (0.83 g/mL; 0.85 g/mL)	T_m: 21.3 T_s: 19.5		H_m: 205.9 H_s: 205	(Yang et al. 2020)
LA-SA (LA 90 wt%)	T_m: 50 (peak)	–	–	(Xiao, He & Wang 2021)
LA-SA (LA 65 wt%)	T_m: 42 (peak)	–	–	(Xiao, He & Wang 2021)
LA-SA (LA 20 wt%)	T_m: 58 (peak)	–	–	(Xiao, He & Wang 2021)
SAT-STP	T_m: 41.58	–	H_m: 211.9	(Chen et al. 2021b)

MA-TD	T_m: 28.5-42.5 T_s: 30.1-21.1	–	H_m: 198	(Dong et al. 2020a)

2.1.4 **Distinctions among different classes of PCM**

Most of them have good latent heat, bringing the possibility for energy storage, but the applicability is different based on the phase change temperature. The organic PCMs showed phase change temperature varying between 20 °C to 60 °C that is close to the suitable temperature in civil engineering (Park et al. 2019; Shi et al. 2020). Paraffin as the special one had a wide range of melting point and latent heat based on its various mixing constituent. This characteristic supports paraffin to work well in various conditions without great unexpected affects. On the contrary, the point of most inorganic PCMs is much higher than environmental temperature leading little phase change. This difference proved that organic PCMs may have a larger application range in civil engineering and inorganic PCMs can perform better in high temperatures like in battery, vehicle, and industrial waste heat recovery (Kawaguchi et al. 2020). Although there were inorganic PCMs (Fang et al. 2021; Islam & Ahmed 2021) used in construction with low phase change temperature, the used energy mostly contributed to the bound water rather than the main part. The melting points of $Na_2SO_4 \cdot H_2O$ and $CaCl_2 \cdot 6H_2O$ are only 32.4 °C and 28.84 °C but the counterparts of Na_2SO_4 and $CaCl_2$ are 884 °C and 772 °C.

As for eutectic PCMs, some properties can be modified from pure PCMs meeting the requirement, but the designs need much development for better results. The eutectic PCM had the bigger potential to show the perfect chase change temperature and latent heat.

In addition, some factors severely affect PCM performance. High supercooling posed negative effects on the phase changing in the expected state (Jin et al. 2014). This problem

was mostly shown in inorganic PCMs like hydrate salt but it can be reduced by additives (Chen et al. 2021b) and exact effective investigation was necessary (Thonon et al. 2021). The potential corrosion of inorganic PCMs was another major problem that required highly for incorporation techniques. Alkaline and metallic materials in civil engineering were prone to suffer from this threat.

In contrast, organic PCMs generally were stable in most aspects except flammability. Although the ignition point was higher than the environmental and working temperatures, the flammable property will cause a catastrophic consequence once any fire hazard occurs. As a kind of PCM with the most promising prospect, there still was a long distance to go so the concluded feature is not systematic but the high cost definitely was the immediate problem.

2.2 Incorporation methods

PCMs have great power in TES that bring novel development applied in structures. It is notified that PCMs struggling to work effectively if they are added without any supportive process. Directly adding PCM may cause an unexpected chemical reaction or microstructure changes, leading to decreasing working performance of both PCM and matrix materials. Researchers have tried various methods to enhance or maintain the performance of PCMs; anyway, incorporation is an indispensable part as presented by near all PCM application. The positive incorporation maintains the thermal properties of PCM and allows them to keep away from potentially unstable changes. There are 2 popular incorporation methods called shape stabilization and encapsulation. The encapsulation method is further classified into micro-encapsulation and macro-encapsulation but the difference is more than the literal change (size). The former showed that numerous capsules filled with PCM can be randomly and uniformly introduced into

matrix materials. The latter usually was made as a part of structures like a layer embedded in a wall or a panel bonded at the surface.

2.2.1 **Micro-encapsulated PCM (MicroPCM)**

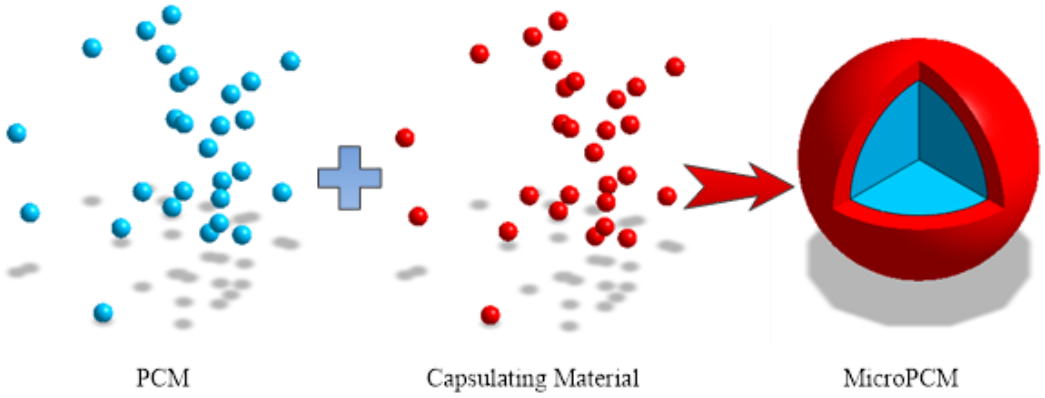

Figure 2.1 Scheme of microencapsulation in PCM

Figure 2.1 demonstrates the production of MicroPCM and the methods are diverse. The metallic oxide is compacted becoming an accepted capsule material. Kawaguchi et al. (2020) produced a kind of MicroPCM with a mean diameter of 35.7 µm. There were two main steps for manufacturing. The first was boehmite treatment to form an AlOOH-based shell coating PCM particular (Zn-Al alloy). The second was heat-oxidation treatment to make the shell as Al_2O_3 and ZnO shell with the help of a pure O_2 atmosphere at 800 °C. Finally, the PCM was coated by ZnO and Al_2O_3 layers with 500 nm and 300 nm.

The SiO_2 has brilliant reliability as an inorganic shell. Do et al. (2021) designed a SiO_2 shell to encapsulate PCM. The core materials and tetraethyl orthosilicate (TEOS) were mixed in the same mass and stirred at 50 °C lasting 1 h. Then cationic surfactant solution with CTAB ($C_{19}H_{42}BrN$) and HCl were added. The final products were obtained after cleaning. The combination was strong and the morphological stability was great. The double-layer method was preferred by researchers. Yu et al. (2020) fabricated a double inorganic shell based on silica coating paraffin PCM. The inner layer was TEOS

hydrolyzed silica. This manufacturing process went at 60 °C and a stirring speed of 400 r/min then the PCM particles were encapsulated by SiO_2. The manufacturing process of the outer layer was more complicated, modified spherical silica. The spherical silica was obtained from the mixture solution of ammonia water, anhydrous ethanol, deionized water, TEOS, and anhydrous ethanol. The spherical silica was modified by propyl trimethoxy silane in the ethanol solution. Next, modified spherical silica (after ultrasonic oscillation in deionized water) and SiO_2 coating PCM (in anhydrous ethanol-added ascorbic acid aqueous solution) were mixed and stirred. Designed PCM with double layers was finally produced after purification. The results demonstrate that the layers can be very tight without unexpected products. Although the latent heat reduced dramatically after encapsulation, thermal stability was higher by 47 °C and TC was increased dramatically.

2.2.2 **Macro-encapsulated PCM (MacroPCM)**

Unlike microencapsulation, macroencapsulation is operated on the macroscale. Therefore, there is a wide range of operation space and choices and various macroencapsulation are applied. For example, Rathore & Shukla (2020) took aluminium tubes with a dimension of 0.5 mm thickness, 16.7 mm diameter, and 900 mm or 370 mm length as the container to store PCMs. Li et al. (2018) filled PCM in a stainless steel capsule that was a spherical shell with a diameter of 34 mm and thickness of 2 mm. Besides good compatibility and the moderate energy density of MacroPCM, the positive heat transfer capacity of the capsule was tested. Grabo, Acar & Kenig (2021) simulated MacroPCM in super-ellipsoidal-based shapes with a radius of 27.4-71.6 mm. The prismatic capsule shapes presented higher packing density and higher energy storage. Talebizadehsardari et al. (2021) filled paraffin into a zigzag plate heat exchanger and revealed the influence of different zigzag angles shown in Figure 2.2.

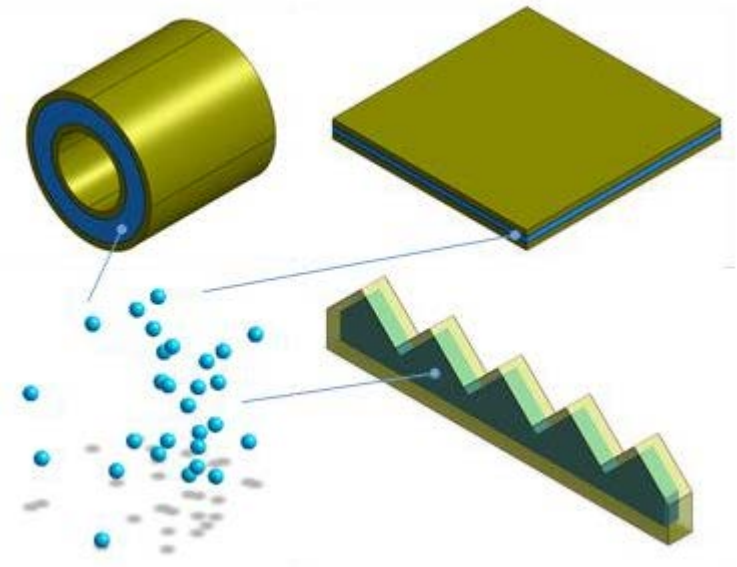

Figure 2.2 Scheme of macroencapsulation in PCM

Although there was little change in the earlier duration, the remarkable enhancement occurred with time elapses, when the melting and solidification rates increased by 38.3% and 16.3% due to higher zigzag angles from 15° to 60°. Zhou et al. (2021) designed a kind of similar model but the zigzag wall was replaced by the sinusoidal wall and the amplitude of sinusoidal was the key variable. With increasing amplitude, the higher temperature of PCM, higher melting rate, higher earlier heat flux and lower later heat flux were observed.

Some researchers embedded PCMs between different structure layers to conduct their research, mostly focusing on the heat flux and energy-saving except mechanics. These methods can be defined as special macroencapsulations. Liu et al. (2018) filled the gap between two pieces of glass by PCM with a volume fraction of 97%. The 3% is left for volume expansion in the phase change process. Similar applications were shown in experiments (Jin et al. 2014; Khan, Bhuiyan & Ahmed 2020) and numerical models (Arıcı et al. 2020; Li et al. 2019) for investigating the optimal location of PCM in walls, roofs (Al-Yasiri & Szabó 2021) and other parts.

Compared to MicroPCM, MacroPCM has extremely high PCM content because the process is more controllable leading to great energy store density. Besides, MacroPCM is often used as an independent structure only for thermal control, while MicroPCM is mixed with building materials, bringing additional influences on the matrix material. Due to less inner structure and continuous void, the percentage of PCM occupation of MacroPCMs can reach a very high level. However, The MacroPCM application heavily relies on a specific structure that is unfriendly for commercial processes and demands much for in-situ construction. On the contrary, the usage of MicroPCM is similar to a conventional additive that is positive for mass production and universal application. By the way, the SSPCM has these features of MicroPCM, shown in this paragraph.

2.2.3 **Shape stabilized PCM (SSPCM)**

Shape stabilization is another welcomed incorporation technique. It impregnates PCMs into the supporting material rather than coated by a shell. As shown in Figure 2.3. The application method of SSPCM is similar to that of MicroPCM. For leakage prevent and high absorbing rate, the supporting material has a porous structure in most cases. In a sentence, PCMs are absorbed into porous supporting materials become SSPCM composites. The most prevailing processing methods are vacuum impregnation and melting (direct) impregnation (Ramakrishnan et al. 2015), also others like the self-acting combination. Many factors determined the incorporation of SSPCM. For example, a high temperature of liquid PCM could accelerate the absorbing rate but may affect the maximum absorption proportion, and vacuum impregnation did not always work better than direct impregnation (Dehmous, Franquet & Lamrous 2021).

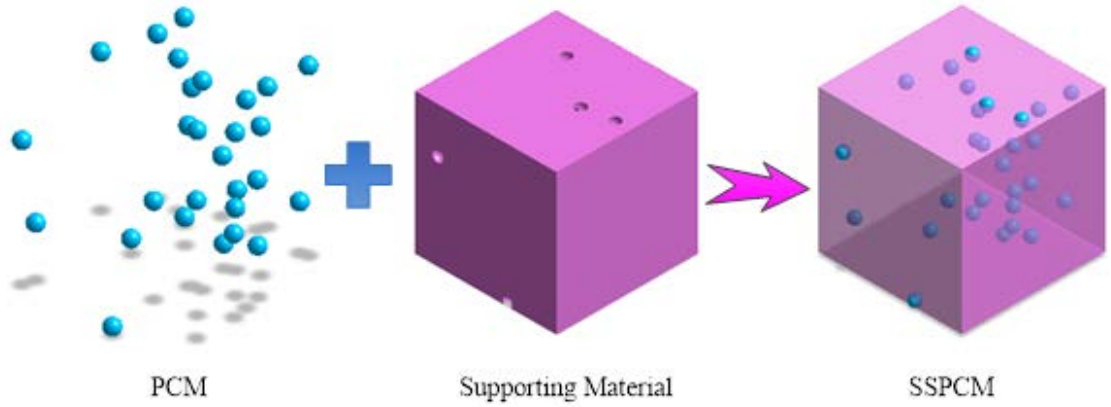

Figure 2.3 Scheme of shape stabilization in PCM

Inorganic porous materials were welcomed as supporting materials. Chen et al. (2021c) selected SBA-15, a superior representative of mesoporous silica materials. Furthermore, dopamine biomimetic modification was introduced to fabricate carbon layer-modified mesoporous silica (CLMS). The phase change enthalpy and TC were increased after incorporation with SBA-15, and then the application of CLMS expanded these advantages. Karaman et al. (2011) selected dried diatomite to absorb melted PEG. The vacuum process lasted for 90 min under 65 kPa. In this condition, the maximum absorption was 50 wt%. In the reference (Meng & Wang 2020), The impregnation was operated at 50 °C and the composite was obtained with 49wt% of PCM. This SSPCM showed good thermal reliability and stability and leakage prevention even though it suffered a thousand thermal cycles. The cheap ceramsite with an average porosity of 42.3% and a pore diameter of 8-11 mm was selected by Yang et al. (2020). The mixed core material (PCM and metal particles) and dried ceramsite were heated to 80 °C in a vacuum environment that lasted over 3 hrs. The recycled expanded glass aggregate (EGA) with a size of 0.25-4 mm was selected by Yousefi et al. (2021) to absorb PureTemp 23. After the trapped water was removed, an 80% absorption ratio was achieved based on EGA. The thermal stability was kept well.

Metallic and carbon-based materials with high TC played important roles (Fan et al. 2021; Kao et al. 2012). Yang et al. (2016) selected copper foam with a high porosity of 0.92 to contain the paraffin wax. The extremely high impregnation ratio was achieved at 96.7% via the vacuum method for 90 min. Shi et al. (2021a) produced inexpensive carbon foams derived from starch as supporting materials. The maximum mass percentage of PCM reached to 72.79%. Apart from chemical stability and leakage prevention, the benefits of this incorporation included a higher TC that was 1.93 times than that of pure paraffin.

As for organic materials and containing organic materials, there were also many achievements. In the research (Chen et al. 2010) the mixture was heated at 74 °C in a vacuum oven for 1.5 h pushed the LA into the pores of organic montmorillonite (OMMT). The great compatibility between LA and OMMT was proved. Dong et al. (2020a) connected kapok fibre with hollow PET (Polyethylene Terephthalate) playing as a mixed supporting material with a large lumen. The proportion of kapok fibre and PET was 40% and 40% with the addition of 20 % polypropylene/polyethylene sheath-core fibre. PCM and supporting material with a mass ratio of 50:1 were vacuumed repeatedly at 60 °C lasting for one day. The PCM can fill up to 40.5% of lumens. It was noticeable that the composite's heat insulation capacity was great due to low TC caused by many air voids.

Other than impregnation, some self-acting combinations were used. The PCM was added in the process of production of supporting materials. The SSPCM was obtained when the production of supporting materials was finished. Tang et al. (2016) mixed hexadecanol in the process of dye-linked PU production to get a SSPCM where the hexadecanol played as core PCM and PU presented both functions of supporting materials and PCM. Meng et al. (2020a) incorporated paraffin in polymethyl methacrylate (PMMA) by bulk

polymerization method in different mass ratios from 50% to 85%. The 70 wt% was proposed as the optimal proportion with a high enthalpy and good decomposition ability.

2.3 Applications of PCM in construction

Constructs have various structures and functions so multiple application modes are available for energy-saving (Rodriguez-Ubinas et al. 2012). In civil engineering, the thermal control of buildings is foremost. As it is known in building applications, the thermal behaviour of PCMs is affected by the oscillation of the external environment temperature that cannot be controlled (Lakhdari, Chikh & Campo 2020). PCMs delay and decrease the temperature peak in most fluctuations (Akeiber et al. 2016), which is the basis of application in structures as a thermal regulator. Although a few universal methods were proposed (Jiang, Wang & Zhang 2011), the successful use of PCM buildings applications depends on various factors, which is why specific working conditions are necessary to promote research and popularize the application of PCMs (Bhamare, Rathod & Banerjee 2020). The wide application range of PCM is benefited from unremitting potential exploration as shown in Figure 2.4. As for civil engineering, the hottest topic is energy-saving, which is room temperature regulation. Besides that, PCM has feasibility on novel applications.

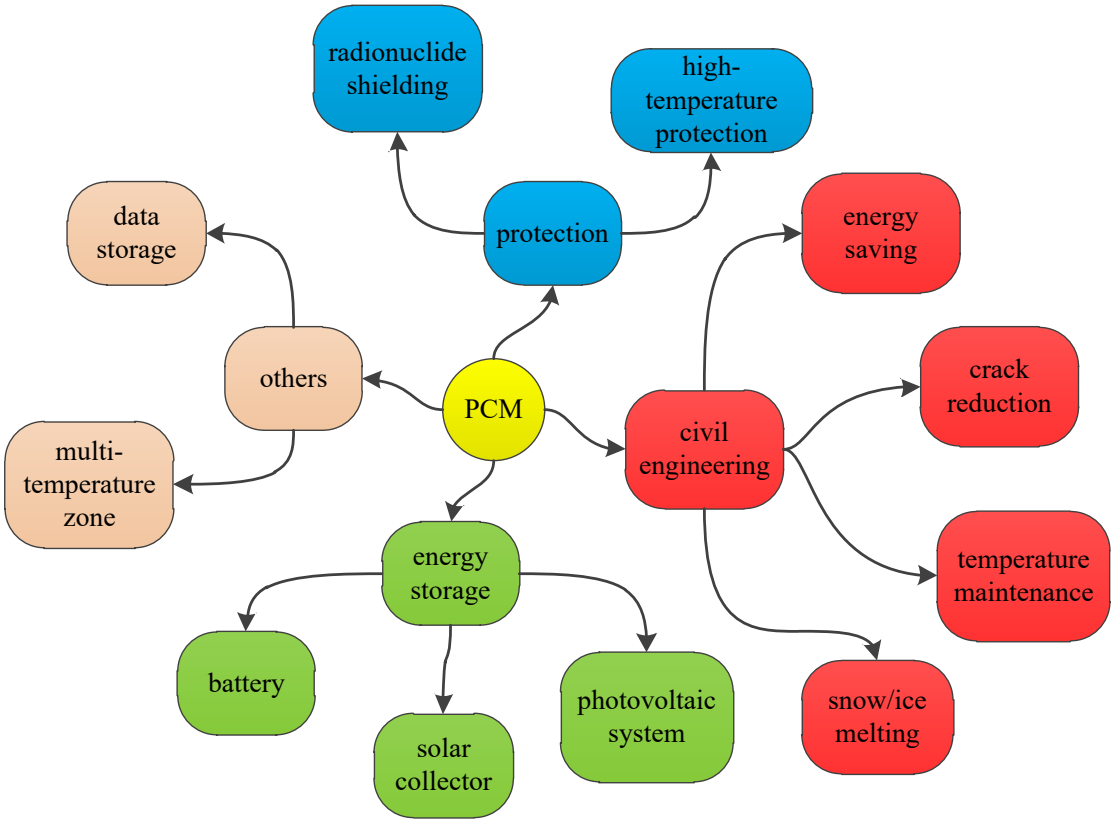

Figure 2.4 Specimens of PCM application in various areas

2.3.1 **Applications in wall**

The wall is the most important part of the building for energy control, and there is a lot of work to find the optimum application of PCMs in the wall. Rathore & Shukla (2020) embedded aluminium tubes filled with PCMs into the walls and roof of the experimental cubicle. A moderate reduction of peak temperature of 7.19%-9.18% and a time lag of 60-120 min were observed. As a result, around 0.4 US dollars can be saved on the electricity bill. Yan et al. (2021) connected a nocturnal sky radiator to the pipe-encapsulated PCM that was embedded in a wall. In hot weather, when the room needs cooling, the designed system can reduce the internal surface average temperature by 0.7 °C and heat flow by 53%, which brought a 16.1% reduction in energy consumption. A PCM thermal shield was designed by Lee et al. (2015) that was thin sheets containing polymer pouches laminated with aluminium foil on both sides to allow the PCM to fully melt and solidify

over daily cycles. The peak heat flux was reduced by 30-50% and the maximum delays were 2.3h-6.3h thanks to PCMs. Zhu et al. (2021) improved the energy-saving capacity of PCM Trombe wall by computing simulation. With the optimization of six important factors, the annual total building load was reduced by 13.52% compared with the reference. Wu et al. (2021) took the moisture changes into consideration. The thermal inertia and hygric inertia were both increased due to the PCM layer.

Different parameters of PCM, based on material and environments, may affect the performance (Al-Absi, Mohd Isa & Ismail 2020). During the process, some proposals for PCM were given. Jin, Medina & Zhang (2016) revealed that the optimal position of a PCM layer embedded in walls was affected by the thermal properties of PCM and environmental conditions. The PCM layer was supposed to be close to the interior surface if the interior surface temperature was high. In another research done by the same group (Jin et al. 2014), the reason was that this position enabled the PCM to absorb and release latent heat during all the thermal cycles compared with other positions. In the research on a conventional wall embedded by a PCM layer, the optimal position of PCM installation was close to the exterior because it improved the melting proportion of PCM (Li et al. 2019). The enhanced performance of PCM was affected by various factors. The optimum location, melting temperature, and monthly optimum thickness of the PCM layer were largely determined by the climate (Arıcı et al. 2020a). For example, Lagou et al. (2019) took the probability density function (PDF) of temperatures as the criterion to propose optimal PCM. According to the PDF data of conventional walls in this paper, the PCM layer should be embedded near the interior edge, and ideal phase change temperatures were different at 16 °C, 11 °C and 20 °C for southern, central and northern European cities. The room temperature was the key to determining the optimal melting temperature, and the insulation layer and changing environments also deserved attention (Zhou, Shire

& Tian 2014). Cao, Bui & Kjøniksen (2019) proved that energy reduction can reach 32% in summer in Oslo. The outdoor and indoor temperature significantly demanded the PCM layer performance while the insulation layer played a key role.

2.3.2 **Applications in roof, ceiling, and floor**

The possible values of PCM in cement-based materials represented by walls were proved as presented above and other building parts also attracted attention. Qu et al. (2021) analysed indoor temperature and energy-saving affected by envelope type, PCM layer layout, PCM thickness, and PCM type. These four factors showed different sensitivity on electricity saving and temperature maintenance where the envelop type was top of the list. With the same PCM layer and testing condition (Al-Rashed, Alnaqi & Alsarraf 2021), the PCM wall reduced the heat gain by around 13.78% but the PCM roof reduced it by 15.37%. Bhamare, Rathod & Banerjee (2020) proposed a new index to estimate the selection of PCMs integrated with the roof depending on ceiling temperature, time lag, decrement factor, and heat absorption. Al-Yasiri & Szabó (2021) fabricated a design of a roof with a PCM layer (melting point was 44 °C). It showed a great effect on cooling indoor temperature in the hot season, which made the maximum reduction of 9 °C. Boobalakrishnan et al. (2021) connected capsulated PCM with metal roofs under natural conditions in India. Great indoor cooling was observed that decreased by 9.5 °C in peak hours and by 5 °C on a daily average. Xiao et al. (2021) evaluated SSPCM in different building enclosures in Boston and preferred the roof to be incorporated in the thermo-optically SSPCM coatings. One of the reasons was the impact of solar orientation. Bogatu, Kazanci & Olesen (2021) took a field study for a PCM ceiling that was fabricated by macroencapsulated paraffin with a peak melting point of 24 °C and pipes filled with water flow. The 20 °C water flow with a high flow rate increased the heat discharge rate and

improved the cooling system, which led to a relatively stable indoor temperature and lower peak temperature. González & Prieto (2021) designed 2D models to reveal the performance of radiant heating floors embedded with PCM. The heat transfer decreased moderately by about 18% and TES rocketed by over 155% attributed to PCM, which led to more stable indoor temperature and less energy consumption. Larwa, Cesari & Bottarelli (2021) proved the benefits of MacroPCM in hydronic radiant floor heating systems on energy-saving and comfortable temperature while many factors like the position of PCM also had influence.

2.3.3 **Applications in gypsum board**

Gypsum is another important building material in construction that comes into contact with indoor air directly that is a good matrix material of PCM incorporation to reduce room cooling load (Shukla, Fallahi & Kosny 2012). The gypsum showed latent heat of 28 J/g with 25 wt% of MicroPCM with enthalpy of ~120 J/g (Shukla, Fallahi & Kosny 2012). The thermal conductivity increased from 0.35 to 0.6 W/(m·K) by 71.4% besides improved enthalpy to 15.24 J/g (Jeong et al. 2017). Zhou, Darkwa & Kokogiannakis (2015) investigated the thermal performance of laminated composite phase change material gypsum boards by simulation and experiments. The research was done under dynamic temperature controlled by a climate chamber. The board with 4 mm of PCM layer showed high heat exchange of up to 15.6 W/m^2 and great energy storage of up to 363.7 kJ/m^2. This ability caused more temperature reduction by 3.2 °C compared with traditional gypsum board.

2.3.4 **Applications under severe environments**

In addition to the above applications, PCMs have much beneficial capability more than energy storage. Above all, cracks have been a major problem for civil constructs seriously

affecting the structural safety of the concrete. The hydration heat of cement is generated and dissipated during the curing period leading to volume change that is the primary reason for cracks. Šavija & Schlangen (2016) gave some theoretical thoughts. Then Šavija (2018) reviewed the PCMs applied to reduce the cracks in various conditions including fresh concrete in early age and under freeze-thaw cycles. PCMs showed a positive influence in easing temperature fluctuation and smoothing temperature gradient, leading to fewer cracks.

Apart from concrete, this concept was used in pavement materials. When it comes to freeze-thaw cycles, the ice and snow on pavement pose a threat to traffic safety but conventional melting methods may damage the pavement. PCM incorporation becomes an alternative method. Esmaeeli et al. (2018) developed a one-dimensional model and relevant large-scale and small-scale experiments that suffered temperature variations of -10–10 °C and -40–24 °C, respectively. The freezing time and depth in nearly 143 of 210 cities were reduced by at least 10%, demonstrating the huge application region of PCM. If the transition temperature was over and close to 0 °C the enhancement was bigger. Farnam et al. (2017) designed and analysed two PCM, paraffin oil, incorporation methods into the pavement. One was placing PCM in LWA, expanded shale, and then mixed into concrete. Another was placing PCM in metal pipes and then embedded in concrete during the casting process. Both incorporation methods allowed the PCM to accelerate snow melting but had different performances with different ambient temperatures. Before the snow event, if the ambient temperature was relatively high or over the solidification point of PCM, the pipe method made faster snow melting than LWA method. However, if the ambient temperature was near or below the solidification point, the performance of the former decreased considerably when the latter still helped to melt snow gradually.

Many special concretes were innovated in the last decades showing great ability and a bright prospect. The connection of different functions is an available way for multifunctional concrete. Some researchers have conducted research showing the practicability. Uthaichotirat et al. (2020) made recycled aggregate concrete impregnated with a PCM where the PCM showed good performance to improve thermal properties. The PCM and recycled aggregates had good compatibility. Ren et al. (2020) attempted to introduce PCMs in ultra-high-performance concrete. These results proved that PCMs have the potential to enhance the capability of ultra-high-performance concrete. Moreover, the composite showed satisfying chemical stability. Ren, Liu & Gao (2020) also proved the reliability of lightweight aggregates (LWA) incorporated with PCM and carbon nanofibers at the same time that have electric thermal storage performance. Hunger et al. (2009) represented encapsulated PCMs that were able to maintain the self-compacting ability and enhanced thermal properties in self-compacting concrete.

2.4 Enhancements and impacts of PCM concrete

2.4.1 **Thermal properties and Phase change efficiency enhancement**

(a) Nano-particles

Nano-particles of metal or metallic oxide were popular additives to optimize the process of phase change that was inefficient due to the low TC of PCMs. Sheikholeslami & Mahian (2019) numerically investigated the influence of inorganic nanoparticles and magnetic fields on PCM solidification. The reliability of the Galerkin FEM code was verified. The CuO nanoparticles with a conductivity of 18 W/(m·K) and heat capacity of 540 J/(kg·K) were added into pure PCM. TC improvement was the main reason for solidification time reduction (Sheikholeslami 2018a) that was affected by some factors like the diameter of nanoparticles (Sheikholeslami 2018b). Two parameters were

considered that solidification time will decrease with decreasing Rayleigh number or increasing Hartmann number.

Besides copper-based particles, aluminium-based particles are also prevailing. Based on results obtained from experiments (Yang et al. 2020), the Al_2O_3 nanoparticle had a higher efficiency than Fe_2O_3 and TiO_2 in the matter of TC enhancement, and the 0.5 wt% Al_2O_3 nanoparticles were proposed in (Yang et al. 2020) but 1% (Chen et al. 2021a) and 3 wt% in (Peng & Sadaghiani 2021). Adding some nanoparticles could enhance the phase change rate but superabundant particles will increase the viscosity leading to weaker natural convection (Ren, Xu & Luo 2019). The melting time was reduced up to 26.8% but energy storage decreased by up to 31% in (ul Hasnain et al. 2021).

The property of single particle is crucial but the hybrid method has outstanding capability. Hosseinzadeh et al. (2021) tested the impacts of hybrid nanoparticles (MoS_2-Fe_3O_4) with various factors including volume concentration, radiation, and shape. Results proved the most noticeable influence of radiation that reduced the solidification time by 70 s and the most contribution of 74.58% of radiation. In addition, the different particle incorporation methods can be applied simultaneously. Do et al. (2021) introduced Fe_3O_4 and Cu particles to produce the n-eicosane-Fe_3O_4@SiO_2@Cu composite with higher performance. The Fe_3O_4 was mixed with n-eicosane to enable the composite to have a magnetic function with little influence on thermal performance. The Cu was distributed on the surface of the SiO_2 shell to enhance the TC. However, hybrid nanoparticles were not always better. Nitsas & Koronaki (2021) added Cu and Al_2O_3 nanoparticles simultaneously. Around 11.5% of heat storage capacity was lost for both single or hybrid conditions. Because of the higher TC of Cu, the addition of Al_2O_3 nanoparticles showed little advantages in this experiment.

The carbon-based materials were more prevalent when the brilliant TC was proved. Karaman et al. (2011) added EG in the PEG/diatomite composite for further higher TC. The testing results demonstrated good compatibility and strong improvement on TC that increases linearly. The improvement of EG was also significant in (Chriaa et al. 2021; Sun et al. 2020; Zhang et al. 2018). For instance, TC was improved by 114.4% because of 7 wt% of EG (Rathore & Shukla 2021). In addition, the 0.02 wt% of carbon particles provided a better energy storage rate (Sun et al. 2020). The different morphology contributed to various impacts.

The range of additives should be expanded and not limited to metallic and carbon materials. To further enhance the thermal stability after numerous cycles, Kawaguchi et al. (2020) introduced glass frit as a sintering agent on a Zn-Al PCM in the microencapsulation process. In the second step before heating, the same weight of glass frit was added and the mixed material was milled. After one hundred cycles with a temperature range of 300 °C to 600 °C, the composite showed brilliant thermal durability when around 80% of the material was intact. However, a reduction in heat storage was observed.

(b) Conductive fins

What has been mentioned are micro technologies for MicroPCM and SSPCM. The macro technology is also feasible especially for MacroPCM and it can improve the performance of most PCM. Although Hamad et al. (2021) took the aspect ratio as the factor to analyse the PCM performance in a rectangular enclosure, more concerns were concentrated on inner technologies including fins metal structure. Fins were the most used components to improve the phase change process. The added fins enhanced the effective TC of PCM (Gil et al. 2018) and more fins could make the temperature distribution more uniform

(Joneidi et al. 2020) as well as faster phase changing (Acır & Emin Canlı 2018). Although the transfer area was also increased, more fins posed threat to natural convection and heat transfer coefficient at the same time (Cao et al. 2018). Adding fins sometimes was more efficient and economical than nanoparticles (Peng & Sadaghiani 2021; Ren, Xu & Luo 2019; Sarani et al. 2020). The material with high TC, like copper, usually performed better (Hosseinzadeh et al. 2021; ul Hasnain et al. 2021). With the same volume percentage, copper strip fins with a thickness of 4.5 mm saved 89.48% melting time when the longitudinal copper fins and Al_2O_3 particles counterparts were 76.69% and 19.59% (Sarani et al. 2020). Even though strip fins had half (2%) volume, they still showed better thermal performance than longitudinal fins (Sarani et al. 2020). The longer fin made more contribution to faster melting. With the help of 1% volume CuO, 30% of the length of the fin can be reduced, but the same influence was maintained (Arıcı et al. 2020b). The position of fin also generated effects energy storage that was 11-36% higher than no fin situation. In (Rabienataj Darzi, Jourabian & Farhadi 2016), the melting process could be accelerated by a vertical-oriented elliptical cylinder, adding nanoparticles and fins. The highest effectiveness was attributed to fins, and the maximum time reduction reached 82% by 20 fins compared to a 45% reduction caused by 4% nanoparticles. Similar results were presented in the solidification process, but only 16% of the time was saved by 4% nanoparticles.

The different configurations and shapes of fins generated various impacts on PCM working. Researchers investigated many shapes of fins (Desai, Shah & Singh 2021). Ji et al. (2018) assembled two rectangle fins in Figure 2.5 (a) with different length ratios (upper: lower) and constant total lengths**.** The lower length ratio caused intensive natural convection and a longer solid-liquid interface, leading to fast melting. Ren, Xu & Luo (2019) divided the copper rectangle fin into 2 triangle fins in Figure 2.5 (b) having the

same length and total volume. The melting process was accelerated which could be the consequence of a larger heat transfer area. Yao & Huang (2021) investigated the effect of longitudinal triangular fins in Figure 2.5 (c) on solidification in a triplex-tube system. These fins decreased the solidification time of PCM by 30.98% compared to rectangular fins. The height and TC of the fin prominently affected the required time. Zhang, Li & Chen (2020) analysed the effects of tree-shaped fins in Figure 2.5 (d) in LA solidification via a verified model. The length ratio and width ratio between branches and trunks changed the aluminium alloy fin performance significantly. Results proved the improvement of tree-shaped fins compared to traditional fins as well as positive and negative effects of higher length ratio and width ratio.

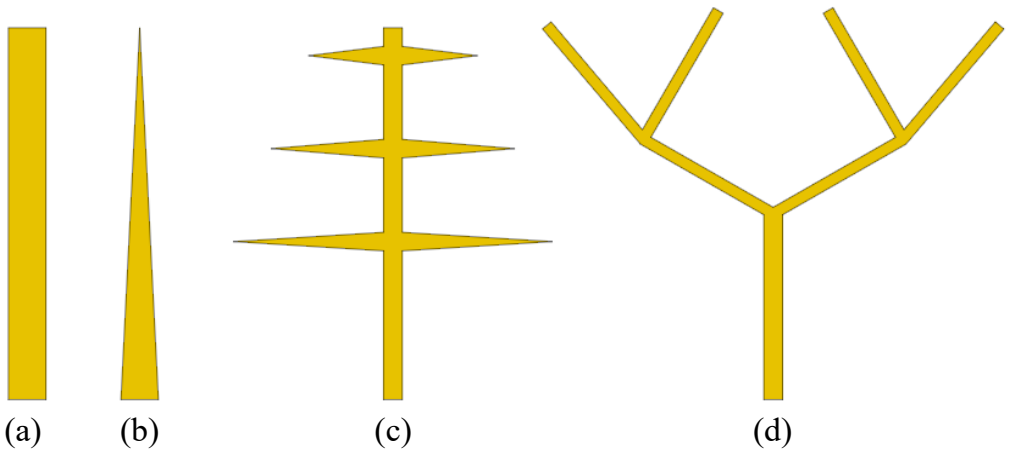

Figure 2.5 Specimens of PCM fins

More works were achieved to investigate the influence of the configuration of fins, and an optimizing algorithm was effective. Pizzolato et al. (2017) designed a computational optimization method for effective fins. The impacts of fluid convection were given and optimal configurations for melting and solidification were different. Xie, Lee & Xiang (2019) used an efficient program code for 3D topology optimization (Liu & Tovar 2014)

to design the shape of fins. The optimized fins improved the conduction heat transfer with close metal volume, leading to a faster melting process.

(c) Conductive structure and pre-treatment

Porous structures with high conductivity had a similar function to fins. Zhang et al. (2020) investigated the influences of copper fins and copper foam on a PCM enclosure encasing the part of a heat pipe. The combined methods enhanced most heat transfer although weakened the natural convection (Chen et al. 2021a). According to the evaluation indexes like heat flux and heat storage, Meng et al. (2020b) analysed the effects of porosity of copper foam on PCM. The lower porosity improved the heat transfer but decreased the energy storage. Li et al. (2021a) improved the melting rate further by optimizing the partial porosity of copper foam. The results gave an important conclusion that enlarging the top and middle pore density can augment natural convection and strengthen the vortex at the bottom, leading to a higher melting rate. Li et al. (2015) combined PCM and SiC-honeycomb with a density of 0.741 g/cm^3. With the 30 wt% of SiC-honeycomb, the TC increased by 454%, which generated major impacts on heat transfer. Zhao et al. (2021) set periodic structures made of 4 kinds of metal to reveal the impacts of exact parameters. The porosity density was defined as pores per inch (PPI) that affected the heat transfer significantly and when the PPI exceeded the critical value the further positive effects can be neglected.

The improvement method was not restricted to particle addition. Konuklu et al. (2020) took microwave and calcination as pre-treatments to enhance latent heat energy storage capacity. According to the results, the microwave method showed better influence on latent heat for both diatomite and sepiolite based SSPCM composites. Summarily, many

auxiliary methods have excellent abilities to enhance the properties of PCM composites. The valuable performance of PCM enhancements are shown in Table 2.4.

Table 2.4 Enhancement for phase change efficiency of PCMs

Methods	Consequences	Refs.
Volume fraction of 4% CuO nanoparticles	Solidification time was reduced by 14%	(Sheikholeslami & Mahian 2019)
Employ external magnetic field with Hartmann number from 0 to 10	Solidification time was reduced by up to 23.5%	(Sheikholeslami & Mahian 2019)
0.5 wt% Al_2O_3 nanoparticles mixed with PCM	TC raised from 0.198 to 0.2843 W/(m·K) by 43.3%	(Yang et al. 2020)
0.1% Al_2O_3 nanoparticles mixed in PCM	Melting time decreased by 184 s	(Chen et al. 2021a)
1%, 5% and 10% Al_2O_3	Melting time decreased by 11.5%, 19.2% and 26.8% Energy storage decreased by 11%, 19% and 31%	(ul Hasnain et al. 2021)
2% and 4% of Cu nanoparticles	Solidification time decreased by 9% and 16% Melting time decreased by 25% and 46%	(Rabienataj Darzi, Jourabian & Farhadi 2016)

Cu nanoparticle covering the shell	TC ascended excellently up to 83%	(Do et al. 2021)
Cu nanoparticle	energy storage rate increased under 324 K	(Ren, Xu & Luo 2019)
Blade MoS_2 – Fe_3O_4 with radiation of 0.5 and 1 (fixed volume fraction of 0.025)	Solidification time decreased by 40 s (21%) and 70 s (36%)	(Hosseinzadeh et al. 2021)
Addition of EG	TC raised linearly from 0.32 to 0.67 W/(m·K)	(Karaman et al. 2011)
EG up to 7wt%	TC raised from 0.145 to 0.311 W/(m·K)	(Rathore & Shukla 2021)
EG up to 15wt%	TC raised linearly up to 4.6%	(Chriaa et al. 2021)
0.06 wt% NG nanoparticles	TC raised from 0.3 to 0.38 W/(m·K)	(Sun et al. 2020)
0.1 wt% NC nanoparticles	TC raised from 0.3 to 0.34 W/(m·K)	(Sun et al. 2020)
4 wt% EG	TC raised to 0.944 W/(m·K) by 307%	(Zhang et al. 2018)
50 wt% glass frit as sintering agent	Brilliant thermal durability 41% (117 to 48 kJ/kg) latent heat reserved	(Kawaguchi et al. 2020)

Microwave for no more than 1 min	H_p of diatomite-based SSPCM raised from 51.71 to 65.24 kJ/kg	(Konuklu et al. 2020)
Microwave for 3-6 min	H_p of sepiolite-based SSPCM raised from 40.54 to 59.54 kJ/kg	(Konuklu et al. 2020)
196 transversal squared fins	Effective TC increased by 4.11-25.8%	(Gil et al. 2018)
4, 10, 15 and 20 fins	Melting time decreased by 39%, 73%, 78% and 82% Solidification time decreased by 28%, 62%, 75% and 85% Convection was enhance with ratio lower than 1	(Rabienataj Darzi, Jourabian & Farhadi 2016)
Double fins with different length ratio	Melting time decreased by 40.5% with ratio of 0.11	(Ji et al. 2018)
triangle fins compared to rectangle fin	melting rate increased	(Ren, Xu & Luo 2019)
Single or double branched fins	Melting time decreased by 35.4% and 45.9% Energy storage increased by 17% and 20%	(ul Hasnain et al. 2021)

Tree-shaped fins with length ratio of 1 and width ratio of 2	Complete solidification time decreased by 66.2% Complete melting time reduced by 4.4%	(Zhang, Li & Chen 2020)
Optimized fins by program code with metal volume fraction of 20% and 30%	Melting time for 0.7 PCM reduced by 3.1% Melting time for 0.7 PCM reduced by 6.4%	(Xie, Lee & Xiang 2019)
Copper fins	Complete cycle decreased by 82.70%	(Zhang et al. 2020)
Copper foam	Complete cycle decreased by 89.03%	(Zhang et al. 2020)
Combining copper fins foam	Complete cycle decreased by 93.34%	(Zhang et al. 2020)

2.4.2 **Impacts of PCM composites on cement-based materials**

The types and proportions of raw materials are decisive factors for concrete ability which are changed due to PCM introduction (Richardson, Heniegal & Tindall 2017). Generally, pure PCMs cannot be directly used due to their severe threat to the chemical stability and mechanical properties of building materials, but PCM composites are available. Besides thermal influence, the physical and mechanical properties' impacts of PCM composites on construction materials deserve much attention to guarantee the performance. For instance, Dehmous, Franquet & Lamrous (2021) tested concrete with various PCM composites and fabrication methods. Many factors could make the changes in mechanical performance and the fabrication method was proposed as the critical one.

Qu et al. (2020) introduced the paraffin/fumed silica SSPCM in foam concrete. When the percentage of PCM composites increased the TC fell gradually. At the same time that heat storage capacity was improved, the ability to insulate heat was also enhanced. The improved thermal properties (higher energy storage, lower pick temperature, etc.) and weaker mechanical properties (lower bearing stress) were commonly shown (Shen et al. 2021; Yang et al. 2020). Yousefi et al. (2021) replaced the sand of mortar with EGA-PCM based on volume with a constant cement. The smooth surface and porous structure of EGA caused the higher flow, lower density and weaker strength. The weak bond of EGA-PCM and fly ash was also attributed to the reduction of compressive and flexural strength. In thermal performance tests, the EGA with low conductivity reduced the temperature increasing rate by up to 0.6 °C/min and further by 2 °C/min due to PCM. The sand was replaced by EPO-PCM according to different volume percentages (Ramakrishnan et al. 2017). There was an obvious and continuous reduction of apparent density and TC of concrete samples with an increasing proportion of PCM composites that were believed to be positive for TES. The dramatically decreased compressive strength (S_c) and the increasing shrinkage strains were given. The low stiffness of PCM composites may be the reason for this phenomenon leading to early age shrinkage cracks. Djamai et al. (2021) designed a textile-reinforced concrete slab with PCM. The thermal enhancement was great, with an energy saving of 37% and a lower peak temperature of 4 °C. Moreover, detailed information for cracks under three-point bending was presented. The load-bearing capacity was decreased significantly with the addition of PCM and further deteriorated if the content rate of PCM was higher.

The commercial PCMs showed the potential for mass production and valuable application. Snoeck et al. (2016) tested various commercial PCM composites including Micronal series and Mikrathermic series in the cement mortar. The lower value of flow

was shown in all samples. The PCM posed a threat to flexural strength and compressive strength, and the samples of dispersed PCM reduced two times more than others, which presented the preference for dried PCM encapsulation. Moreover, the additive method (PCM was added at the end of the mixing process with various mass percentages) led to a higher reduction than the replacement method (the sand was replaced by PCM). Essid, Loulizi & Neji (2019) investigated the various performance of concrete incorporated by Micronal DS 5038X. The compressive strength became weaker but the damaged PCM brought less reduction because the broken structure asked fewer pores. The higher porosity and lower adhesive properties were the important reasons leading to less strength. The higher porosity didn't change the permeability because these pores were not connected. Joulin et al. (2014) made a cement mortar plate with Micronal DS 5001X microcapsules. The PCM caused decreasing TC and increasing energy storage in both specific heat and latent heat.

As shown in Table 2.5, the impacts of PCM composites on construction materials were diverse. Many influences, like lower density and compressive strength, directly change the performance of construction materials. It is hard to remedy all drawbacks in a short time; instead, it is reasonable to select proper PCMs and incorporation methods based on the requirements of matrix elements. However, the research data is insufficient to reveal the exact relationship.

Table 2.5 Effects of PCMs on construction materials

Construction materials	Impacts	Refs.
Cement mortar	Specific heat from 925 ±46 to 1238±62 J/(kg·K) at liquid and 1255 ±63 at solid	(Joulin et al. 2014)

Concrete	specific heat capacity increased from 946 to 1145 J/(kg·K) by 21%	(Dehmous, Franquet & Lamrous 2021)
Concrete	average specific heat capacity increased by 76.5% (6wt% PCM)	(Shen et al. 2021)
Cement mortar	Longer time delay and lower pick temperature	(Yang et al. 2020)
Cement mortar	Temperature increasing rate from 3.6 °C/min to 1.6 °C/min (EP100)	(Yousefi et al. 2021)
Cement mortar	Latent heat of 19 kJ/kg	(Joulin et al. 2014)
Cement mortar	Latent heat up to 21.3 kJ/kg	(Qu et al. 2020)
Cement mortar	With 80% PCM, thermal storage increase from 47.39 to 126.04 kJ/kg by 166%	(Ramakrishnan et al. 2017)
Concrete	Energy storage increased from 23.65 to 29.43 kJ/kg by 24.4%	(Dehmous, Franquet & Lamrous 2021)
Concrete	thermal resistance increased by 6.35% (6wt% PCM)	(Shen et al. 2021)
Cement mortar	TC decrease up to 65.8%	(Ramakrishnan et al. 2017)
Cement mortar	TC decrease from 0.65 ±0.02 to 0.37 ±0.01 W/(m·K)	(Joulin et al. 2014)

Concrete	TC decrease from 0.65 ±0.02 to 0.37 ±0.01 W/(m·K)	(Dehmous, Franquet & Lamrous 2021)
Cement mortar	Apparent density decrease from 2039 to 1244 kg/m^3 by 39%	(Ramakrishnan et al. 2017)
Cement mortar	Apparent density decrease from 2.20 g/cm^3 to 1.45 g/cm^3 (34%) with 20 wt% PCM composite	(Yang et al. 2020)
Cement mortar	Density decrease from 2001 kg/m^3 to 1248 kg/m^3	(Joulin et al. 2014)
Cement mortar	Density increased from 2367 kg/m^3 to 111.2 kg/m^3 by 53% (EP100)	(Yousefi et al. 2021)
Cement mortar	Density increase from 545 to 565 kg/m^3 (PCM by 30wt%)	(Qu et al. 2020)
Cement mortar	Shrinkage strains increase up to 0.125%	(Ramakrishnan et al. 2017)
Cement mortar	Up to 8% reduction on flow with dried PCM	(Snoeck et al. 2016)
Cement mortar	Up to 8% reduction on flow with dispersed PCM	(Snoeck et al. 2016)
Cement mortar	Flow diameter increased from 21.75 cm to 23.50 cm (EP100)	(Yousefi et al. 2021)
Cement mortar	Maximum bearing strength declined from 0.58 to 0.37 MPa with 20 wt% PCM composite	(Yang et al. 2020)
Cement mortar	Up to 50% on 28-day S_c from 60 to 35 MPa	(Snoeck et al. 2016)

Cement mortar	With 80% PCM, 28-day S_c decrease from 53.77 to 16.36 MPa by 70%	(Ramakrishnan et al. 2017)
Concrete	28-day S_c decrease from 36 MPa to 27 MPa when 5% damaged PCM composite	(Essid, Loulizi & Neji 2019)
Concrete	S_c decreased non-linearly by minimum 36%	(Dehmous, Franquet & Lamrous 2021)
Concrete	S_c decrease from 18.56 MPa to 4.37 MPa by 76.5% (6wt% PCM)	(Shen et al. 2021)
Cement mortar	28-day S_c decrease from 76.7 MPa to 8.8 MPa by 89% (EP100)	(Yousefi et al. 2021)
Concrete	28-day S_c decrease from 39 MPa to 19 MPa when 5% undamaged PCM composite	(Essid, Loulizi & Neji 2019)
Cement mortar	28-day flexural strength decrease from 2.6 MPa to 0.6 MPa by 77% (EP100)	(Yousefi et al. 2021)
Concrete	Flexible strength decrease non-linearly by minimum 14%	(Dehmous, Franquet & Lamrous 2021)
Cement mortar	Flexural strength decrease gradually	(Snoeck et al. 2016)

2.5 Valuable topics deserve further development

2.5.1 **Novel PCM with enhanced properties**

PCM is the most significant part of determining the relevant research but there is no perfect PCM by far (Tyagi et al. 2022). A novel PCM may be capable of solving most problems in current programs. Although comprehensive research of pure PCM is

indispensable as it is a conventional and well-directed method, the exploitation of novel eutectic PCMs has a huge potential ability to overcome the inherent defects of pure PCMs. It is a high-demanding and tough process that needs support from multiple disciplines like chemistry and material. As long as the development of PCMs gains constructive progress, a substantial contribution will be made to other research processes.

2.5.2 **Reliable and economical PCM composites**

Besides core PCMs, there are some crucial criteria for PCM composites including corrosion protection, TC, structural integrity, etc. Although some methods were proven reliable, the operating process is complex and requires highly time-consuming and costly. These problems must be solved before mass production and applications.

Reducing cost is a positive result and purpose based on the great development of novel PCMs and incorporation techniques, which seems like an assignment with less importance and lower priority compared to PCM and incorporation (Liu et al. 2020; Yu et al. 2023). Even so, it is also reasonable to work right now. For example, Boussaba et al. (2018) made coconut fat recovered from underused feedstock as low-cost and eco-friendly PCM. To maintain these features, supporting materials were cellulose fibres prepared from recycled cardboard, and natural clay was selected as a binder. Additionally, a direct immersion method with no vacuum treatment, a simple incorporation process, was adopted. This composite had a fine performance with a phase change temperature of about 20 °C, latent heat of about 107 kJ/kg and absorption of 56 w%. Although some deficiencies were observed like uniform distribution, it is still acceptable and is a meaningful attempt.

2.5.3 **Targeted optimisation**

The performance of PCMs is affected by various impacts like ambient climate, heating/cooling rate, orientation and inner structure of constructs (Cao, Bui & Kjøniksen 2019; Qu et al. 2021; Rolka et al. 2021), etc. Take ambient climate as an example, Mi et al. (2016) numerically investigated energy-saving and economic efficiency led by the same PCMs via EnergyPlus. The models took different cities (Shenyang, Zhengzhou, Changsha, Hong Kong and Kunming) with climates classified into severe cold, cold, hot summer and cold winter, hot summer and warm winter, and mild, respectively. Except for climates, other parameters were the same. The highest energy-saving occurred in Shenyang. The amount is 10 times that in Hong Kong. Considering electricity prices, money-saving was great in Shenyang, but PCM application in Hong Kong may take no economic benefits. These demonstrated that research on PCM should consider different application conditions. Similar works proposed the various optimum melting temperatures and masses of PCM depending on climatic conditions (Arıcı et al. 2020a; Jia et al. 2021b). In addition, PCM performance may have a huge gap in different months. According to data in the reference (Xie et al. 2018), changing latent heat and phase change temperature of PCM can improve its performance only in some months like June and September. Maybe in other months, the effect is adverse. The disadvantageous impacts of PCM are not rarely seen if the optimisation is not targeted well (Guo & Zhang 2021).

However, there are opposite requirements for TC in different purposes and experiments. What is mentioned in the previous paragraphs is the higher conductivity but Li et al. (2019) proposed that the lower conductivity helps reduce heat in an indoor room. Therefore, a huge data is required to build a comprehensive system to determine the optimal properties of PCM in various conditions.

2.5.4 **Workability of PCM concrete**

The capability ceiling of PCM in buildings depends on the total heat storage. In consideration of limited absorbed energy density, a higher quantity of PCM can enhance the thermal regulation effectively. The concrete takes the majority volume of building materials in most buildings leaving great space for PCM incorporation. Additionally, the thermal conductivity of concrete is higher than that of gypsum and plaster (around 10 times) enabling the heat to be absorbed and released more efficiently (Adesina 2019). Hence the concrete is the most important component in which PCM composites are introduced. With PCM addition, the workability and physical characteristics of concrete are changed significantly which poses a fatal impact on the practical application (Richardson, Heniegal & Tindall 2017). The benefits of energy efficiency and the drawbacks of mechanical properties are observed simultaneously (Hekimoğlu et al. 2021a; Kastiukas, Zhou & Castro-Gomes 2016; Pilehvar et al. 2017). The drawbacks are generally caused by the fabrication methods (e.g., post process and supporting material for SSPCM) and low compatibility with additives (e.g., microPCM composites). Nevertheless, the workability, mechanical property, and time-stability require more research work.

2.5.5 **Multifunctional concrete**

PCMs had the potential to cooperate with functional concrete (Hunger et al. 2009; Kuzmenko et al. 2022; Medved' & Trník 2018; Wang et al. 2024). In addition to the energy and environmental issues, specific PCM concrete can bring interesting benefits, like low-temperature PCM concrete to melt snow and reduce freeze-thaw damage. Deicing salt has been popular for decades, but the damage can destroy concrete structures (Farnam et al. 2015). In this case, PCM with low transition temperature may release the heat to prevent ice and snow. A convincing result is completed where the snow with

depths of 0.7 and 1.7 inches is melted by PCM (Deb et al. 2024). The improved resistance to freeze-thaw cycles and weaker incidental deterioration can extend the service life by 20.7% - 35.9% contributed by 20% PCM addition (Urgessa et al. 2019). On the other hand, The self-heating concrete is electrically conductive and aims to raise the temperature of the concrete by current application, when ice removal is one of the significant advantages (Rahman et al. 2022). Many remarkable achievements have been presented about efficient ice/snow removal by self-heating concrete (Moman, Butt & Nassiri 2023). It is noticeable that carbon-based additives are also prevailing for self-heating improvement (Farcas et al. 2021; Guo et al. 2022; Li et al. 2022; Lu et al. 2023), which shows the protentional combination with PCM concrete. A few studies have been carried on for PCM concrete with self-heating ability (Jang et al. 2023; Niu et al. 2023) but the way to ensure the effective multifunction needs a great deal of research.

2.5.6 **Long-term efficiency**

Civil engineering has been designed for decades, even hundreds of years, bringing forward high demand for long-term reliability. The evaluation should involve multiple perspectives on a long-term performance like carbon footprint, energy saving, cost payback period, and so on (Arumugam & Shaik 2021; Fang et al. 2022; Yu et al. 2022).

For another, a lot of construction waste has been a severe problem that is solved by recycling. The chemical stability of PCM is lower than conventional construction materials, and PCM addition breaks the original, which challenges the service life, recycle utilisation and environmental impact. More environmental data is required for life cycle assessment than ordinary buildings (Struhala & Ostrý 2022). In addition, the type of PCMs is huge and the properties may be extremely different, like flammability. Many parameters are crucial to make an accurate assessment.

CHAPTER 3. STABLE SSPCM COMPOSITE BASED ON COARSE AGGREGATE AND PARAFFIN

The PCM incorporation in concrete often shows the improved ability of energy saving. The critical adverse impact of PCM addition on concrete is weaker strength (Fang et al. 2022; Kastiukas, Zhou & Castro-Gomes 2016; Pilehvar et al. 2017). It is proved that the weaker strength of PCM composites compared with conventional aggregates plays an important role where a part of aggregates is substituted by PCM composites (Hekimoğlu et al. 2021a; Hekimoğlu et al. 2021b; Hekimoğlu et al. 2022). At the beginning stage, PCM was introduced in conventional aggregates directly to test the possibility of strength maintain.

3.1 Material and sample preparation

Based on the literature review, fly ash ceramsite and paraffin were selected to fabricate the PCM composite as shown in Figure 3.1 (Fang et al. 2022; Ren, Liu & Gao 2020; Shen et al. 2021). The fly ash ceramsite was produced by JiangSu Houde Ceramsite Co.,Ltd (China) that had high moisture absorption and low density (high porosity factor) due to the requirement of high paraffin absorption and light weight. In this experiment, the ceramsite with size from 7-13 mm was used because this diameter played the most amounts of the coarse aggregates. All ceramsites were dried for 12 h at 80 ℃ to remove the moisture in the pores before experiment.

The refined paraffin was purchased from ShangHai Joule wax Co.,Ltd (China) that was recommended PCM for building energy storage. This paraffin with high purity had the melting temperature of ~28 ℃, enthalpy of ~220 kJ/kg, specific heat of 3.22 J/(kg·K) and thermal conductivity of 0.21 W/(m·K). Considering potential degradation and impurity

during packing and delivery, some parameters were revised in this experiment according to the test results.

(a) Dry ceramsite (b) Paraffin

Figure 3.1 Raw materials

Generally, an incorporation process is necessary to improve the working compatibility, such as being mixed in concrete, gypsum and asphalt. Popular incorporation methods are macro-encapsulation, micro-encapsulation, and shape-stabilization. Impregnation is a prevailing shape-stabilization method that is suitable for porous supporting materials where the liquid PCM is absorbed into the pores as PCM composites. The impregnation method has many advantages, and the low cost is the significant one. Vacuum impregnation gives higher pressure on the liquid PCM to fill the pores, leading to a higher absorption rate than direct impregnation. Therefore, the vacuum impregnation was selected in this experiment. The temperature was maintained at 40°C to ensure the paraffin attained a highly fluid state, while the vacuum pressure was set to approximately 70 kPa. In this condition, the process lasts for 4 hours, enabling the pores to be filled enough. Three groups were processed as shown in Figure 3.2.

(a) Dried samples

(b) Immerged in paraffin

(c) Vacuum oven

(d) Paraffin/ceramsite composites

Figure 3.2 Incorporation process

3.2 Essential properties of raw materials

3.2.1 **Basic physical properties of ceramsite**

The porosity is the key feature of ceramsite that is presented by density and moisture absorption. As shown in Table 3.1, the ceramsites were sieved and the residues between 7 mm to 13 mm were used. There were three groups of dried samples with weights of 73.26 g, 80.99 g, and 85.61 g, respectively. Apparent density and bulk density, two important parameters of light aggregates, were tested as 915.94 kg/m^3 and 536.87 kg/m^3. As for the moisture absorption test, the ceramsites were immerged in water under hydrostatic pressure and normal atmosphere. The moisture absorption reached to 15.85% after 1 hour and 23.80% after 24 hours. In this experiment, the moisture absorption means

the mass ratio of absorbed water to dried cemasite and it is also same for the paraffin absorption in the following parts.

Table 3.1 Physical parameter of ceramsite

	Dried weight (g)	Apparent density (kg/m^3)	1h Moisture Absorption (%)	24h Moisture Absorption (%)
Sample 1	73.26	915.75	16.19	24.13
Sample 2	80.99	930.92	15.74	23.99
Sample 3	85.61	901.16	15.61	23.27
Average	-	915.94	15.85	23.80
Notes:	Diameter size: 7 mm-13 mm; Bulk density: 536.87 kg/m^3			

3.2.2 **XRD result of ceramsite (constituent)**

X-Ray Diffraction (XRD) is a popular method to obtain the composition of the material, the structure or form of the atomic or molecular material. The constituent of ceramsite could affect the connection and reaction between ceramsite and PCM, although paraffin showed good chemical stability. Therefore, the XRD test is a basic and essential step in this experiment.

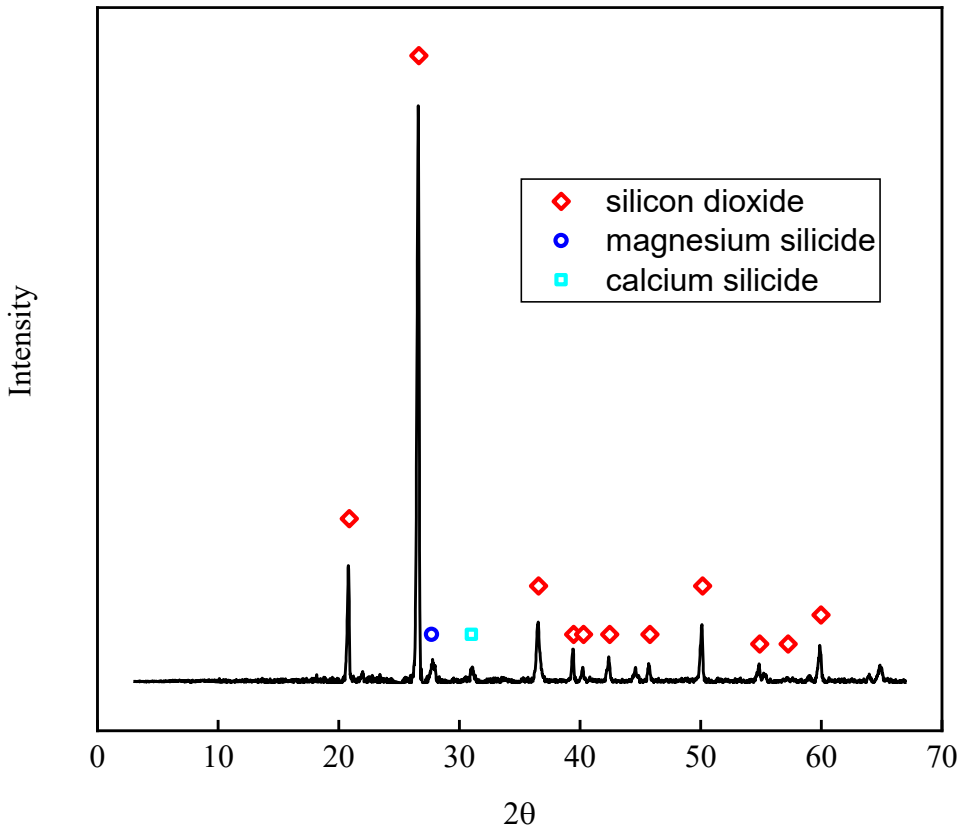

Figure 3.3 XRD result of ceramsite

The constituent of ceramsite was tested by XRD and the result was shown in Figure 3.3. The silicon dioxide was prominent, contributing to most peaks. The magnesium silicide and calcium silicide were respectively observed by a single peak. These elements were stable and would not react with paraffin nor affect paraffin impregnation. The silicon dioxide, a little magnesium silicide (27.78°) and calcium silicide (31.08°) were common in concrete, which were good for the inter bonding with cement matrix. Therefore, the ceramsite, used in this experiment, was reliable and harmless to paraffin and concrete showing good potential for SSPCM fabrication. The incorporation process had little relationship with chemical reactions.

3.2.3 **DSC results of paraffin (thermal properties)**

Differential Scanning Calorimetry (DSC) is an important method to measure a variety of thermodynamic parameters that was conducted via NETZSCH DSC 200 F3 in this experiment. The crucible was aluminum and the inert gas was nitrogen. The heating rate was set at 5 ℃/min to reduce the time lag because the thermal conductivity of paraffin was low. The 13 mg of sample was tested every time and the negative heat flow presented the exothermic process.

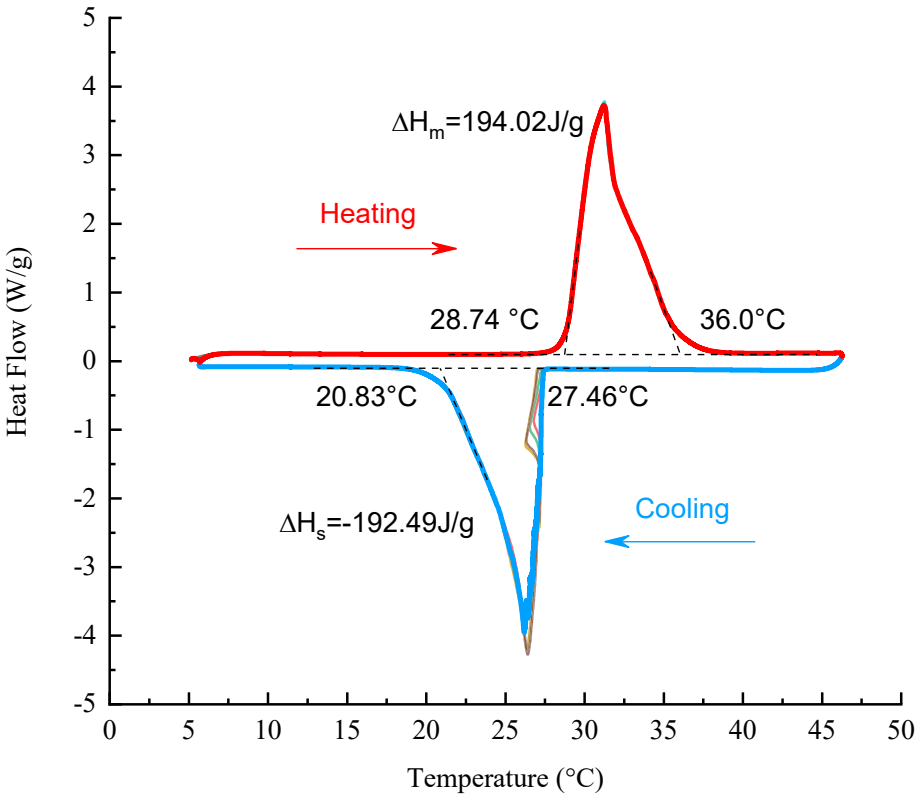

Figure 3.4 DSC of paraffin in heating and cooling

The thermal properties of paraffin were tested by DSC with five heating and cooling cycles as shown in Figure 3.4. Based on the points of rise and decline rate, the phase change temperatures were received. The melting and solidification start at 28.74 ℃ and 27.46 ℃, which end at 36 ℃ and 20.83 ℃. In the same time, the values of enthalpy were

also calculated showing 194.02 J/g and 192.49 J/g of melting and solidification process respectively. These properties were shown in Table 3.2.

Table 3.2 Thermal parameter of paraffin

Melting start point	Melting end point	Melting enthalpy	Solidification start point	Solidification end point	Solidification enthalpy
28.74 ℃	36.0 ℃	194.02 J/g	27.46 ℃	20.83 ℃	192.49 J/g

3.3 Properties of paraffin/ceramsite composite

3.3.1 **Incorporation results**

The density of the paraffin used was 846.5625 kg/m^3 (liquid). After vacuum impregnation at 40 °C for 4 h, the PCM impregnation ratio of 45.33 wt% with a standard deviation (SD) of 0.799 was reached, shown in Table 3.3, indicating good potential for building applications. Compared to the references (Cárdenas-Ramírez et al. 2022; Gencel et al. 2022; Hekimoğlu & Sarı 2022; Karaman et al. 2011; Qu et al. 2020; Ramakrishnan et al. 2015; Shen et al. 2021; Yang et al. 2020; Yousefi et al. 2021) as shown in Figure 3.5, the fabricated PCM composite in this work carried moderate raw PCM, where most cases had an impregnation ratio of around 40-45. It was believed that the paraffin-impregnated ceramsite in this experiment was able to regulate the heat flux and thermal energy.

Table 3.3 Incorporation results of paraffin/ceramsite composite

	Sample 1	Sample 2	Sample 3	Average	SD
Percentage of paraffin (wt%)	45.77	46.02	44.21	45.33	0.799

Notes: Paraffin density: 846.5625 kg/m^3 (liquid); Method: vacuum impregnation at 40 °C for 4 hr

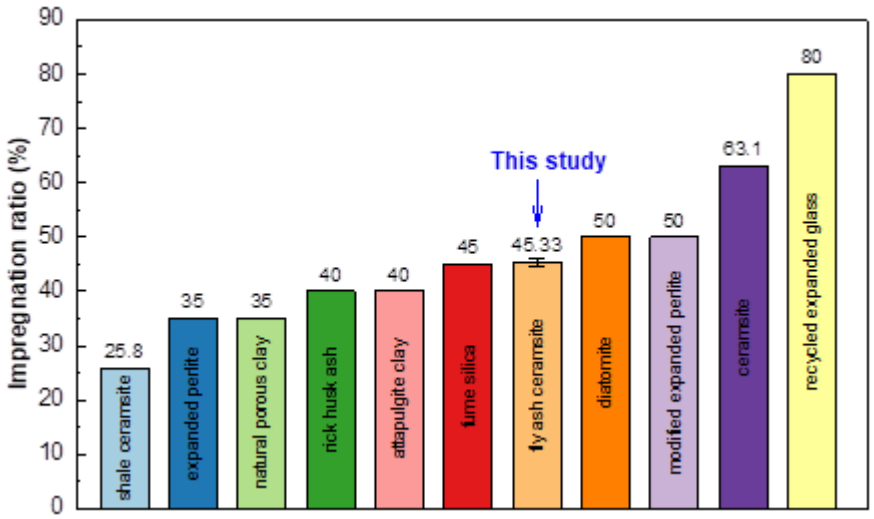

Figure 3.5 PCM impregnation ratios of building material based SSPCM composites

3.3.2 **Leakage prevention**

(a) Original condition (b) 1st cycle (c) 2nd cycle

(d) 3rd cycle (e) 4th cycle (f) 5th cycle

Figure 3.6 Leakage performance of sample 3 under freezing thaw cycle

The groups of samples were heated at 40 ℃ and cooled at -10 ℃ for 1 h repeatedly to examine leakage prevention. A piece of filter paper was under the sample to absorb excurrent PCM and the samples were sealed by a bag to eliminate the influence of moisture. After each cycle, the weight of sample (container and paper were removed) was tested to illustrate the leakage level more precisely.

Based on Figure 3.6, some paraffin did leak from composites and absorbed by the filter paper but the increase with cycle was not significant especially after 3rd cycle. The quantitative changes for all samples were illustrated in Figure 3.7. The extensive weight loss was observed in all samples after 1st cycle with the maximum mass loss of 1.87% for sample 3. That was mainly caused by surface residue although tissue cleaning was applied. Then the loss increased slowly that was contributed by the leaked PCM from the superficial layer. Finally, the weight tended to be constant revealing the stop of PCM leakage. This conclusion was drawn from the overall performance of three groups. The fluctuation and final stage were not totally consistent as shown in Figure 3.7(b). Considering the quantity of each sample was not large, the varying inner structures contributed to this difference among groups. In summary, the leakage performance was acceptable because the quantity was small and mainly occurred after the first cycle (Yousefi et al. 2021; Zhang et al. 2021). In addition, the leaked PCM (after the first cycle) could be cleaned before concrete casting and the optimal structure of ceramsite will minimize the leakage.

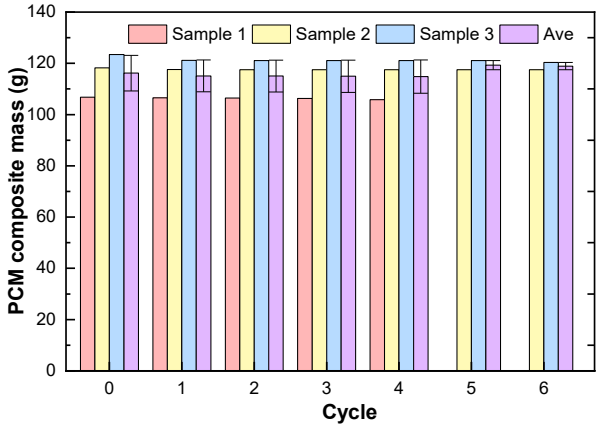

(a) PCM composite mass of each sample

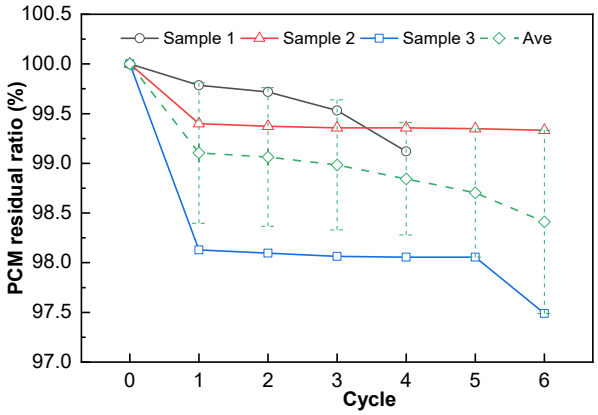

(b) Residual PCM ratio after cycles

Figure 3.7 Leakage performance of SSPCM after heating and cooling cycles

3.3.3 **Strength performance**

(a) Cylinder before assembly

(b) Cylinder after assembly (c) Pressure meter

Figure 3.8 Facilities for cylinder compressive strength

The strength of PCM composites was represented by cylinder compressive strength (GB/T 1981) that was conducted by cylinder and pressure meter as shown in Figure 3.8. The loading speed was controlled between 0.3 – 0.5 kN per second. When the displacement reached 20 mm, the value of force was recorded and transferred to stress. The compressive strength tests were performed at room temperature (around 20 °C), lower than the melting point of paraffin, and therefore the paraffin in the paraffin-impregnated ceramsite was at the solid state. The test for each sample was repeated five times.

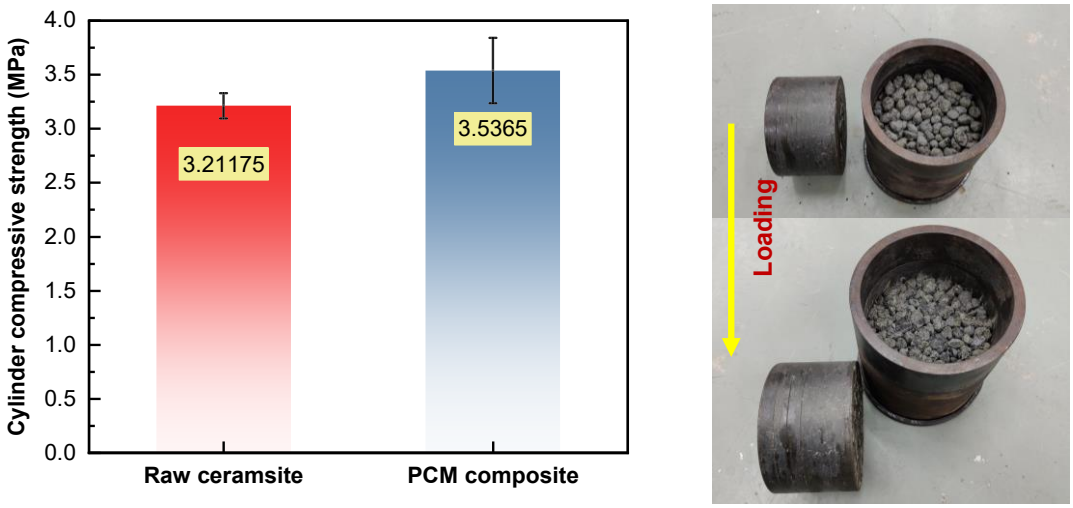

Figure 3.9 Cylinder compressive strength of ceramsite with and without PCM

According to Figure 3.9, the average cylinder strength was 3.2 MPa for the raw ceramsite, and it increased to 3.5 MPa for the paraffin-impregnated ceramsite because the solid-state paraffin filled the pores of the raw ceramsite. The paraffin-impregnated ceramsite samples were tested after being subjected to 5 - 6 heating and cooling cycles, which suggested that the paraffin-impregnated ceramsite was not damaged after the heating and cooling cycles. That was attributed to the low volume expansion of paraffin. The improved strength was expected to be advantageous to concrete production while many other PCM composites showed a negative influence on concrete strength. Unlike the post coating in (Kastiukas, Zhou & Castro-Gomes 2016; Ren, Liu & Gao 2020; Yang et al. 2020), the surface of the PCM composites in this experiment kept relatively natural condition.

3.3.4 **Optical microscope for microstructure**

The inner microstructure of a ceramsite controls the porosity, PCM absorption, PCM leakage, and strength of the ceramsite. In this experiment, the ceramsite's microstructure was observed using a KH-7700 digital microscope manufactured by HiROX. The magnification of 50x was used to observe the pores in the ceramsite. To ensure the quality

of results, samples were sealed in epoxy resin and cut into two parts by a low-speed diamond saw. It enabled a relatively stable plate to observe the inner structure of the ceramsite, as shown in Figure 3.10.

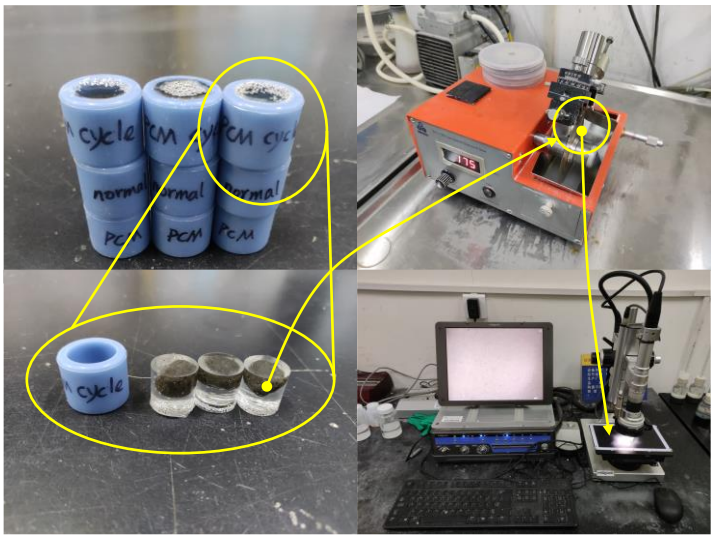

Figure 3.10 Process for microstructure observation

The raw ceramsite samples were denoted as N (not-impregnated), which were dried samples, while paraffin-impregnated ceramsite samples before and after six heating-cooling cycles were denoted as P (paraffin) and C (cycle), respectively. As shown in Figure 3.11, there were pore, cracks and openings of various sizes and shapes in the raw ceramsite sample, and their amount, connectivity, and geometric parameters determined the degree of the paraffin impregnation and leakage. The microstructures of the paraffin-impregnated ceramsite composites are shown in Figure 3.12 and 13. The orange lines in Figures. 3.11 – 3.13 are the boundary between ceramsite and epoxy resin and the unit in these figures was millimetre.

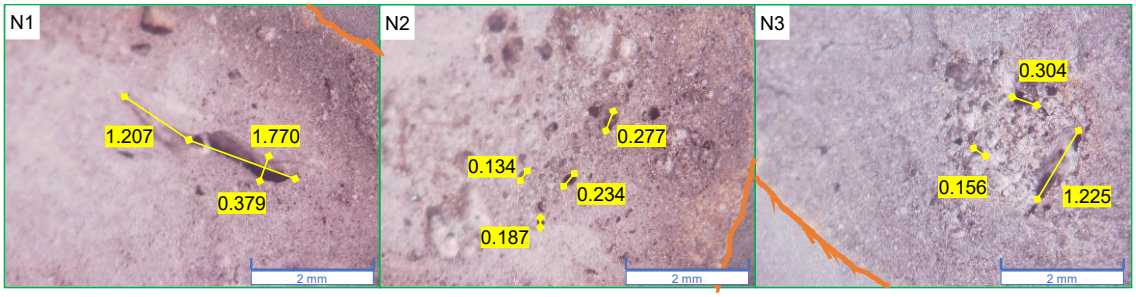

Figure 3.11 Microstructure of raw ceramsite (N)

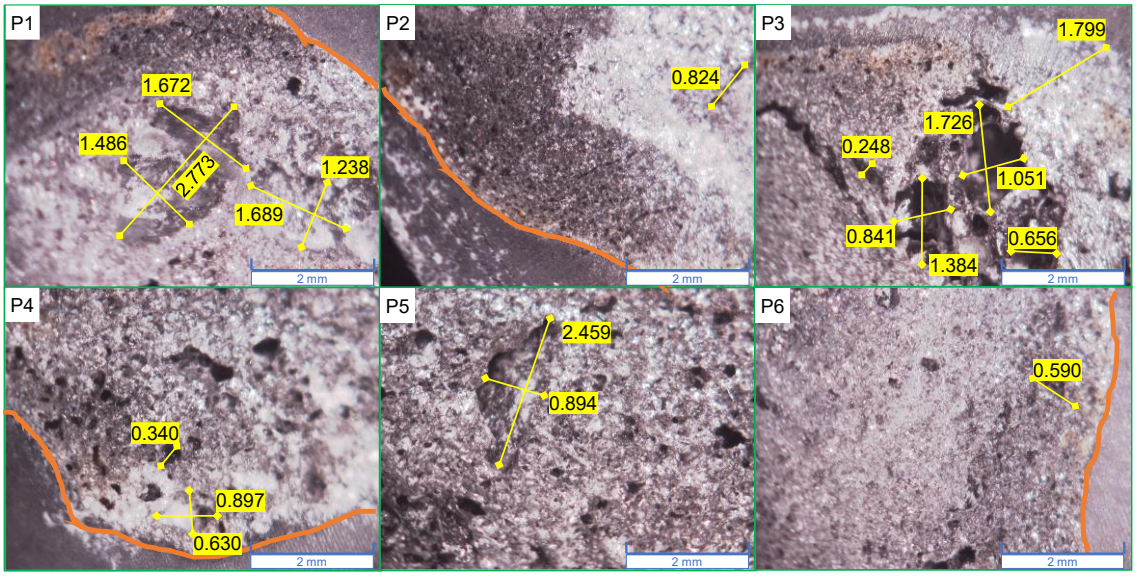

Figure 3.12 Microstructure of PCM/ceramsite composite (P)

Figure 3.12 shows the microstructure of paraffin-impregnated ceramsite without heating and cooling cycles. Based on P2, small pores near a crack were filled with paraffin but the pores close to the boundary did not (it was clear from P6). This revealed that the paraffin incorporation path was not uniform around the surface of ceramsite particles where the crack and opening were important. From P1, P3 and P4, the big pores might have a higher capacity to allow paraffin to penetrate but not to retain. Thus, most of them showed extremely low incorporation rates. On the other hand, the small pores showed a higher capacity for retaining penetrated paraffin (P4 and P5).

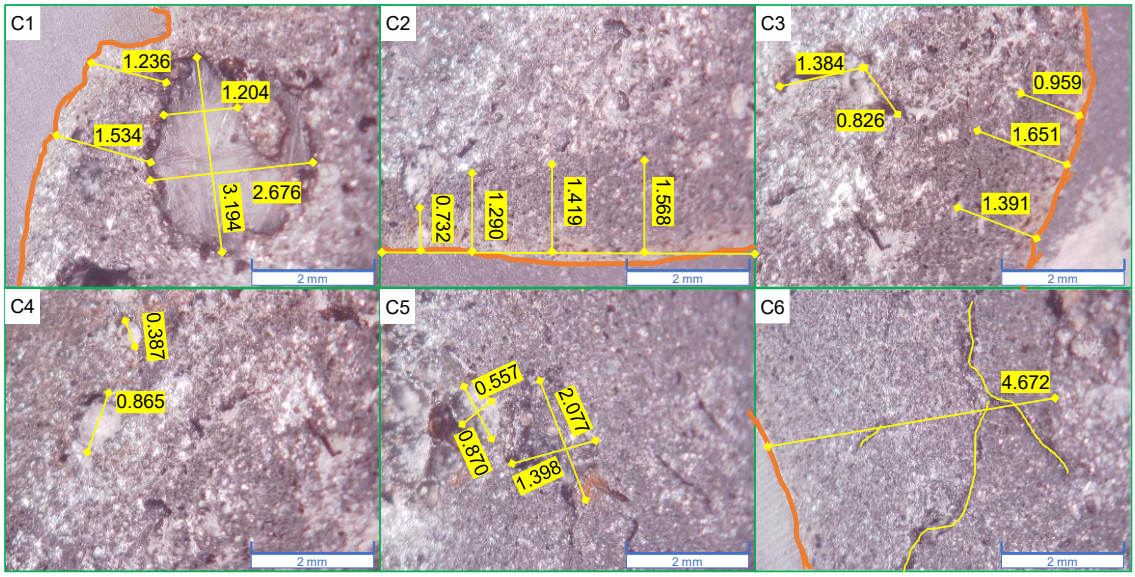

Figure 3.13 Microstructure of PCM composite after heating and cooling cycles (C)

Figure 3.13 illustrates the paraffin distribution after the leakage test. It was clear from C1 and C4 that the paraffin was retained in large pores after heating and cooling cycles. This result was not observed from all pores (C5), and the difference was caused by disconnected paraffin penetration paths. The pores in the area around 1.5 mm from the surface boundaries also showed little paraffin (C2 and C3), probably due to the paraffin loss in leakage tests. Image C6 shows that the cracks performed poorly for retaining paraffin although they were beneficial for paraffin incorporation.

Based on Figures 3.11 to 3.13, the liquid paraffin filled the openings in the ceramsite under vacuum pressure and capillary action. The connected cracks and pores formed the main incorporation paths. The small pores (< 0.3 mm) had a high filling rate, while the large pores showed a lower rate. This may be attributed to weak capillaries with large pores. During heating-cooling cycles, liquid paraffin flowed without vacuum pressure and was prone to present confluence in pores including large pores. Small pores were preferred because large pores had adverse effects on mechanical properties. The storage performance of these pores was different to the pores close to the boundary (< 1.5 mm),

where liquid paraffin flowed easily and caused leakage. The mentioned pores did not include closed ones without connected paths. Uniform cracks with small pores were potentially better for long-term storage of paraffin.

The above analyses are another supplement to the strength performance in the previous section. After the first heating and cooling cycle, resident and leaked PCM will attach to the surface but it is easy to clean the liquid PCM. Then, the rest PCM in the ceramsite is stable that would not affect the surface condition, especially when the microstructure of ceramsite is ideal as proposed in this paper. In summary, the PCM impregnation will not pose a negative effect on the strength.

3.4 Summary

(a) As an economical and reliable PCM material, paraffin is compatible with ceramsite. The porous structure contributes to a 45% incorporation ratio of the paraffin-impregnated ceramsite. Based on the present literature, this incorporation ratio and thermal ability of paraffin are sufficient to provide the energy storage and thermal regulation ability of paraffin-impregnated ceramsite.

(b) After the heating and cooling cycles, the paraffin-impregnated ceramsite has a little leakage issue but the paraffin loss value is < 3%, which is acceptable. The cylinder compressive strength of paraffin-impregnated ceramsite after heating and cooling cycles is 9% higher than raw ceramsite at room temperature. These could contribute to the concrete strength. The leaked PCM may decrease the bond between ceramsite and cement paste, but it could be cleaned before concrete casting because the major leakage happens after once heating and cooling cycle. The leakage will be further weaker if the ceramsite has ideal structures.

(c) The inner structure of ceramsite decides the PCM impregnation and retaining capacity. Connected and porous structure benefits PCM incorporation, and the small pores (< 0.3 mm) are preferred due to good PCM storage and little effect on strength although it does not show an obvious influence on incorporation ratio. Cracks are critical as incorporation paths, but present weak ability on PCM retaining, especially after heating and cooling cycles.

(d) The pores close to the surface of paraffin-impregnated ceramsite particles (in the distance < 1.5 mm) contribute negatively to the PCM retention, which is the main reason for the leakage. The pores distribution and morphology of the ceramsite are the reasons for the fluctuation of leakage test among different samples, although they show similar PCM incorporation and strength.

(e) High porosity of ceramsite is significant but opening distribution is also crucial for PCM incorporation. It is preferred to have interconnected, small pores/defects uniformly distributed inside of the ceramsite particles. This structure is better as PCM supporting material but poses challenges for ceramsite production.

CHAPTER 4. HYDRATION AND MECHANICAL PERFORMANCE CAUSED BY THERMAL INFLUENCE OF INORGANIC SSPCM

The advantages of PCM on concrete have been proven, and the current aspiration is to focus on improving the benefit efficiency and eliminating the adverse effects (Brooks et al. 2021; Pilehvar et al. 2019). From the literature, the various drawbacks on mechanical properties and durability are observed, and there has not been a comprehensive explanation. PCM addition may affect the cement hydration that generates a vital influence on concrete (Šavija 2018). From this perspective, this work investigates the shrinkage performance and strength changes of PCM mortars. The temperature evolution in the hydration process and isothermal calorimetry are tested to directly reveal the influence. Then, effective characteristic methods and microstructures illustrate the results of this influence, and further explain the change of strength and durability.

4.1 Material and sample preparation

The disodium hydrogen phosphate dodecahydrate ($Na_2HPO_4 \cdot 12H_2O$, NHP) and sodium sulphate decahydrate ($Na_2SO_4 \cdot 10H_2O$, NS) were purchased in Australia and selected in this work while they both showed effective results in building material for energy-saving (Hirschey et al. 2022; Islam & Ahmed 2021; Rao et al. 2018). NHP was provided by Glentham Life Sciences and NS was manufactured by Thermo Scientific, which had a purity of 99%. This experiment designed a eutectic PCM by mixing NHP and NS with a weight ratio of 1:1. The NHP and NS were sealed in tubes and mixed by ultrasonic in a water tank at 40 °C. The NHP/NS PCM was fabricated in 6 h before PCM composite incorporation and stored in sealed vessels.

The expanded perlite (EP) is a good lightweight aggregate for mortar and concrete, and it is good at absorbing PCM due to its high porosity (Ramakrishnan et al. 2015; Sun et al. 2023; Zhang et al. 2016). EP was purchased from Ausperl Australia with a dry density of 70 kg/m^3. The size distribution is shown in Table 4.1. The EP was stored in a room with low humidity and was dried in an oven at 80 °C lasting for 24 hours before the experiment every time.

Table 4.1 Size grade of EP (based on the technical sheet)

Size	0.15 – 0.3	0.3 – 0.6	0.6 – 1.18	> 1.18
Percentage	5 – 30%	10 – 40%	30 – 60%	0 – 40%

The silica sand (SS) with a small size (~ 1 mm) and general-purpose cement was used in this experiment, which was stored in a room with low humidity. Bastion general-purpose cement, produced in Australia, consisted of Portland cement (>92%), a little limestone and gypsum according to the technical sheet from the company.

The EP was heated at 50 °C and 80 kPa in a vacuum oven for 12 h to remove the pore moisture and air. According to the capability information from the manufacturer, the water holding capacity by volume of EP was 65%. The incorporation mass ratio of 10:6 (PCM:EP) was selected, which equalled 7:60 by volume. This ratio is much lower than the water holding capacity that is supposed to achieve thorough impregnation and leakage-free. The EP/PCM composite is abbreviated as EPC.

This experiment separately designed 3 groups of mortar with different aggregates (silica sand, EP, and EP/PCM composite), namely SSM, EPM, and EPCM. The cement-to-sand weight ratio of the basic group (SSM) was 4:9, while the aggregate replacement ratio was 100% based on volume for the other groups (EPM and EPCM). The mixing proportion is shown in Table 4.2. The extra water and SP in EPM and EPCM modified the flowability

because much water was absorbed by EP. All samples in this paper had the same dimension of 40 × 40 × 160 mm. For the shrinkage test, the length (160 mm) included the length of the gage studs. In other words, the designed distance of the ends of the gage studs was 160 mm (EN 2002) and the length of the mortar prism was 150 mm (AS 2006).

Table 4.2 Details of mixing proportion

	Cement	Water	SS	EP	EPC	SP	w/c	SP/c
SSM	488 g	195.2 g	1098 g	-	-	3.66 g	0.40	0.75%
EPM	488 g	219.6 g	-	50 g	-	4.88 g	0.45	1%
EPCM	488 g	219.6 g	-	-	133.3 g	4.88 g	0.45	1%

4.2 Temperature change in the prism specimen during hydration

The temperature was collected by K-type thermocouples connected to a data logger. The thermocouples were embedded in the sample during casting. The temperature collection started when the mortar cast was completed. The time gap between water addition in mixing and the first temperature collection was recorded. The time interval of each collection was 10 min. In the first day, the samples were cured at room temperature of ~ 24 °C with plastic film coverage. In the next days, the samples were cured in a water tank with a temperature of ~ 22 °C, as shown in Figure 4.1.

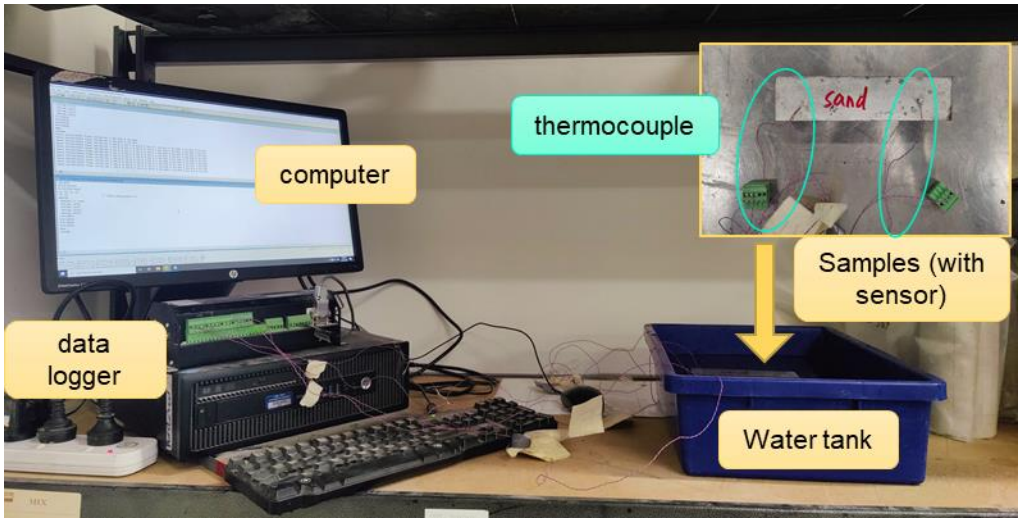

Figure 4.1 Configuration for temperature collection

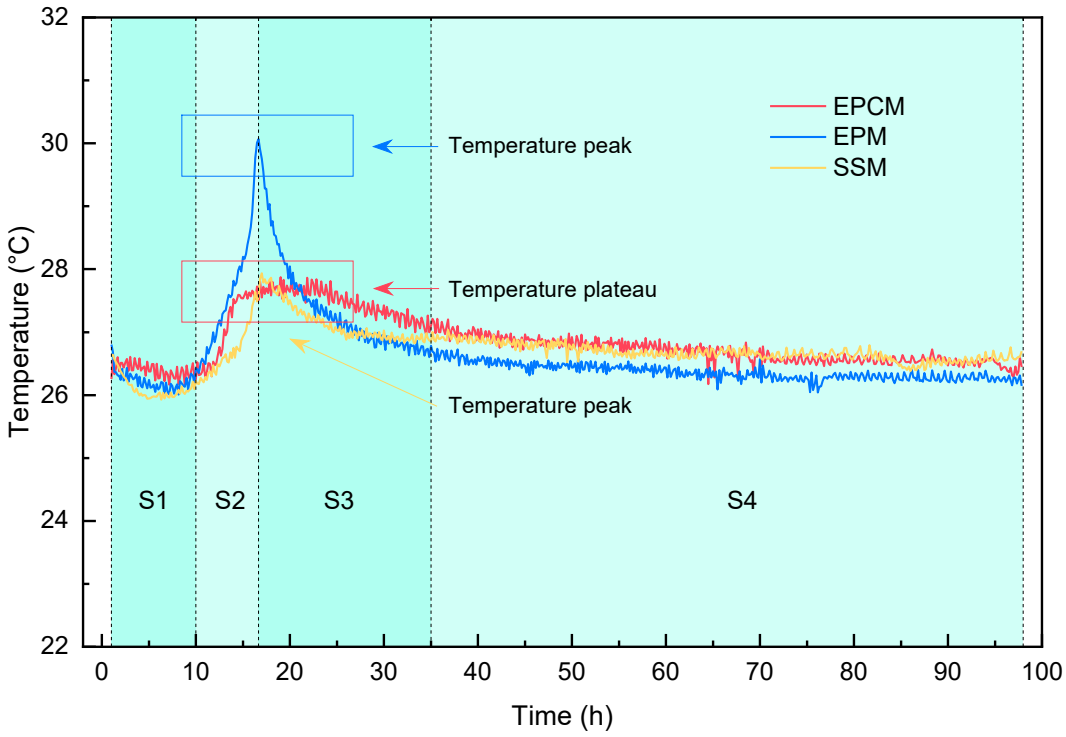

(a) Inner temperature of samples

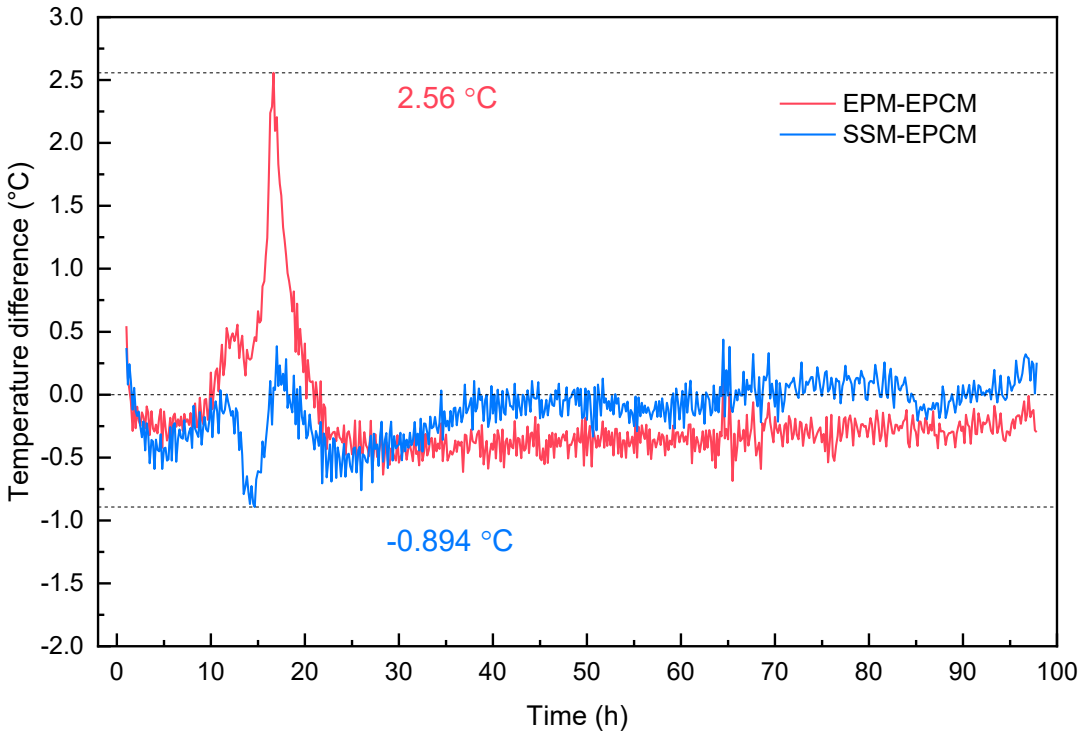

(b) Temperature difference among samples

Figure 4.2 Temperature evolution during hydration

The test lasted for over four days as shown in Figure 4.2. From Figure 4.2 (a), all samples showed temperature reduction and recovery before 10 h,, which was marked as S1 caused by cement dissolution. Then, the huge amount of heat accumulation led to increasing temperature, which was marked as S2. The rapid hydration started made the temperature peak for SSM and EPM. After that, the downward temperature suggested the lower hydration ratio. The peak intensity was different because it was affected by various factors including w/c ratio, SP dosage, etc. The SSM showed later acceleration and lower speed. Anyway, the law was same although the expression level was changing. The critical difference was the temperature plateau (~ 27.8 °C) for EPCM sample, which was caused by the heat absorption of PCM. This plateau occurred at both S2 and S3 that were significant for cement hydration. The distinct plateau of EPCM, especially compared to EPM, regulated the ambient condition may leading to an unexpected hydration process.

The S4 normally was regarded as stable period or curing period. The difference was still observed but the gap was narrowed with time. The temperature of EPCM was higher than the EPM counterpart. Two reasons were proposed: the first was the released heat from PCM that was the main feature of PCM. The second was the delayed exothermic reaction in S2 and S3, which was continued in S4. Both of these reasons also can explain the bridged gap with the passage of time: exhausted energy storage and consumption of raw material. The gap was exhibited in Figure 4.2 (b), where the maximum value was 2.56 °C and verge to 0 °C over time. The effect concentrated from 12 h to 20 h and still played a role until 97 h. It is noticeable that the curve is similar to the heat flow curve in isothermal calorimeter but the feature is different. The temperature is controlled by the specimen dimension, laboratory temperature, and curing condition, apart from the hydration performance. In addition, the temperature is a parameter of heat accumulation in the whole specimen that is less sensitive than heat flow. For example, the heat exchange with curing water tank. Thus, the temperature collection in laboratory is complementary to heat flow data from the standard machine.

4.3 Shrinkage and mechanical strength

4.3.1 **Shrinkage**

The cast samples were covered by plastic film and cured at room temperature on the first day. After 24 h, the samples were demoulded and tightly covered by the aluminium film as shown in Figure 4.3. The distance between the end of two gage studs was recorded as reference. The shrinkage performance in the following days was calculated based on this reference length (ASTM 2017). The moisture evaporation was an important reason for the shrinkage so that the aluminium coverage eliminated the influence of evaporation. The obtained shrinkage was mainly caused by hydration reaction and temperature change.

All samples were placed on the shelf in the shrinkage room, where the temperature was 22.5 °C and the relative humidity was 48%.

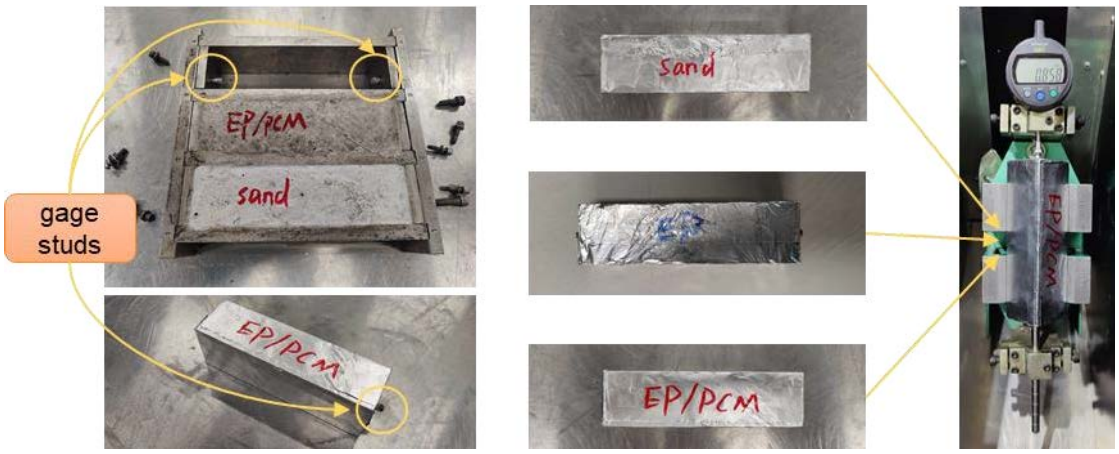

Figure 4.3 Samples and apparatus for shrinkage test

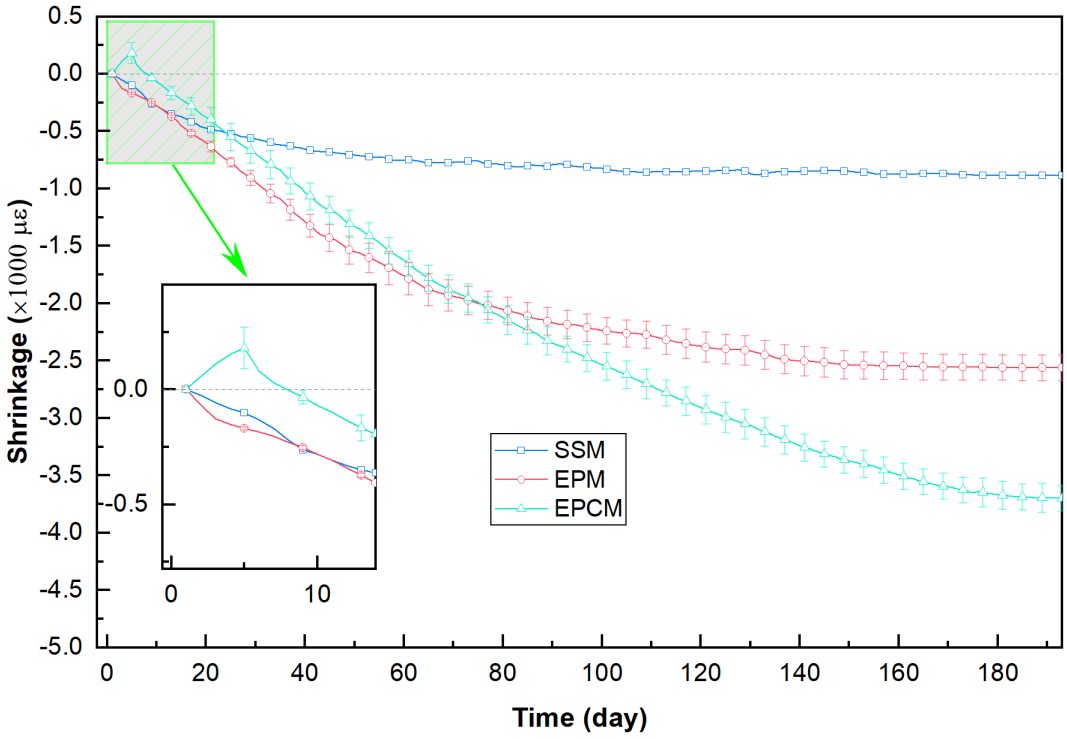

Figure 4.4 Shrinkage results of mortar with different aggregate

As shown in Figure 4.4, the SSM presented little shrinkage ability up to -875 με and became stable from 70th day, which was mainly contributed by the high stability of sand

and less influence on cement hydration. The high water absorption of expanded perlite caused large deformation, and the non-crystal quartz may lead to further reaction, in addition to the low strength of EP providing lower resistance against the shrinkage. All EPM and EPCM samples illustrated continuous shrinkage while EPM became relatively stable from 100th day and EPCM accumulated the shrinkage steadily until 178th day.

The critical feature of EPCM was observed before 8th day. The expansion occurred only on EPCM that should be affected by the PCM while reaching 180 με on 5th day. The direct difference was the temperature plateau as shown in Figure 4.2 that could change the thermal expansion. The present paper showed the effect of PCM on expansion control (Šavija 2018; Šavija and Schlangen 2016). However, the lower temperature was supposed to reduce the expansion, and the key corresponding time was unmatched: 15 – 25 hours in temperature and 0 – 8 days in shrinkage. The sample dimension in this experiment was small, which mitigated the thermal effectiveness. Therefore, the reduced expansion by lower temperature was limited and the varying product could be the main factor. The product could be influenced by two factors, temperature and reaction with PCM. The temperature regulated the reaction ratio and modified the hydration product, which may last for over four days (peak of expansion occurred on 5th day). The EPC was manufactured by vacuum impregnation without post-process. The low quantity of PCM posed little burden on leakage but the residual PCM on the surface during impregnation still may participate in a reaction. The expansion could be contributed by NS, while the SO_4^{2-} was critical to ettringite and gypsum generation that caused expansion. Normally, Na_2SO_4 can accelerate cement hydration and increase the generation of calcium sulphoaluminate (or ettringite) showing an obvious expansion effect. The available Na_2SO_4 was limited and the expansion was offset by the hydration shrinkage on 8th day. The details required evidence from many testing methods.

4.3.2 **Mechanical properties**

The 3-point flexural strength and compressive strength were tested on the hydraulic compression machine with the required apparatus. The compressive strength of mortar was tested based on the specimens' portion of prisms made and broken in the flexural strength test. According to ASTM standards (ASTM 2018, 2021b), the loading speeds were set as 44 N/s and 1.3 kN/s for flexural and compressive strength tests, separately. After being cured at room temperature with plastic film coverage for 24 h, the samples were demoulded and cured in the water tank until the day of testing.

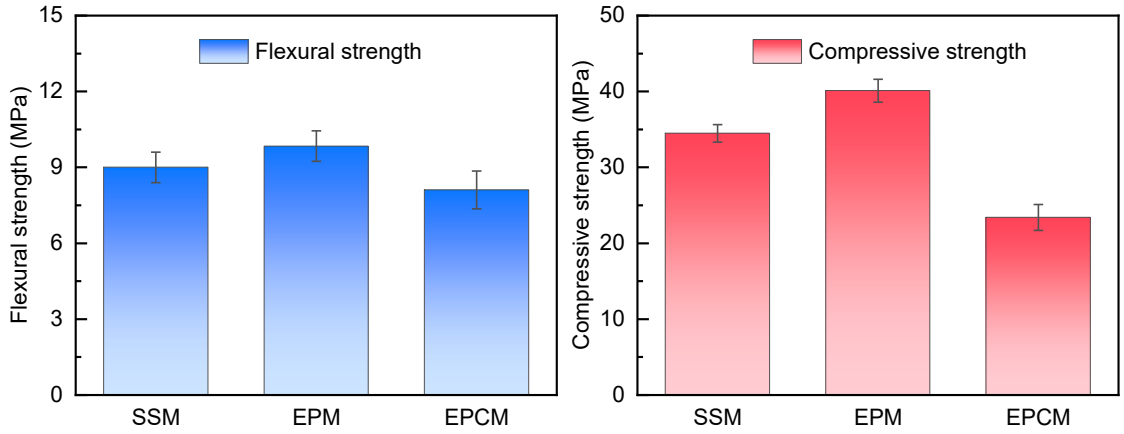

Figure 4.5 Mechanical properties of samples on 28-day

As shown in Figure 4.5, the EPM showed an increase on compressive strength (16%) and flexural strength (9%) compared to SSM. The strength of EP was much lower than SS excepting the possibility of stronger aggregate supporting. The higher value could be caused by the cement matrix and bond. EP had high water absorption that caused stronger bond with cement matrix and the matrix could be denser according to the large deformation in shrinkage test, even though more water was used, which led to the higher strength. In addition, the non-crystal quartz of EP may play a role in cement hydration that can change the quality of the interfacial transition zone (ITZ) and the analyse was provided in next section based on characteristics. The rising compressive was limited by

the weak EP when the aggregate strength was critical for compressive strength. As explained previously, the porous EP improved the bond strength that benefited the bending resistance. The crack mostly occurred at ITZ between aggregate and cement matrix. The reduction of compressive strength on EPCM was evident (42%) while the flexural counterpart was mild (18%). The disadvantage could be explained by the lower capillary effect because the EP was partially filled by PCM in advance. The enhancement on bond strength was eliminated and the crucial weakness of EP became apparent. Similar to the explanation for shrinkage, the potential reaction caused by PCM deserved much attention, which can change the product around the aggregate and the property of ITZ. In another word, the bond strength may suffer damage and the mortar became weak with the weak aggregate.

4.4 Influence on cement hydration

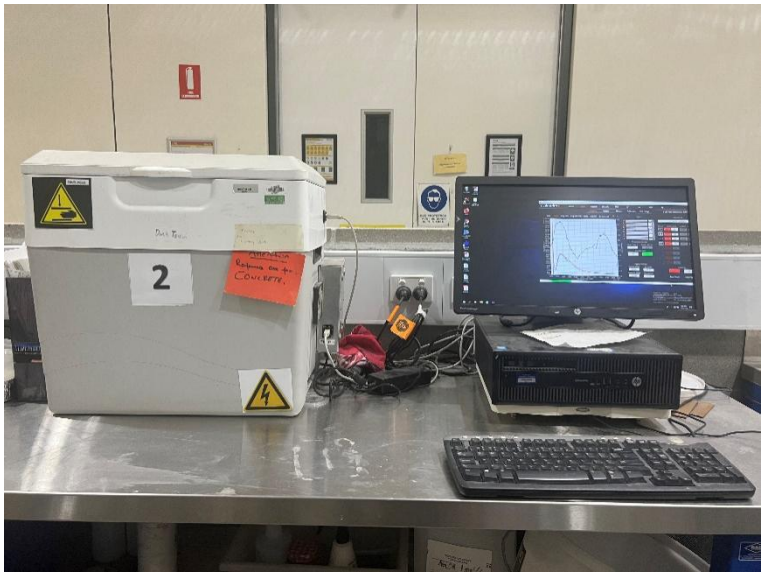

Figure 4.6 Calmetrix I-Cal 4000

The isothermal calorimetry test was done by I-Cal 4000 (manufactured by Calmetrix USA) with four channels to test the cement hydration as shown in Figure 4.6. According to the user guide, two reference metal cylinders were used for each channel. The quantified

testing sample was sealed in a plastic container that fitted well with the sample channel. The container filled with tap water was placed in channel 1 as reference and calibration. SSM, EPM, and EPCM were tested in channels 2, 3, and 4, respectively, as shown in Table 4.3. All channels were turned on 24 hours in advance to maintain the stable thermal environment of channels. The channel temperature was set as 25 °C, which was required by standards for mortar curing. Before the test, the cement and aggregate were weighed and mixed thoroughly in the container for each group. Similarly, the water and SP were weighed and mixed. Then, the water with SP was added to the container, followed by fast manual mixing for 20 seconds. The time of water addition was recorded as the start of hydration. All containers with designed samples were placed in the channel quickly. The heat flow in the first four days was collected and analysed.

Table 4.3 Tested mortar sample in each channel of isothermal calorimetry

	Cement (g)	Aggregate type	Aggregate mass (g)	Water (g)	SP (g)
Channel 1	—	—	—	30	—
Channel 2	20	SS	45	8	0.15
Channel 3	20	EP	2.05	9	0.2
Channel 4	20	EPC	5.46	9	0.2

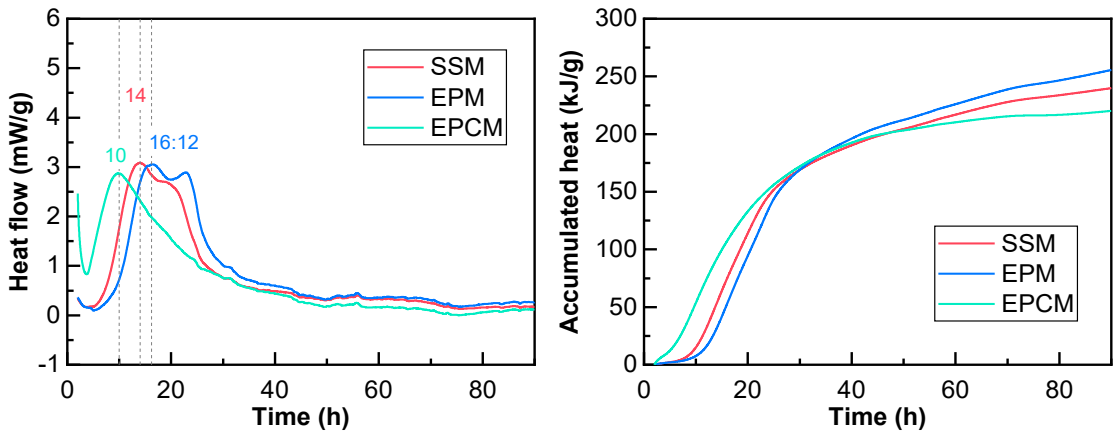

(a) Heat flow for mortar (b) Heat accumulation for mortar

Figure 4.7 Isothermal calorimetry for mortars to investigate cement hydration

The isothermal calorimetry was done as shown in Figure 4.7. The main peak of SSM was found at 14 h with a start at 5 h. When the aggregate was replaced by EP, the hydration was prolonged with the peak delayed to 16.2 h and the lower peak value. From the mix strategy, a higher w/c ratio and more SP were used, which were reasons for the hydration peak changing. The accumulated heat of EPM exceeded its SSM counterpart at 30 h that was also in accord with a high w/c ratio, meaning a higher level of hydration. In this case, the cement matrix was stronger, but the EP was still weak, which proved the deduction in mechanical strength.

The peak of EPCM was hastened to 10 h, which was attributed to the NS attached on the surface of EPC. NS was universally used to accelerate hydration and boost early strength. However, the accumulated heat was the lowest that contributed to the lowest strength. Another noticeable change was the number of main peaks, which was reduced from two to one after PCM incorporation. The isothermal calorimetry was based on the generated heat from the material. After first peak, PCM started work and absorbed partial heat that covered the second hydration peak. In addition, the lower temperature led to weaker hydration speed that reduced the second peak. From temperature change results, the temperature went down from second day and PCM released heat, which summarily did not affect the final accumulated heat result.

In this experiment, NS brought hydration forward but made lower accumulated heat, which was in accord with traditional effect although cooperated with NHP. The effect of PCM on cement hydration may be various. Wang et al. (Wang et al. 2021) tested the heat flow of mortar incorporation capric acid-based SSPCM. The curves of all samples

showed similar regulation and no peak shift was observed, although the increased peak value was found. The different results could be caused by material type, incorporation method, casting method, etc., which deserved further research. Therefore, the selection of PCM should take the possible hydration reaction into consideration.

4.5 Characterisation of raw materials and mortar

4.5.1 **Facilities and methods**

Many reliable test methods were applied to analyse the features of hardened mortar, including XRD, FTIR, TGA and SEM-EDS, which are popular in building material characteristic.

X-ray Diffraction (XRD) is an overwhelming method to analyse the crystal component of cement-based material, which was completed by Bruker D8 Discover XRD, as shown in Figure 4.8, to identify the mineralogical characterization with a 2θ scan range from 5° to 70°. The crushed mortar was ground in fine powder with a size of ~ 20 μm at the laboratory to ensure reliable results. The total number of steps was 3526 with 0.8 s per step. The whole scan for each test cost 50 min.

Figure 4.8 Bruker D8 Discover XRD

FTIR test was completed by Thermo scientific NICOLET 6700 FT-IR as shown in Figure 4.9. The absorption spectrum was measured from 4000 cm^{-1} to 400 cm^{-1} with a resolution of 2 cm^{-1}. The measuring circle was repeated 30 times to enhance the result accuracy. All samples were ground as fine powders and sealed in tubes. The test was completed in dry laboratory conditions to eliminate the influence of ambient moisture.

Figure 4.9 Thermo scientific NICOLET 6700 FT-IR

Thermal gravimetric analysis (TGA) was completed to investigate the material composition via mass change at elevated temperatures. The NETZSCH STA449 F5 Jupiter as shown in Figure 4.10, was used with a balance resolution of 0.1 μg and a maximum chamber temperature of 1600 ℃. The heating rate was 10 ℃/min and N_2 gas was selected with a speed of 20 ml/min. The data collection started at 25 ℃ and stopped at 1000 ℃. 20 – 30 mg powder was placed in an alumina crucible and tested for every sample.

Figure 4.10 NETZSCH STA449 F5 Jupiter

SEM-EDS test was completed by Zeiss EVO LS15 (shown in Figure 4.11) at the low magnification of 500 and Zeiss Supra 55VP (shown in Figure 4.12) at the high magnification of 10k. A gold layer with a thickness of 10 nm was coated by Leica EM ACE600 Coater (shown in Figure 4.13) to form a conductive path. All samples were stored in a vacuum desiccator to prevent moisture and dust from air.

Figure 4.11 Zeiss EVO LS15 SEM

Figure 4.12 Zeiss Supra 55VP SEM

Figure 4.13 Leica EM ACE600 Coater

4.5.2 **Results and analyses**

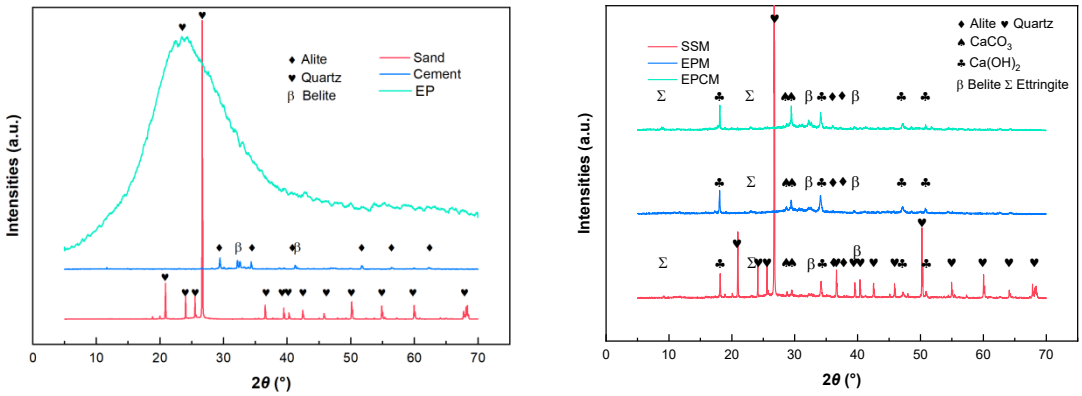

(a) Raw materials (b) Hardened mortar

Figure 4.14 XRD result for raw materials

The XRD tests were done for raw materials and hardened mortar as shown in Figure 4.14. The peaks of quartz in SS was very strong that indicated the stable crystal. Conversely, the quartz in EP showed amorphous state, which may participate in the hydration reaction or pozzolanic reaction. The most peaks of all samples looked weak because the highest peak of quartz was extremely strong that did not present the signal of other products were uncertain. The most peaks of hardened mortar referred to universal mortar composition, including ettringite, alite, belite, Ca_2CO_3, and $Ca(OH)_2$. The highest peaks of SSM, which referred to quartz, were contributed by SS. The strong peaks at around 9° and 23° for EPCM were ettringite. The NS attached on the surface of EP closely contacted with cement particles and was likely to participate in the hydration reaction, which normally resulted in more ettringite generation. In another word, the phosphate was generally regarded as retarder that would not change the final product. This conclusion was also applied to NHP in this experiment and there was not crystal peak of HPO_4^{2-} related product.

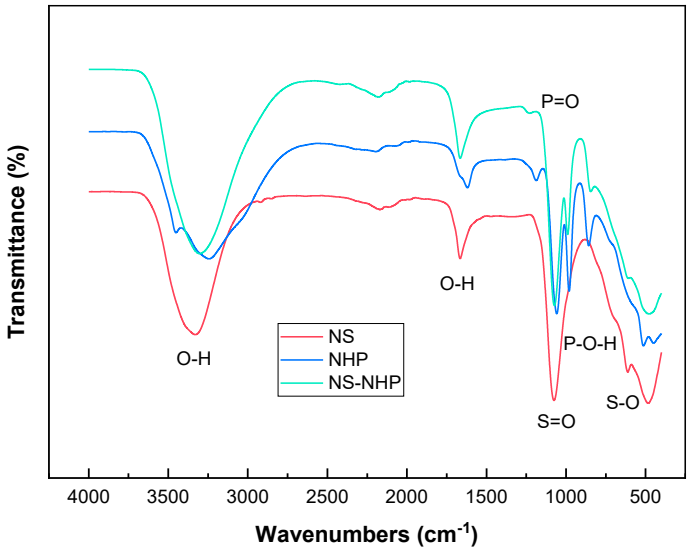

Figure 4.15 FTIR results for PCMs

The pure and mixed PCMs were tested by FTIR in the range of 450 – 4000 cm^{-1} to analyze the eutectic PCM manufacturing process as shown in Figure 4.15. Because of water molecules, the obvious vibration of O-H was found at ~ 3321 cm^{-1} and ~ 1169 cm^{-1} for all samples. The significant vibration occurred in 1300 – 500 cm^{-1}. The vibration as ~ 1078 cm^{-1} and ~ 613 cm^{-1} referred to S=O and S-O, which was contributed by SO_4^{2-}. The vibration at ~ 1187, 1057, 979, and 854 cm^{-1} presented the exist of HPO_4^{2-}. All of these key vibrations were observed for the NS-NHP and there was not new vibration. Although the mild vibration shift was detected, the stability of NS and NHP was still credible. There was not new product and the compatibility was reliable, when the vibration shift was caused by the intermolecular attraction.

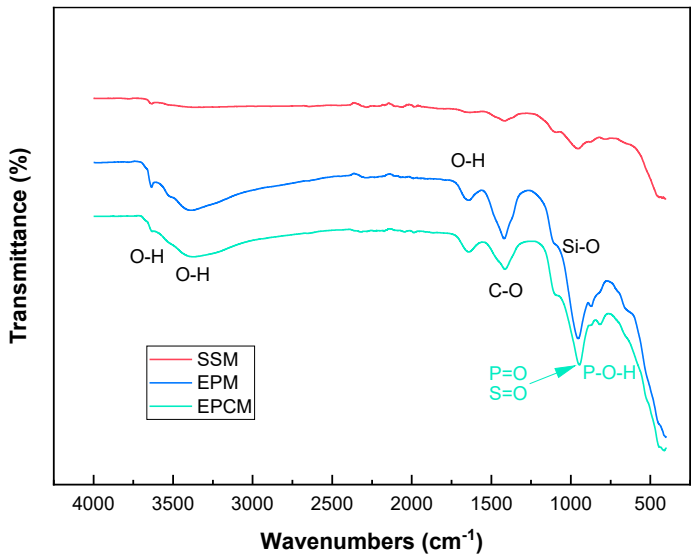

Figure 4.16 FTIR results for hardened mortar

From Figure 4.16, chemical bonds of cement hydration were found at ~ 1411 and ~ 960 cm^{-1} referring to C-O and Si-O, which were key feature of $CaCO_2$ and C-S-H. The O-H vibration was observed at ~ 3637, 3395 (wide), and ~ 1640 cm^{-1} that were contributed by water molecule and $Ca(OH)_2$. These vibrations were detected in all samples but the signal for SSM was relatively weak, especially for O-H vibration. The amorphous quartz of EP, with very fine particle size shown in Table 1, offered important raw material for the reaction that boosted the hydration production. The increasing quantity and stability of products contributed to the stronger vibration signals. For EPCM, the vibrations of PCM at ~ 1000 cm^{-1} was covered by the Si-O that was the most significant chemical bond in hydration products. One vibration of P-O-H at ~ 845 cm^{-1} in NS-NHP was still identified with a minor shift to ~ 816 cm^{-1}. The PCM incorporation showed little effect on the product composition but the amorphous quartz of EP may enhance the cement hydration effectively.

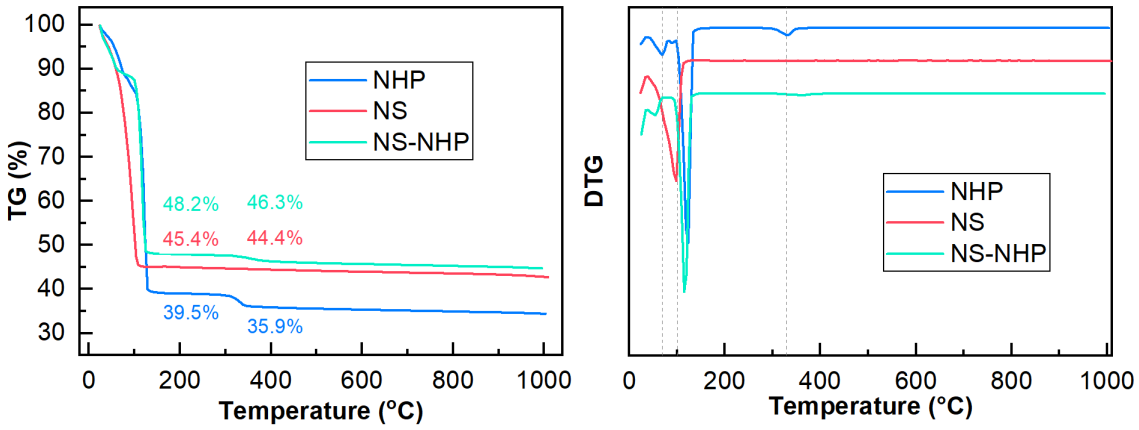

Figure 4.17 TG and DTG results for PCMs

The mass loss of PCM as shown in Figure 4.17 was mainly caused by the dehydration that the chemical equations were presented from Eqs. (4.1) to (4.4). The dehydration of NS was direct and only one peak was found at 100 °C as shown in Eq. (4.1). There were three peaks were observed for NHP. The first two peaks referred water molecule loss at 39 °C and ~ 100 °C as shown in Eq. (4.3), while the third peak at ~ 329 °C showing the decomposition to tetrasodium pyrophosphate and water loss as shown in Eq. (4.4). These peaks were observed in NS-NHP showing the compatibility in accord with the FTIR result.

$$Na_2SO_4 \cdot 10H_2O \rightarrow Na_2SO_4 + 10H_2O \quad (4.1)$$

$$Na_2HPO_4 \cdot 12H_2O \rightarrow Na_2HPO_4 \cdot 7H_2O + 5H_2O \quad (4.2)$$

$$Na_2HPO_4 \cdot 7H_2O \rightarrow Na_2HPO_4 + 7H_2O \quad (4.3)$$

$$2Na_2HPO_4 \rightarrow Na_4P_2O_7 + H_2O \quad (4.4)$$

For the water loss at 39 °C, the material was sealed in the mortar that the water molecule was not leaked. In addition, the dehydration was reversible when the temperature decreased down. In the most building working conditions, the temperature will not reach to 100 °C where the water changed to gas. Based on the TGA result, NS-NHP was regarded reliable to work as PCM in buildings. In the extreme condition like fire disaster,

the dehydration and evaporation of this PCM could relieve the destruction. The deserved precaution was that this PCM mortar was not suitable as the stress-bearing part, which may be destroyed due to inner water evaporation.

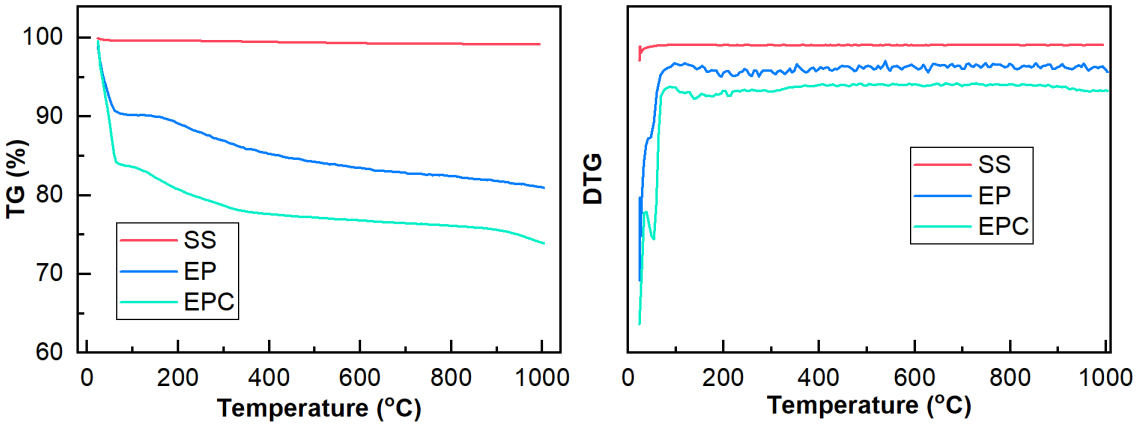

Figure 4.18 TG and DTG results for aggregates

As shown in Figure 4.18, the SS showed extreme thermal stability while others had obvious mass loss up to 1000 °C. The loss of EP was caused by impurities that was introduced during expansion process in the factory. The further loss of EPC mainly occurred at lower than 100 °C and a peak was found in the DTG result, which was attributed to the dehydration of PCM. After 100 °C, all samples showed reliable stability. The fluctuation in DTG test was caused by the low total mass of samples. The volume of the pan was limited that low density made low sample mass (~ 4 mg for EP, ~ 10 mg for EPC and ~ 35 mg for SS). Therefore, the fluctuation of EP was the most significant followed by EPC counterpart.

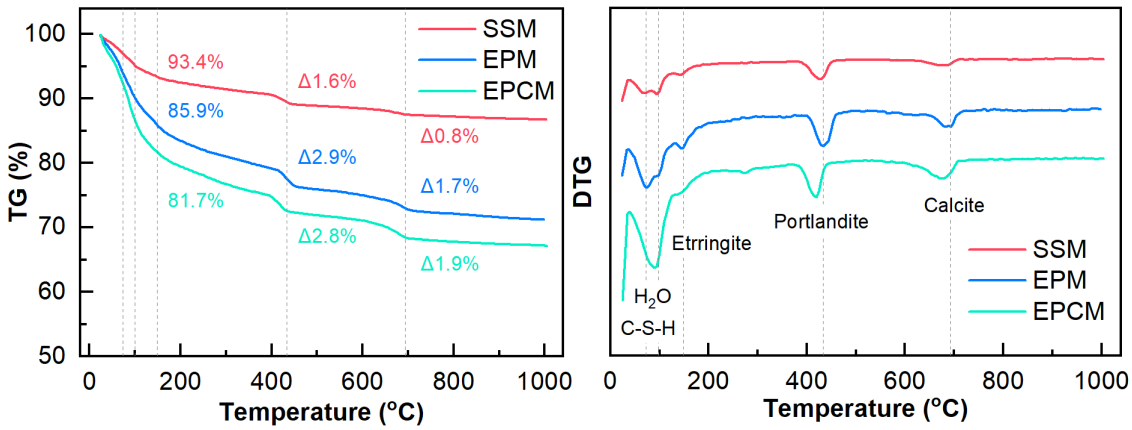

Figure 4.19 TG and DTG results for hardened mortar

After 28 days curing, the hardened mortar samples were tested as shown in Figure 4.19. The mass loss was shown in the TG figure and the peaks referred to different material loss in DTG figure. Take SSM as example, the 93% was the residual mass of whole sample and Δ1.6% was the mass loss referring to portlandite. The portlandite change of EPM was 2.9% while the counterpart of SSM was 1.6%, which demonstrate the more portlandite production. The similar foundation was also noticed for calcite when the reduction of EPM was 1.7% and the reduction of SSM was 0.76%. The difference < 100 °C was hard to make contrast because the raw water content was different and C-S-H decomposition occurred. The summary can be made that the hydration level of EPM was higher. The difference between SSM and EPM was made by higher water proportion that promoted the hydration degree. By contrast, the influence of amorphous SiO_2 in EP was not recognized. The EPCM had same raw material and mixing proportion with EPM, except the impregnated PCM. Comparing the residual mass of 86% and 82%, the mass loss of EPCM was higher than that of EPM, which referred to the ettringite and partial C-S-H mass. The proportion of ettringite in EPCM was likely higher but this estimation was not convincing enough. The loss of water content and C-S-H also played a significant role in this temperature range so more evidence was demanded in the following tests.

However, it was related to the hydration process because the mass of PCM account for only 1% of the raw material that was negligible. The reductions referring portlandite (2.9% and 2.8%) and calcite (1.7% and 1.9%) of EPM and EPCM were very near. The peak in EPCM showed a left shift and the actual value was closer. In summary, the effect of PCM mainly occurred at ettringite while the rest product showed little change. The SO_4^{2-} in PCM promote the production of ettringite.

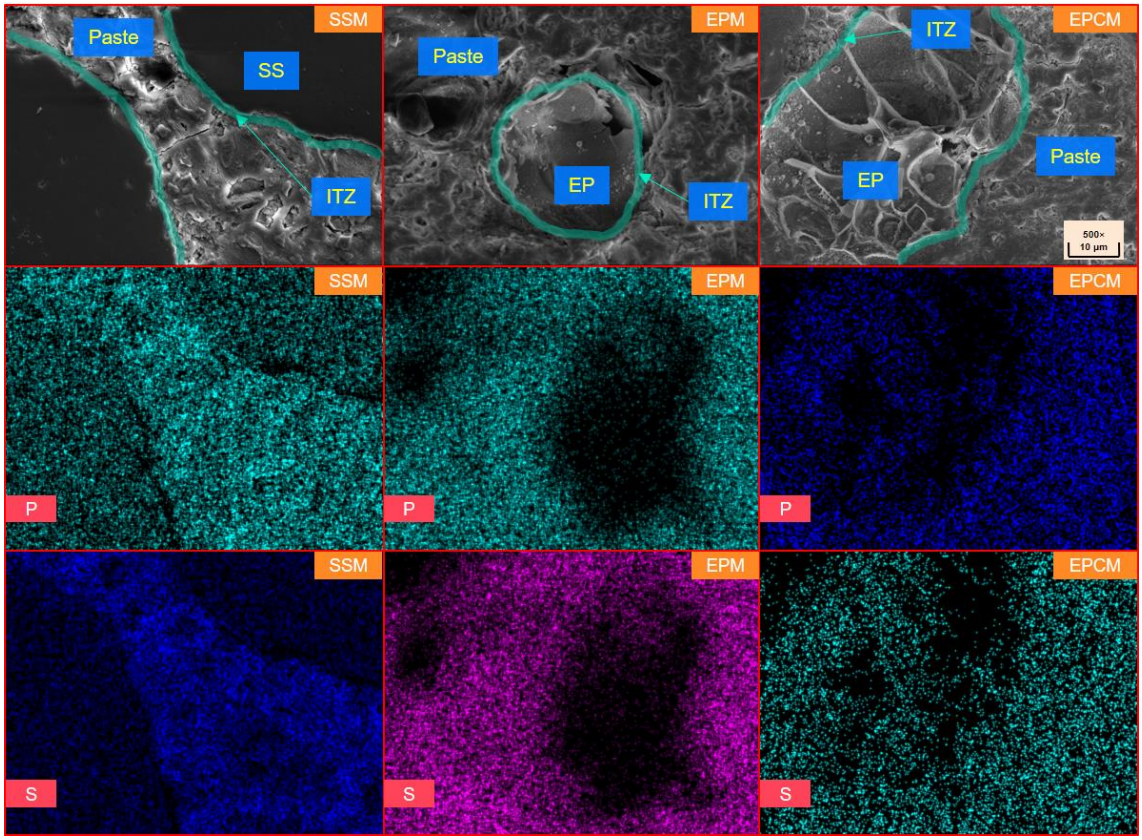

Figure 4.20 SEM-EDS result at the magnification of 500×

As shown in Figure 4.20, SSM illustrates the obvious boundary and minor cracks along the aggregate. This could destroy the integrity and form a weak area, which is adverse for mortar strength. Oppositely, EPM and EPCM show denser ITZ and nearly no crack occurs around the aggregate. EP is porous with an extremely high absorption effect due to capillary. The fresh cement paste with great flowability is sucked and contact closely with

aggregates. More importantly, a part of the water is absorbed by EP, then, leading to an internal curing effect, which is the critical reason for denser ITZ (Qiu et al. 2023). The weak spot in SSM is modified that is the critical reason for the strength enhancement. However, the structure of EP is more brittle than SS and the enhancement effectiveness will be partly offset. These figures explain the changing strength of SSM and EPM, except the EPCM. Chemical element S (sulphur) and P (phosphorus) were slightly observed on the aggregate of SSM, while they should not be observed from aggregate. This found was caused by the sample preparation, especially cutting process, that transferred and dispersed the element on the cutting plane. The uneven cross section of EPM aggregate presented little S and P residual. For EPCM, the concentration rose again and only the deepest part showed black due to the limitation of scanning ability, which prove the existence of NS and NHP in aggregate. Then, the microstructure and product at higher magnification are shown in Figure 4.21.

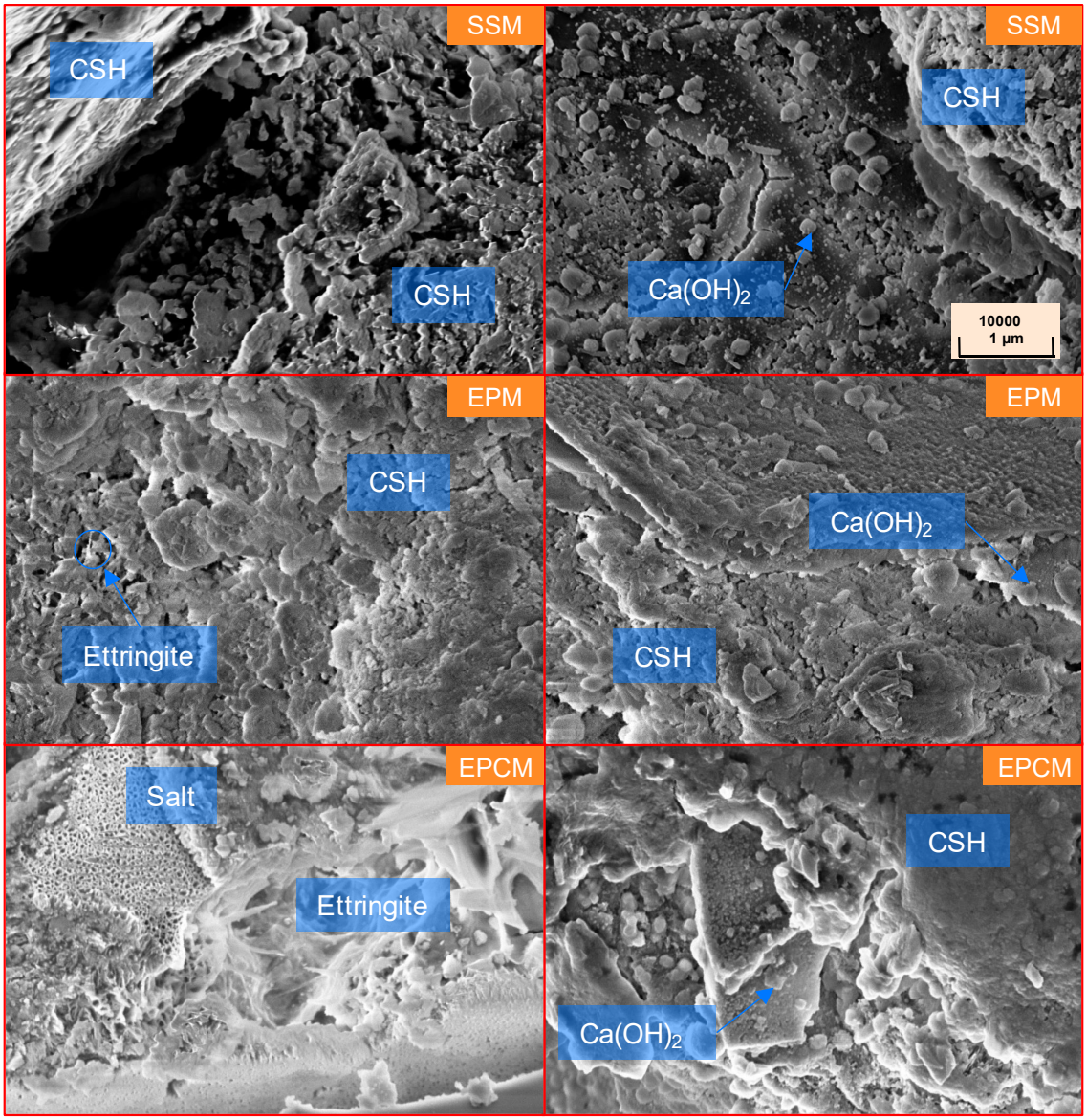

Figure 4.21 Microstructure and product at the magnification of 10k×

All SEM pictures shown in Figure 4.21 were captured around the aggregate. After thorough scanning the area near aggregates, commonly main products, $Ca(OH)_2$ and C-S-H, were distributed as expected. SSM showed lowest compactness and most obvious cracks. That was improved in EP and EPCM. Based on universal cement hydration process, ettringite was mainly generated in the early stage and was consumed later. These results were taken at 28^{th} day when a large amount of ettringite was consumed. A few minor ettringite was observed in SSM and EPM, while the EPCM counterpart was

relatively significant. In addition, the salt with compact porous structure was found near on the ettringite. It proved the above analyses that the salt-based inorganic PCM in this experiment boosted the ettringite generation, which was an important reason for the strength reduction.

4.6 Summary

This study investigated the hydration performance and structure changes of PCM-infused concrete. PCMs are functional additives that have varying influences on cement hydration. Based on the selected material and method in this study, the PCM composite alters hydration performance and temperature evolution. Differences in physical properties are observed, and the significant reasons behind are proposed. The main results are summarised as follows:

(a) The inclusion of PCM significantly affects temperature regulation during cement hydration. While the temperature trend follows the usual increase and decrease, the typical peak is replaced by a plateau at approximately 27.8 °C. This suggests that PCM effectively influences hydration, especially if its phase-change temperature aligns with specific hydration stages.

(b) The presence of PCM leads to notable strength loss, with compressive strength showing a more significant reduction (42%) compared to flexural strength (18%). This loss is primarily attributed to compromised bonding quality, as evidenced by a noticeable gap around the aggregate in the reference sample (SSM). While the porous aggregate slightly benefits bond quality, PCM alters the hydration product—specifically ettringite—on the surface of EP, weakening the bond strength.

(c) SSM and EPM exhibit continuous shrinkage in the early stages, whereas EPCM shows an initial expansion, reaching its maximum on day 5 before stabilizing by day

8. This expansion is mainly attributed to the accelerated hydration caused by the presence of nano-silica (NS), which promotes ettringite formation. Despite the small amount of NS, the maximum expansion is 180 με.

(d) Isothermal calorimetry results indicate that PCM modifies the hydration process. The thermal peak is lower, and hydration begins earlier, likely due to the presence of NS. However, the total heat released in EPCM is the lowest, indicating a reduced hydration level. This lower hydration is a key factor in the diminished mechanical properties of EPCM, a finding supported by thermogravimetric analysis (TGA).

(e) No pozzolanic reaction involving the amorphous quartz in EP was observed in this experiment. There is no evidence to suggest that differences in hydration products or processes are due to the presence of amorphous quartz.

CHAPTER 5. ENHANCED THERMAL AND MECHANICAL PROPERTIES OF PCM MORTAR

PCM concrete meets various challenges for real application, and Chapter 4 has revealed many changed mechanical properties from the thermal influence perspective. Further work is required to improve the comprehensive capability. Two current imperative developments are thermal conduction and strength maintenance, while carbon-based additives have tremendous potential (Li et al. 2023). The carbon black nano-particle (CB) and carbon nano-tube (CNT) are representative 0D and 1D nano-materials (Li et al. 2022). Millimetric carbon fibre (CF) is a universal material to improve the strength (Lu, Wang & Zhong 2022). This work designs hybrid carbon-based material additives to enhance both thermal and mechanical properties that provide a mothed for reliable PCM mortar application. CB and CNT with different dimensions build spatial connections that raise the thermal transfer and energy storage performance. Apart from the benefit of CNT on strength, CF promotes the modification at a visible scale, in addition to the channels in the nano-scale thermal conductive network.

5.1 Materials and sample preparation

The aggregate was expanded perlite (EP) with a size mainly from 0.3 mm to 1.3 mm provided by Australian Ausperl company. This aggregate had a porous structure with a dry density of 70 kg/m^3. Thorough drying was done before the experiment to remove the moisture. The silica sand (SS) had a similar size to EP but a different structure. The Portland cement was purchased from Cement Australia Pty Limited with up to 50% particles smaller than 10 microns and ViscoCrete polycarboxylate-based superplasticizer (SP) was used to modify the flowability.

The hydrated inorganic salt was used as PCM in this experiment. According to the previous chapters, $Na_2HPO_4 \cdot 12H_2O$ (NHP) and $Na_2SO_4 \cdot 10H_2O$ (NS) were selected. All raw materials were analytical reagents with a purity of 99%. The NHP and NS were melted with the same mass in advance to fabricate the binary PCM. The mixing procedure was processed in sealed tubes in a warm tank (60 ℃) with ultrasonic vibration.

Thermal properties, especially phase change performance, were critical for PCM concrete evaluation. Differential scanning calorimetry (DSC) was prominent and selected as a thermoanalytical technique in this experiment for the above object. The advanced NETZSCH DSC 300 Supreme (shown in Figure 5.1) was selected with nitrogen protection gas to complete DSC test. The temperature range was 15 – 65 ℃ with a heating/cooling rate of 5 ℃/min. A heating period and a cooling period composed a cycle while each test had 20 cycles consuming 400 minutes.

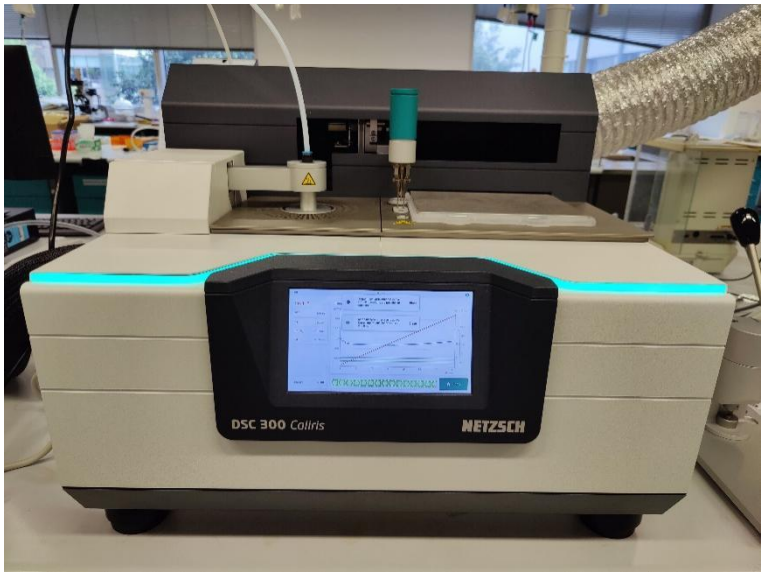

Figure 5.1 NETZSCH DSC 300 Supreme

This experiment selected multi-wall CNT with an external diameter of 8 – 15 nm and a length of 3 – 12 μm. The CB had an average particle size of 20 nm and an apparent density of 0.375 g/L. The dimension of CF was much larger when the diameter was 7 μm, and

the length was 5 mm with a good tensile strength of 4.5 GPa. The mentioned parameters were provided by the manufacture.

The mass ratio of PCM to EP was 10:6 equally 7:60 by volume, which was lower than the volume porosity of EP of 65%. The vacuum of 80 kPa was applied to specified materials for 6 h at the temperature of 50 ℃ that made the EP/PCM composites. Before being removed out the vacuum oven, the composite cooled to room temperature. The solid EP/PCM composite was EPC used in this experiment.

Table 5.1 Raw material proportion for mortar samples

ID	cement (g)	Water/c	SS/c	EP/c	EPC/c	SP/c	CNT/c	CF/c	CB/c
SE0	2000	0.46	1:1	6%	-	0.50%	0.00%	0.00%	0.00%
SC0	2000	0.46	1:1	-	16%	0.50%	0.00%	0.00%	0.00%
SC1-25	2000	0.46	1:1	-	16%	3.00%	0.10%	0.50%	0.25%
SC3-25	2000	0.46	1:1	-	16%	3.50%	0.30%	0.50%	0.25%
SC5-25	2000	0.46	1:1	-	16%	4.00%	0.50%	0.50%	0.25%
SC1-5	2000	0.46	1:1	-	16%	3.00%	0.10%	0.50%	0.50%
SC3-5	2000	0.46	1:1	-	16%	3.50%	0.30%	0.50%	0.50%
SC5-5	2000	0.46	1:1	-	16%	4.50%	0.50%	0.50%	0.50%
SC1-75	2000	0.46	1:1	-	16%	3.00%	0.10%	0.50%	0.75%
SC3-75	2000	0.46	1:1	-	16%	4.00%	0.30%	0.50%	0.75%
SC5-75	2000	0.46	1:1	-	16%	4.50%	0.50%	0.50%	0.75%

The proportion of raw materials for the mortar samples in this experiment was shown in Table 5.1. EP and EPC partially replaced the SS as aggregates with the volume percentage of 50%. SE0 and SC0 was used as references with and without PCM. Both references did

not contain carbon additives. All percentage indication in Table 5.1 was calculated by mass and c represented cement. For example, SS/c was the mass ratio of SS to cement. Most indication was constant expect the CNT, CB (two critical variates for the research) and SP (to compensate the dropping flowability due to more carbon additives). CF was thoroughly mixed with dry materials, cement and aggregates, in mortar mixer at low speed in advance. A part of water was used to disperse CNT and CB. The measured CNT and CB were mixed with tap water that was kept in ultrasonic wave for 30 minutes until fully dispersion. The suspension was poured in dry mixed materials gradually followed by slow mixing for one minute. Then, the rest water and SP were added before mixing at medium speed for 2 min. Fresh mortar was casted in the mould as 50 × 50 × 50 mm cubes following curing requirements in (ASTM 2021a). The test started after 28 days.

5.2 Performance of free thermal convection in the laboratory

All samples were heated in an oven at 57 ℃ for 3 hours to ensure the PCM was in a liquid state. The test started once the sample was taken out of the oven as soon as possible. The record continued until the temperature was close to room temperature (23 ℃). This process was done at the laboratory. The temperature was tested by a HIKMICRO H21 infrared thermal imaging camera that had a resolution ratio of 256 × 192 and the testing temperature range from -20 – 350 ℃. The distance between the sample and the camera was 0.5 m, and the testing mode was set as a rough surface corresponding to the concrete feature. A piece of fabric was placed under the sample to prevent thermal reflection from the desk surface.

The temperature difference forced reducing the temperature of samples and heat loss from multiple directions. The camera was only able to capture the surface temperature, which

was the cooling frontline. The stored heat in the inner part flows out via the surface gradually, which finally causes the temperature of the sample to.

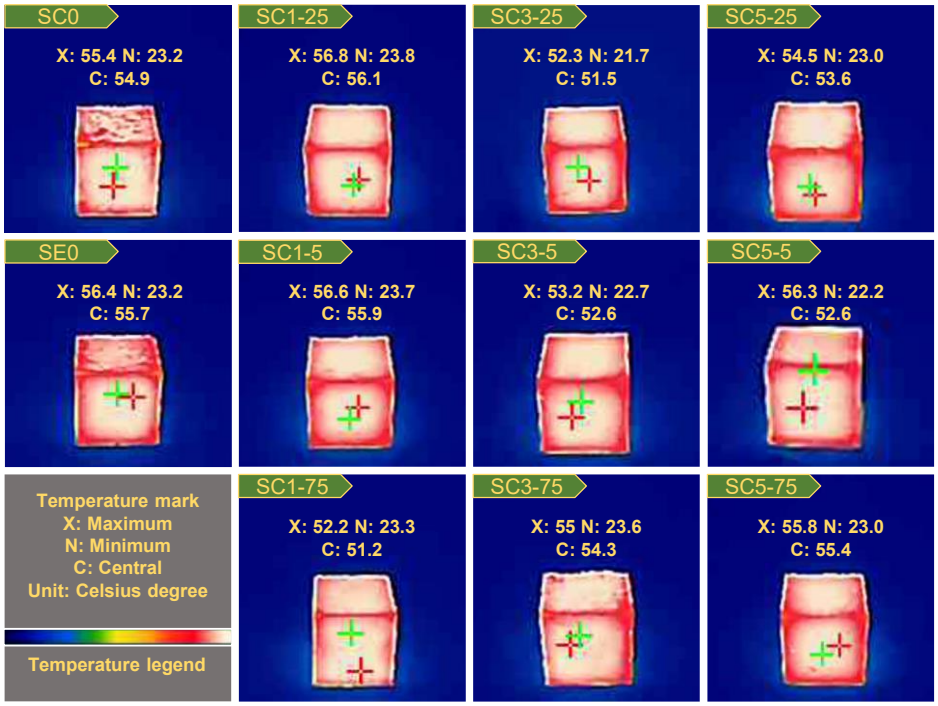

Figure 5.2 Initial temperature distribution

As shown in Figure 5.2, all samples reached high temperatures in an oven. The minimum temperature was captured in the room, and the maximum one was captured from the sample surface. At the ideal conditions, the temperature distribution should be uniform after oven heating. In fact, the temperature at the edges was lower than that at the surface central. Heat mass was transferred from samples to the air, leading to the temperature reduction, while the heat mass at the inner core was transferred to the surface due to the temperature gradient. The edges were affected by more than one surface, which meant faster heat loss and a longer distance to the sample's inner core, making less heat recovery efficiency. This phenomenon is illustrated in Figure 5.3. In the test, there was a time gap between the sample removed from the oven and temperature capture, which enabled the influence as explained above.

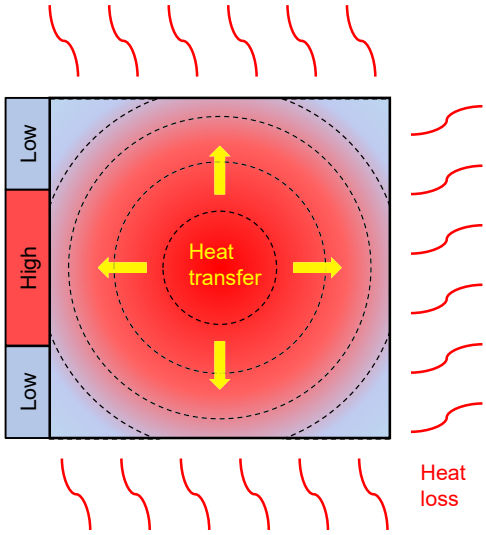

Figure 5.3 Heat transfer and heat loss illustration

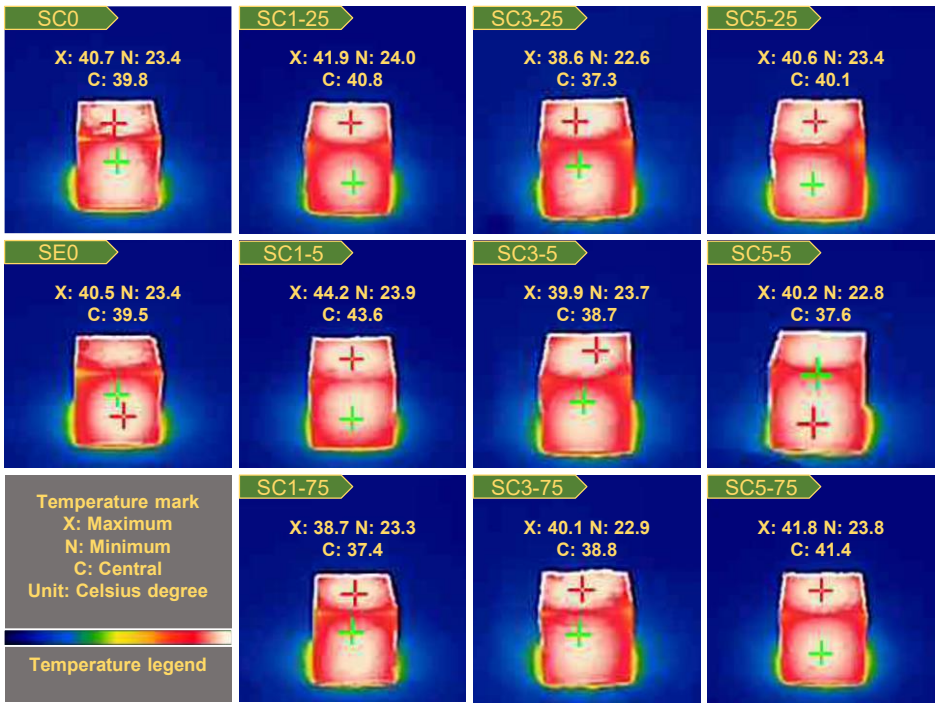

Figure 5.4 Temperature distribution after 10 min

All samples' temperatures dropped remarkably without the oven heating as shown in Figure 5.4, which showed a maximum temperature difference of around 10 ℃ compared to the initial state. The high-temperature difference between the sample and the environment, over 30 ℃, facilitated the heat transfer and heat loss leading to the fast

temperature decrease. The temperature distribution was similar to the results at the initial state, but the relatively low-temperature area near the edge became larger. After 10 min, the inner temperature gradient became more significant than that was at the initial state (more similar to the Figure 5.3).

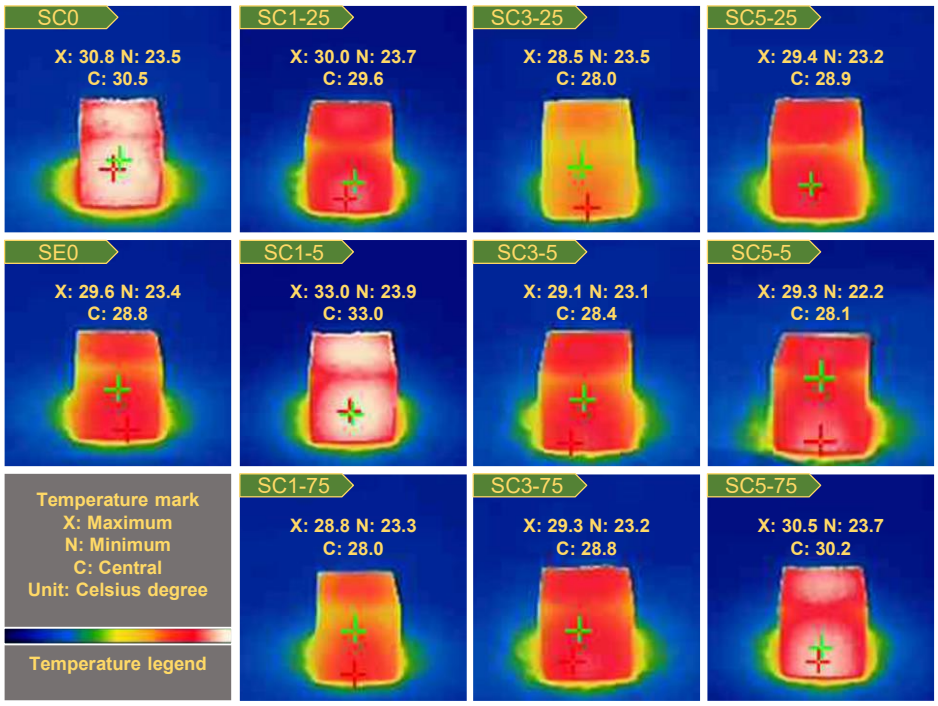

Figure 5.5 Temperature distribution after 30 min

With the passage of time, the temperature distribution feature in Figure 5.4 became weak because the heat mass at the core area was not sufficient. As shown in Figure 5.5, most samples showed uniform surface temperature and the temperature kept decreasing. At this stage, the temperature difference between samples was significant although it was minor at the beginning. For example, SE0 and SC1-5 had only 0.2 ℃ different for both maximum and central temperature but it was enlarged up to 4.2 ℃ in Figure 5.5. According to the mixing proportion, it was attributed to PCM and various carbon additives. The former affected the original heat mass, and the latter influenced heat conduction. The details will be analysed in the following part.

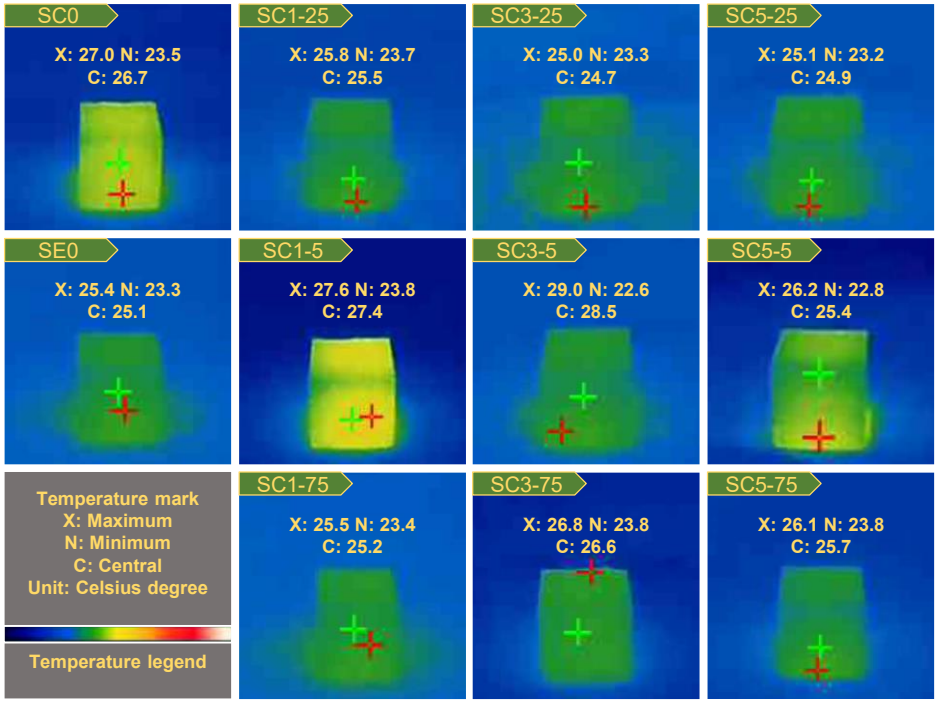

Figure 5.6 Temperature distribution after 60 min

After 60 min cooling, the sample temperature mostly became close to room temperature, as shown in Figure 5.6. The minimum temperature shown in Figure 5.2, Figure 5.4, Figure 5.5 and Figure 5.6 was about 23 ℃ but it was not the room air temperature. The minimum temperature in the figures was captured from the table surface and the lab room thermometer provided the room temperature of around 25 ℃. Therefore, it was concluded that the surface of most samples reached room temperature approximately.

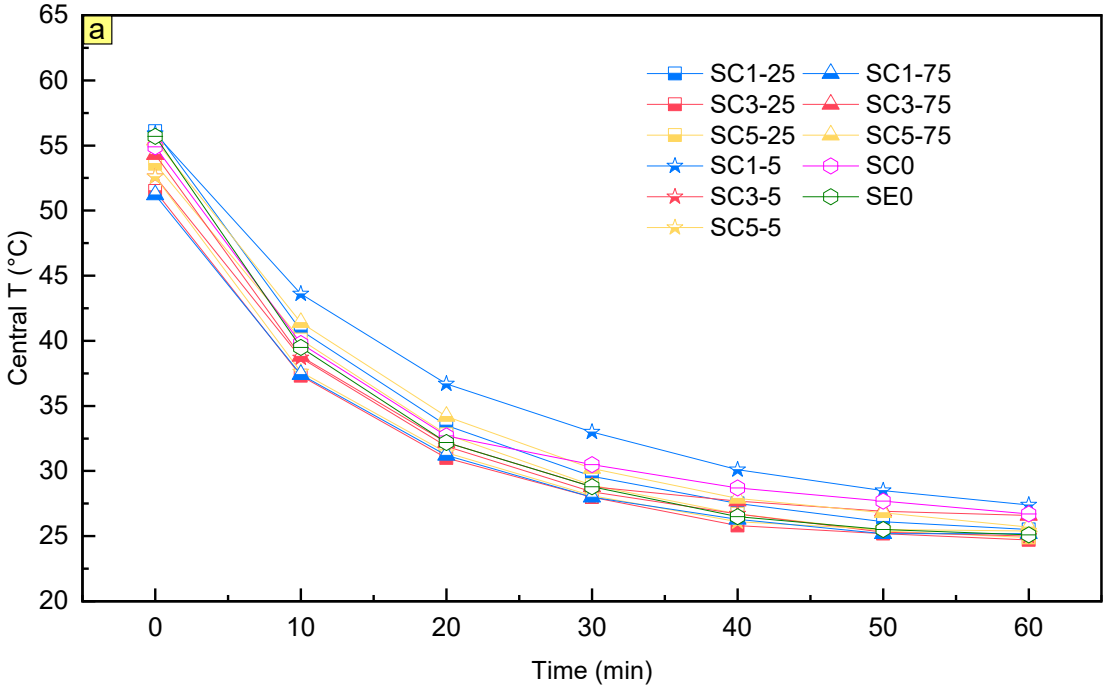

(a) Whole data for temperature development

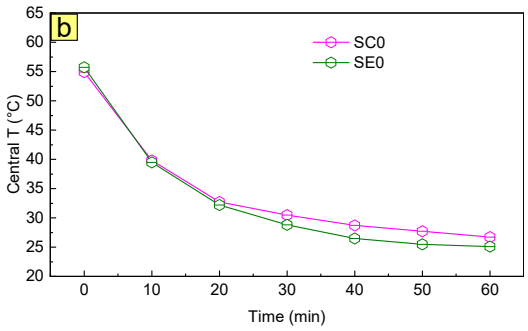

(b) SE0 and SC0

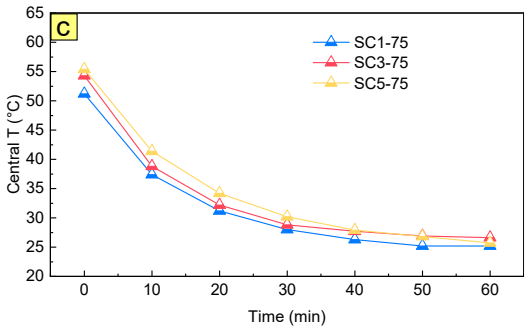

(c) Groups with CB75

Figure 5.7 Central point temperature development

The central temperature development with a time gap of 10 min was illustrated in Figure 5.7 (a). All samples' temperatures decreased continuously and tended to a stable state close to room temperature. Overall, the temperature decline rate became lower with time because the temperature difference was lower, which was a main force for thermal convection. To explain the data clearly, many critical and representative lines were extracted. The effect of PCM is clearly illustrated in Figure 5.7 (b). SE0 and SC0 had close start temperatures and decreasing rates in 20 min. After that, a considerable gap was

when SC0 showed a temperature of 30.5 ℃ higher than the SE0 counterpart of 28.8 ℃. These temperatures reached the melting point of the PCM in the previous chapter, and the released heat eliminated the temperature decline. The temperature gap between samples kept around 2.2 ℃ but fell to 1.6 ℃ at 60 min explained by the inadequate heat in PCM. In addition, the temperature lag was obtained in 10 – 20 min (same temperature: a. SE0 at 30 min and SC0 at 40 min; b. SE0 at 40 min and SC0 at 60 min).

Roughly, the temperature dropped faster because of the effect of carbon additives on thermal conductivity. The influence of various additives was not the same and not always advantageous. On the one hand, the accelerating of CB was relatively stable for most samples, which enhanced the thermal convection ability with the same CNT and CF. On the other hand, CNT showed various effects although it was normally regarded as thermal conductivity. Take the CB 5 groups as examples as shown in Figure 5.7 (c), the decreasing rate was lower with more CNT amount. Choi et al. (2022) got great electrical conduction enhancement but slight thermal conduction reduction on concrete by CNT addition, although pure CNT had both excellent electrical and thermal conduction. They believed the CNT strand was the energy barrier that allowed electron transportation but stopped phonon cross. This phenomenon was affected by CB amount and the comprehensive results are presented in Figure 5.7 (a).

5.3 Thermal properties of mortars

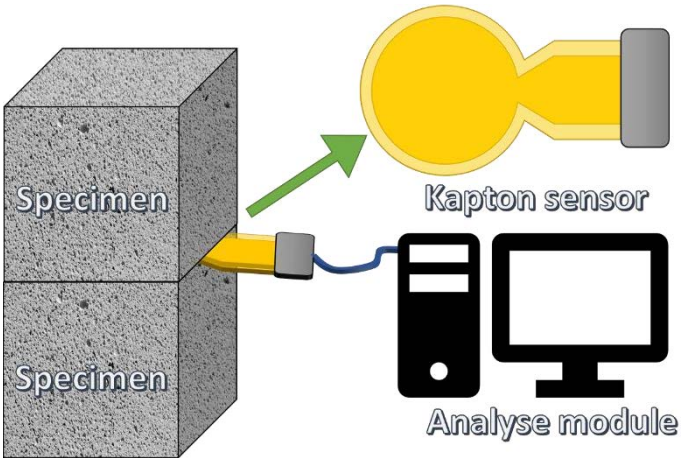

Figure 5.8 Configuration for thermal property test

The thermal convection performance is affected by the intrinsic properties. The critical thermal conductivity was tested by a popular Hot Disk facility based on the transient plane source method. A Kapton 5501 F2 sensor with a radius of 6.403 mm and an output power of 10 mW were used. The sensor was embedded between two specimens with the same properties as shown in Figure 5.8. The test was completed in a laboratory with a temperature of 22.5 – 23.5 ℃. The results of thermal conductivity and thermal diffusivity were analysed.

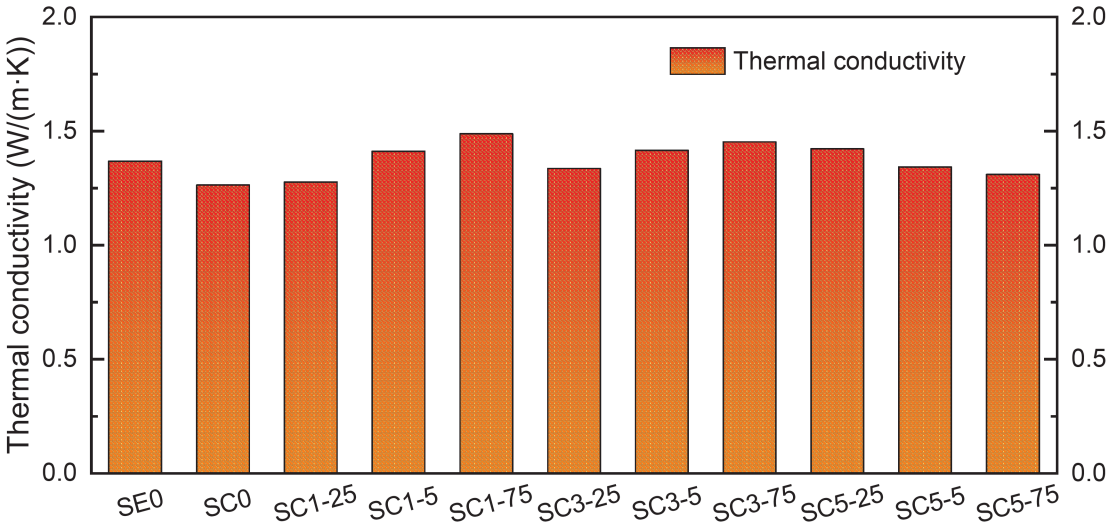

Figure 5.9 Thermal conductivity in room temperature

To analyse the performance of free thermal convection and evaluate the designed PCM mortar, crucial parameters were tested including thermal conductivity (T_C) and thermal diffusivity (T_D). As shown in Figure 5.9, T_C presented moderate regular fluctuation. SE0 represented normal mortar with a T_C of 1.368 W/(mK) while the PCM addition made a lower value of 1.263 W/(mK). The thermal conductivity of the crystal salt was very low and the PCM addition could weaken the contact between aggregate and cement paste. The density was shown in Figure 5.10 that SC0 met a remarkable drop. SC1-75 gave the maximum T_C of 1.488 W/(mK) with an enhancement of 18%. The carbon-based material was supposed to enhance the T_C, but the result of SC1-25 was not satisfying. It was contributed by the looser structure and lower density due to CF addition when the small number of nano-materials provided slight enhancement. The density summarily rose with increasing nano-materials from SC1-25 to SC1-75. Then, the CB generally improved the T_C except for samples with CNT of 0.5%, when it decreased from 1.422 W/(mK) to 1.309 W/(mK). It was explained by the bad distribution of nano-carbon materials with the growing amount.

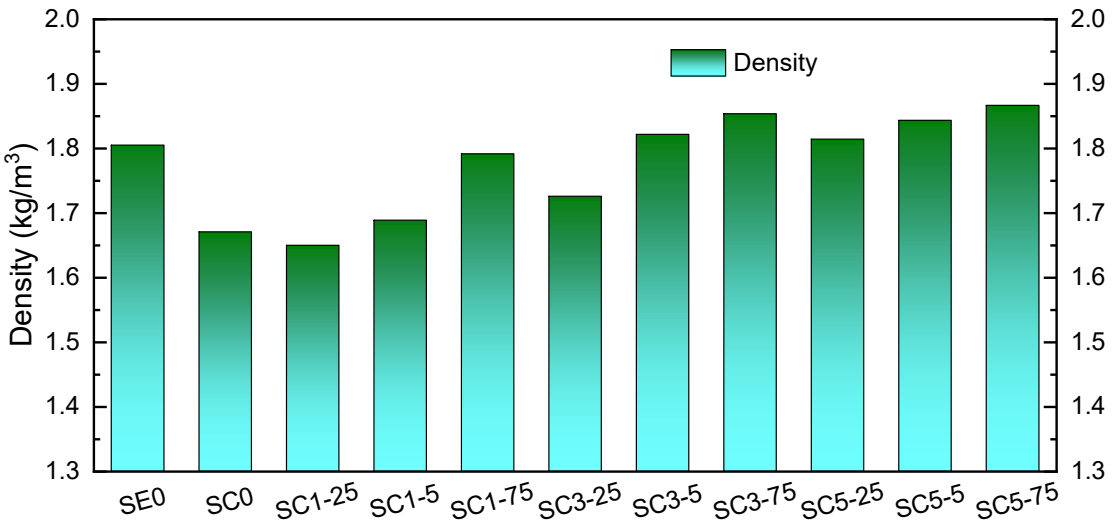

Figure 5.10 Density of specimen

CB was illustrated as a benefit for TC, but CNT sometimes played an adverse role. Although pure CNT had both excellent electrical and thermal conduction, it was found that electrical conduction enhancement but slight thermal conduction reduction in concrete by CNT addition (Choi et al. 2022). CNT strand was the energy barrier that allowed electron transportation but stopped phonon cross. The lattice vibration energy of the phonon was scattered, as shown in Figure 5.11. Therefore, the influence on density and thermal conductivity were opposite (like among SC1-75, SC3-75, and SC 5-75). The T_C uptrend of SC1-25, SC3-25, and SC5-25 was mainly caused by the significantly improved density. In contrast, the differences of others (samples with CB of 0.5% and 0.75%) were not compelling.

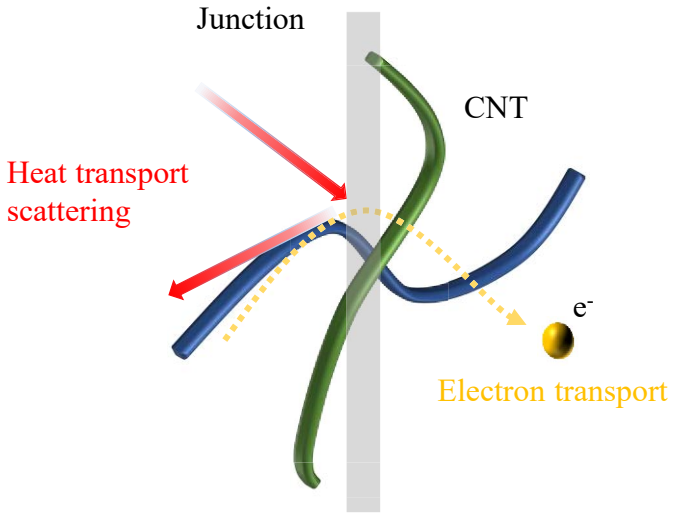

Figure 5.11 Schematic diagram for thermal conduction (Choi et al. 2022)

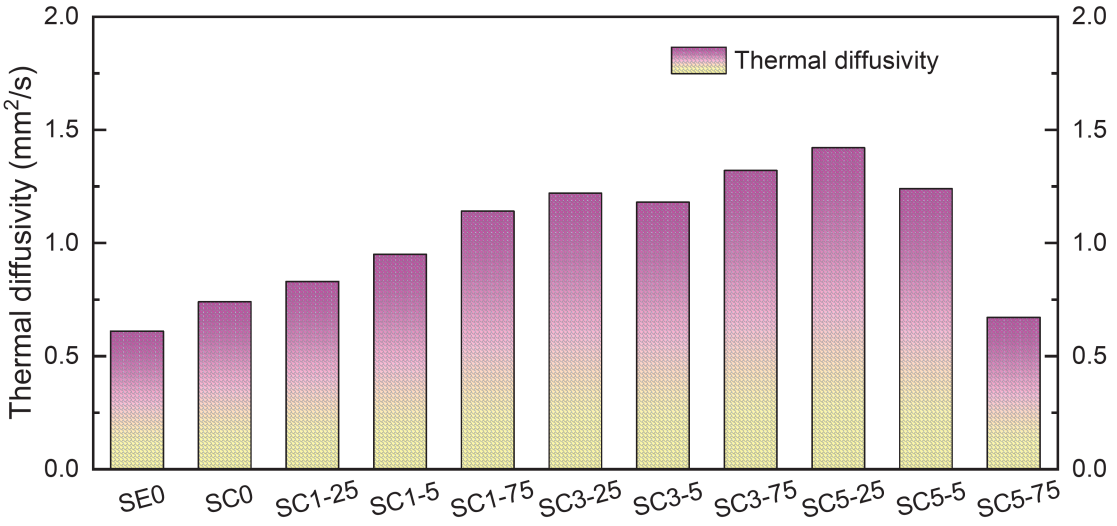

Figure 5.12 Thermal diffusivity at room temperature

Another valuable parameter was thermal diffusivity (T_D), as shown in Figure 5.12, which was not highly consistent with T_C. The improvement on T_D was attractive although the impact on T_C was various, when more carbon materials were incorporated. The uptrend of T_D continued until SC5-25, and TD kept rising from 0.6 to 1.42 mm^2/s, with a difference reaching 136%. CNT did not directly show amazing benefits on T_C but performed well on T_D cooperating with CB and CF. The downward change of both T_C and T_D in samples with CNT of 0.5% was found. However, the density did not show the same regulation and was raised, while higher density was expected as helpful for heat transport. This contradictory result was attributed to the incorporation quality of nano-material, especially at a very large amount. Summarily, both CNT and CB could improve the T_D, although they had different performances of T_C. It is improper to regard CNT addition as harmful just due to the unfavourable influence on T_C.

5.4 Strength enhancement

This experiment investigated the compressive strength of cubic samples as shown in Figure 5.13. The strength drop of SC0 is a common problem for PCM concrete as

proposed in the above chapter. The result shows a remarkable reduction of 28% compared to SE0. The benefits of carbon additives on concrete strength were overall significant. The overall rules of compressive strength presented great similarity with density change in Figure 5.10. The enhancement was clear. Even minor reduction was observed with a few additives like SC1-25 and SC1-5. The millimetre CF may interfere with the formation of uniform cement paste and aggregate, which led to an adverse impact on both density and compressive strength. The CF was supposed to raise the concrete strength, but the mixing plan in this experiment made the insufficient bond between cement paste and CF at a low level of nano-material addition. With increasing additives, the enhancement became compelling, which occurred from SC1-75 with a moderate increase of ~10%. This enhancement was attributed to both nano and millimetre carbon materials. The effectiveness of CNT soared significantly, between 0.1% and 0.3%. The continuous benefit of CB with the same CNT content also happened but the enhancing efficiency was lower. With the same CB quantity, higher CNT brought higher strength, and the efficiency was the best with a CB of 0.25%. The highest compressive strength was provided in SC5-75 followed by SC3-75. The optimal group made an enhancement of 24% compared to SC0.

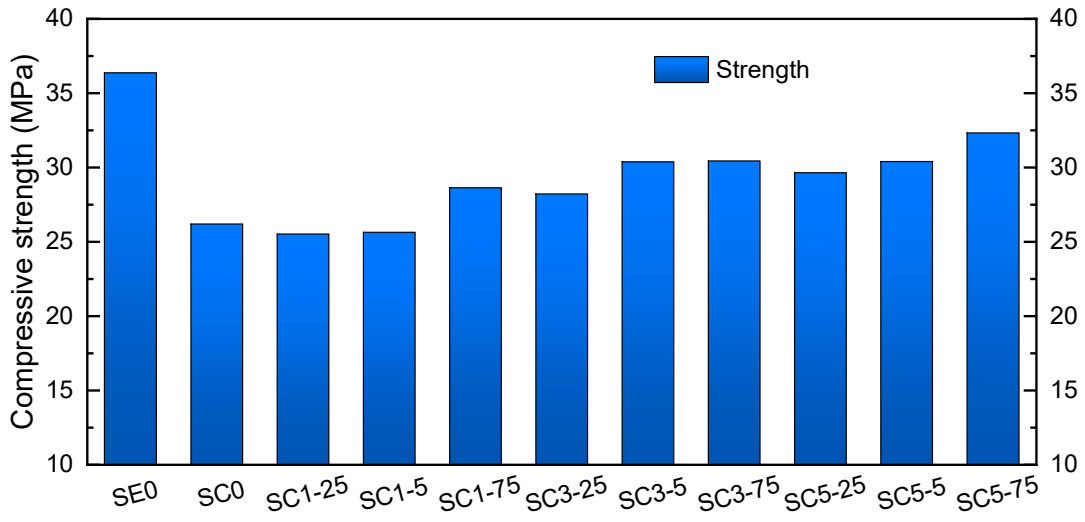

Figure 5.13 Compressive strength of cube with an edge of 50 mm

5.5 Characterisation of mortar

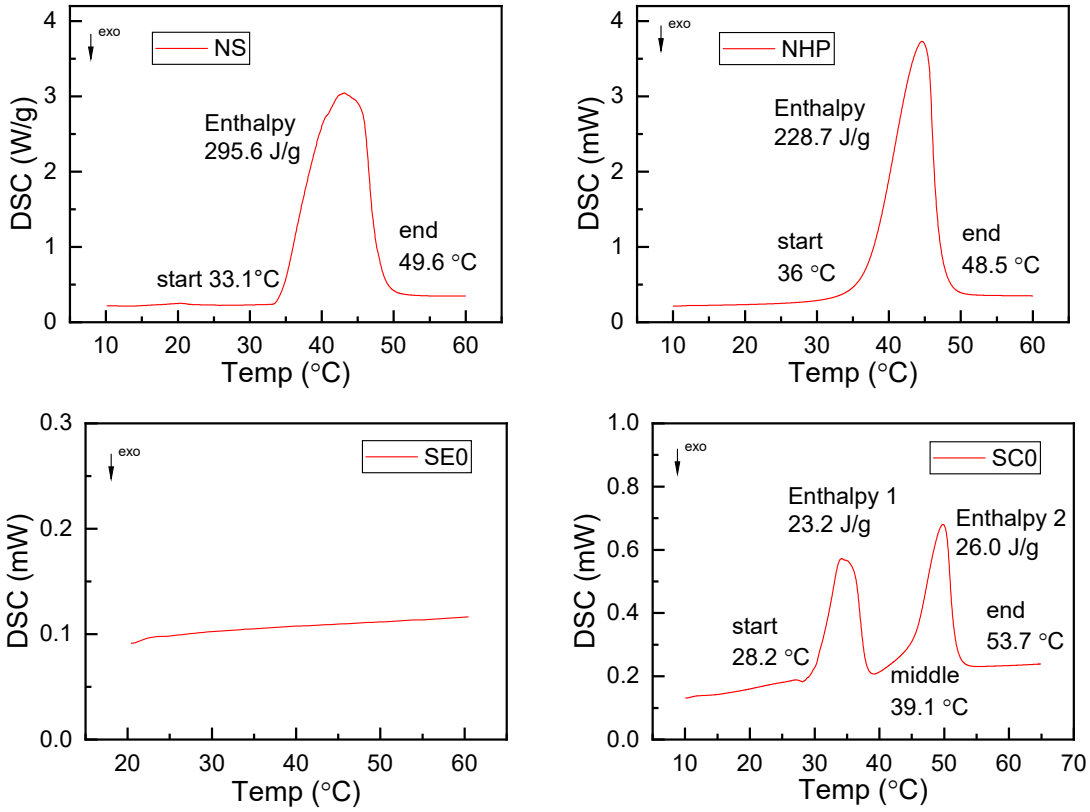

Figure 5.14 DSC results and thermal properties of important materials

Many critical samples were selected to present the thermal properties based on DSC results as shown in Figure 5.14. Both NS and NHP had an ideal enthalpy of 295.6 J/g and 228.7 J/g, which were close to the theoretical values. The conventional sample, like SE0, had no latent heat. The specific heat is able to store thermal energy, but the efficiency is far behind latent heat, while the stable temperature of latent heat is quite advantageous. After PCM addition, SC0 presented obvious latent heat. Compared with raw PCM, the biggest difference was the peak number. It was caused by the moderate multi-effect between two PCMs when the different molecules showed force on the hydrone combination and separation. The melting point became lower reaching 28.2 ℃, but the final end point was higher than 53.7 ℃. The endpoint of the first peak was closely

connected with the start point of the second peak, which proved the continuous performance of the phase-changing effect. The melting range was much broader than raw PCMs providing more appropriate application conditions. The enthalpy of SC0 was remarkably lower than that of raw PCMs, around only one-tenth. The enthalpy was almost provided by PCM and the conventional concrete components had little influence. In addition, from the mixing plan in Table 5.1, the mass of PCM took just a small part of the whole sample, thus reducing enthalpy. However, the SC0 still presented a large ability for thermal energy storage.

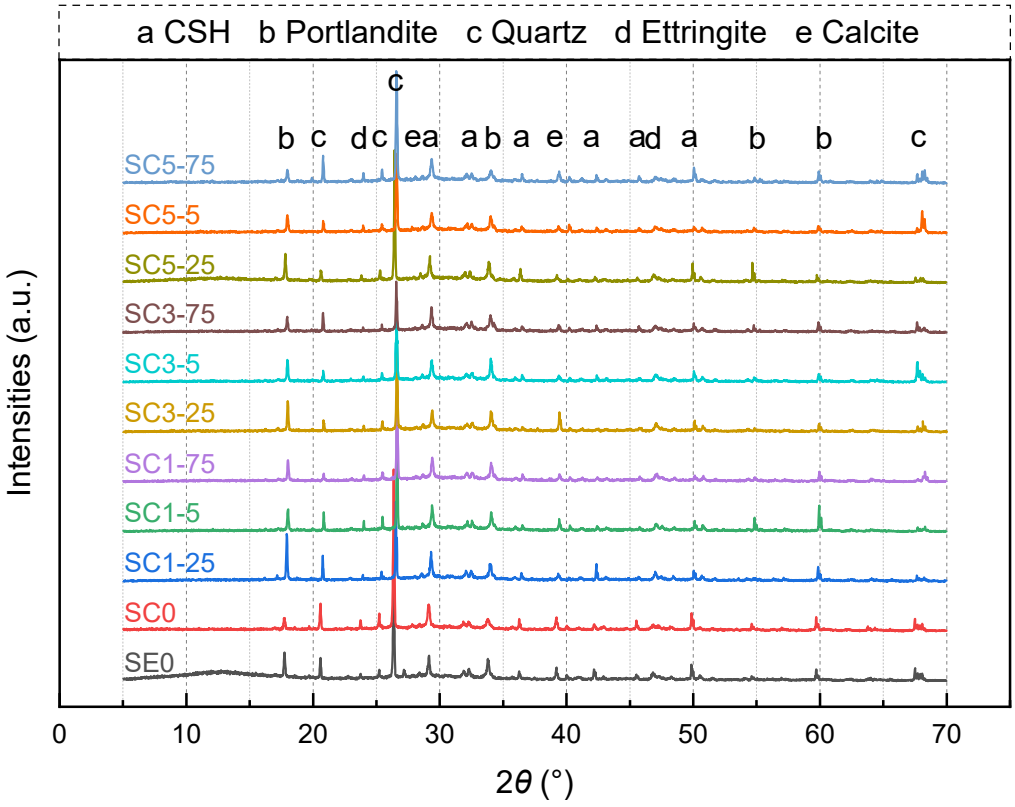

Figure 5.15 XRD results of samples at 28d

The crystal characteristics of XRD are shown in Figure 5.15 where the major peaks and products are marked. Most samples with carbon additives showed similar peaks with the reference, and the variety of products was the same. The peak at around 42° for CSH was slightly weaker with carbon additives. The comparable feature also applied to the peak at

around 50° for CSH, although the SC5-25 group had a stronger peak. On the other hand, the main peaks for CSH at around 29°, 33°, 36° and 45.5° were quite stable. The peaks for portlandite were also stable even though fluctuation was observed at around 55° and 60°. Meanwhile, the peaks for quartz, ettringite, and calcite were extremely stable, proving that there was little influence. The sample difference was peak intensity, but the position and number were not changed. It was concluded that the carbon additives did not bring clear effects on the mortar composition.

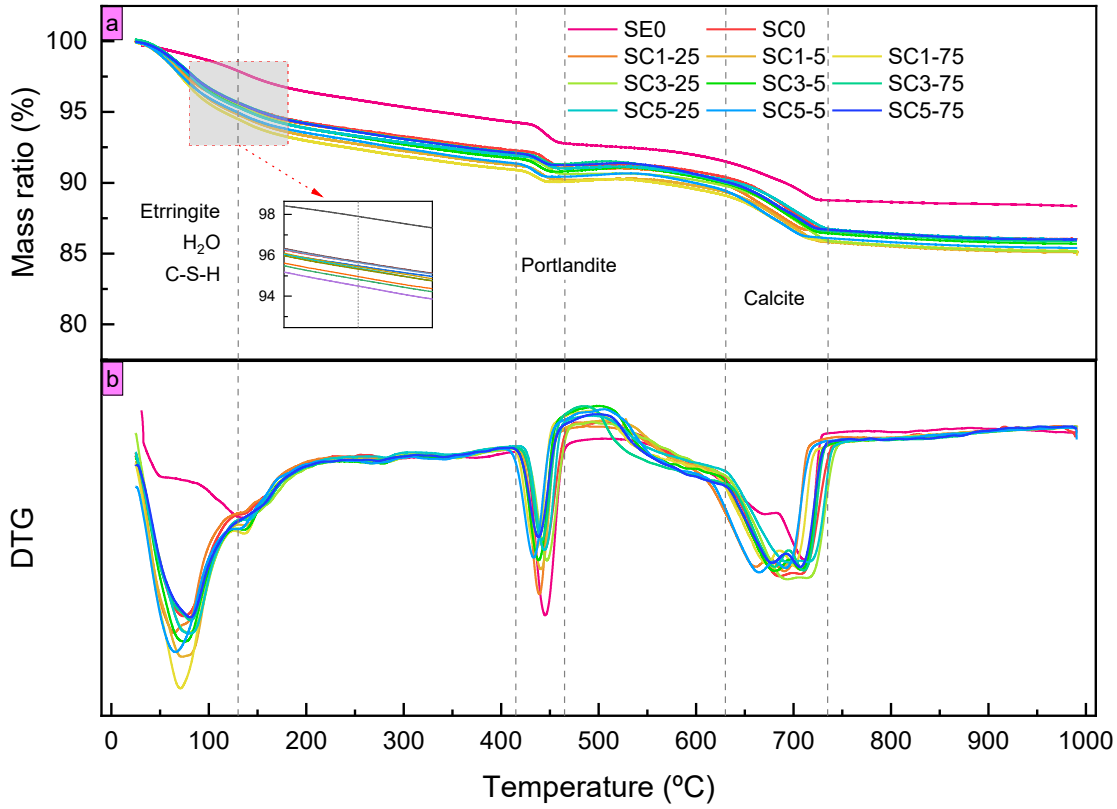

Figure 5.16 TGA results (a. Thermal gravimetric; b. Derivative thermal gravimetric)

The mass loss of samples at elevated temperatures is shown in Figure 5.16. The number and position of peaks were similar but the difference in features was still obvious. The total weights of carbon-based materials were in the range of 0% - 0.65% based on the raw material proportion, which showed little effect on TGA results. The influence of varying

SP was double that was in the range of 0.2% - 1.7%, while it mostly was decomposed at the first loss peak. In contrast, the PCM occupied around 3.75 wt% except SE0. The inorganic hydrated salt PCM was dehydrated and lost moisture at the first peak. The peaks at around 450 ℃ and 700 ℃ were contributed by the cement hydration products.

For the first peak, SE0 showed the best stability with a residual mass of 98% and other samples were far behind with values lower than 96%. In addition to the reasons presented in the last paragraph, it was also proposed that more ettringite was produced, although the contribution may not be dominant. The dehydration reaction of PCMs was still the primary reason. Based on Figure 5.16 (a), the mass loss of all samples for Portlandite was comparable at 420 – 470 ℃. The mass loss in SE0 with a ratio of 1.5% was more than other samples' values of around 1%. Meanwhile, the mass loss in 600 – 700 ℃ varied from 2.7 – 3.9%, and SE0 presented the lowest loss ratio. It was proposed that SE0 had lower calcite with a mass loss of 2.7% while other samples had more calcite loss of about 3.5%.

The DTG peaks showed moderate similarity in high temperatures. There was a mild difference in start and end temperatures. This phenomenon did not affect the proportion of hydration products and had little impact on thermal stability. Finally, most samples' mass became constant at about 85%, and the SE0 counterpart was around 88%. The gap of 3% was close to the condition after the first peak proving the similar thermal stability at high temperature.

Considering the size of objectives, ZEISS SUPRA-55 VP field emission scanning microscope (FE-SEM) was selected to investigate the microstructure of cement hydration products and additives distribution. It had a maximum magnification of over 80k. The resolution can reach 1 nm at the accelerating voltage of 5 kV with the detector of In-lens.

To maintain the original features, samples were cleaned by compressed air blow and dried without polishing or fine cutting, although a polished plane is beneficial for image quality eliminating electric charging. All samples for SEM test were collected pieces after mechanical tests, which had been cured for 28 days and suffered compression.

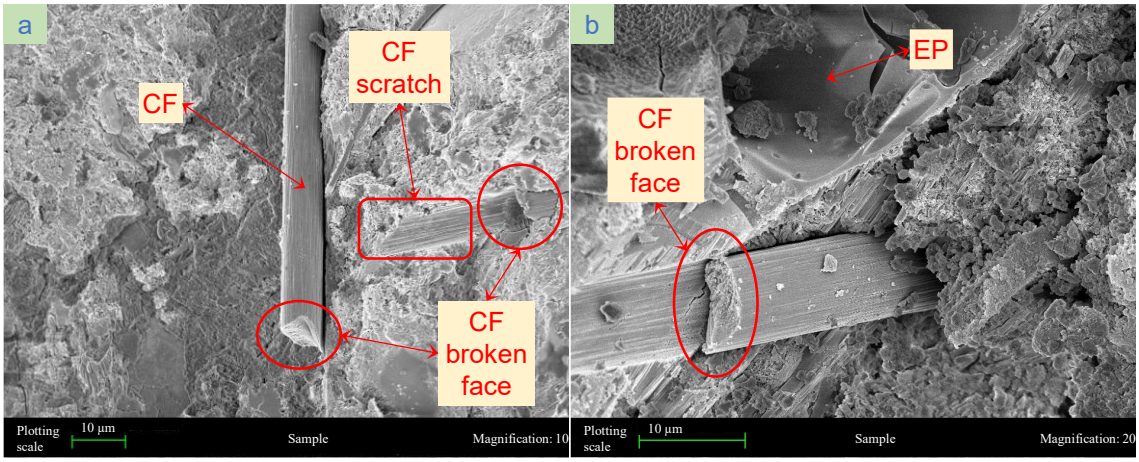

Figure 5.17 Microstructure of (a) SC3-5 and (b) SC5-25

Many properties presented in the above sections are affected by the microstructure, so specific SEM results are analysed in this section. As shown in Figure 5.17, CF was incorporated in the mortar. The CF is quite longer than other components like aggregate and is able to bridge cracks. The figures were captured from the crushed samples that suffered broken. The scratch on mortar and broken face of CF were commonly observed, which proved the support of CF to bearing force. This micro-visible impact contributed to one important reason for the enhanced mechanical compared with SC0. The further influence of various carbon additives is analysed next.

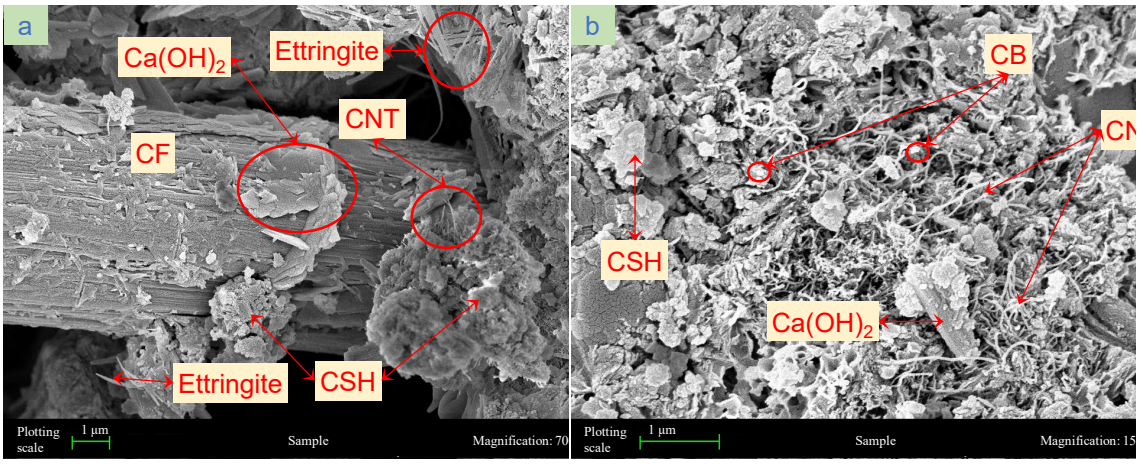

Figure 5.18 Microstructure of (a) SC3-75 and (b) SC5-5

As shown in Figure 5.18 (a), cement hydration products and carbon additives can attach to the CF surface, showing a stable connection. The CF was able to bridge discrete parts and run through the sample at a millimetre level, like the presentation in the above paragraph. Meanwhile, a long conductive path may be generated by the CF attached with materials, besides mechanical bond. EP and CF had millimetre size, but EP was fragile and non-conductive. CF played a remarkable role in modifying the mechanical and thermal properties at the millimetre level. CNT and CB were incorporated with cement hydration products and attached on CF, which improved mechanical and thermal properties of cement paste (Li et al. 2022). However, the superfluous additives may interfere with the stability of mortar. As shown in Figure 5.18 (b), a lot of CNT and CB can agglomerate together to form larger clusters in specific area. The benefit of additives on both mechanical and thermal properties relied on a favourable distribution. In addition, redundant carbon additives will break the excellent stability of cement hydration products. The SEM result verified the phenomena and analyses for thermal convection and strength.

5.6 Summary

This experiment designs a PCM mortar with carbon additives. Besides modified thermal properties, the mechanical properties are also investigated. The carbon additive shows

obvious effects on the PCM mortar performance and the optimal value is sensitive to the various content of additives.

(a) The surface temperature of hot cubes is not equal, which mostly shows higher temperatures in the surface central area. In the temperature-decreasing period, the cube's inner core supplies heat mass to the surface, resulting in a spherical temperature gradient. In addition, the area close to the edge makes it easier to lose heat, which makes the relatively higher temperature of the surface central. The total heat energy storage of PCM mortar is higher and causes a slower temperature decrease. The temperature of all samples decreased to near room temperature after one hour. Take SE0 as the reference; SC0 shows a higher temperature of 1.6 ℃ at 60 min. From the time perspective, a temperature lag of 10 – 20 min is obtained.

(b) Most samples show faster temperature reduction with more additives, but it is changed with over-high additives. This change is clearer in CNT. With 0.5% of CB, a higher CNT amount causes lower temperature reduction. The excellent thermal conduction of CNT does not fully present advantages. CNT strand may generate an energy barrier to stop phonon cross, leading to low thermal convection in concrete. On the other hand, the advantage of CNT on thermal diffusivity is convincing, which still prove the value of CNT in PCM concrete.

(c) The benefit of CB on thermal conductivity is proved in most samples. Higher thermal conductivity is achieved with more CB additives. An exception occurs in groups with a large amount of CNT. Gradual decrease is constant with increasing CB. In this circumstance, agglomerated CNT negatively changes the CB distribution, which interferes with the thermal conductive path. Similar to CNT, increasing CB also makes higher thermal diffusivity obviously. Apart from the activation of carbon material, the absorption effect on structure is an important reason.

(d) Lower strength is still a defect of PCM concrete, but the enhancement of nano additives is great. The sample of this experiment improves the compressive strength by 24%. SEM results prove the distribution and connection of additives. CF runs through the large area of mortar connecting cracks and gaps. CNT and CB are wrapped in paste, attached to CF, and connected to hydration products. The cooperation supports the improved properties of thermal convection and mechanical properties. However, the well-distribution of nano-materials is challenging. The agglomeration occurs with high additive content that hinders the improvement and even poses adverse effects.

(e) Carbon additives and PCM introduce unstable components that affect the thermal stability at around 100 ℃. The intrinsic property of raw materials is the dominant reason. On the other hand, the proportion of portlandite is reduced, and the calcite counterpart is increased, which proves the good thermal stability in high temperatures. The latent heat of mortar with PCM is remarkably improved, and the effect of temperature during self-heating is illustrated.

CHAPTER 6. SELF-HEATING PERFORMANCE OF PCM MORTAR WITH CARBON-BASED ADDITIVES

PCM concrete is a prevailing topic for energy-saving that can store thermal energy (Wang et al. 2023a; Wang et al. 2022; Yang et al. 2022). The primary function of PCMs is passive, whereas self-heating concrete possesses the active ability to modulate temperature. The fundamental mechanism underlying self-heating concrete involves the conversion of electrical energy into thermal energy, as described by Joule's law. This experiment explores the self-heating capability of the modified PCM concrete, which aims for multifunctional concrete development. Carbon additives are beneficial to the efficiency of PCM concrete and critical to the conductive path of self-heating (Ramezani, Dehghani & Sherif 2022; Wang et al. 2023b). The effect of properties (like shape, size, etc.) is different and the attempt for various material combination is attributive (Wang et al. 2023b). Three carbon additives are incorporated with various amount in a hydrated inorganic salt-based PCM mortar. The self-heating capability is evaluated by the temperature distribution and increment under constant DC voltage, in addition to the key parameter of electrical conductivity. FTIR, SEM, and electrical impedance techniques are used to analyse the inner differences and explain for the changing self-heating capability. The sensitivity of raw nano carbon additives is also calculated and the optimal group is proposed. This work will push forward the multifunctional PCM concrete with self-heating.

6.1 Materials and sample preparation

This work used the mixing proposal as shown in Table 6.1. The water-to-cement ratio was kept at 0.46 while the SP-to-cement ratio varied from 0.5% to 4.5% to modify the

flowability. All samples had the same proportion of EP-based PCM composite (EPC). Analytical reagents of $Na_2HPO_4 \cdot 12H_2O$ and $Na_2SO_4 \cdot 10H_2O$ were selected as core PCMs (Fang et al. 2020). To fabricate EPC, same amount of tow PCMs was melted and mixed at 60 ℃ in advance, before being impregnated in EP at 50 ℃ with a vacuum pressure of 80 kPa. The mass ratio of EP to PCM was 0.6. The composite was taken out after four hours and naturally cooled to room temperature, completing EPC fabrication. The sample name illustrates the content of carbon additives. Take T3B25 as example, the mass ratio of CNT to cement was 0.3% and CB counterpart was 0.25%. The CF percentage was 0.5% in most samples except T0B0. The fresh mixed material was cast as 50 × 50 × 50 mm (ASTM 2021a).

Table 6.1 Mix proposal for all samples

Name	Cement	Water	SS	EPC	SP	CNT	CF	CB
T0B0	2100	966	2100	336	3.5	0	0	0
T1B25	2100	966	2100	336	21	0.7	3.5	1.75
T3B25	2100	966	2100	336	24.5	2.1	3.5	1.75
T5B25	2100	966	2100	336	28	3.5	3.5	1.75
T1B5	2100	966	2100	336	21	0.7	3.5	3.5
T3B5	2100	966	2100	336	24.5	2.1	3.5	3.5
T5B5	2100	966	2100	336	31.5	3.5	3.5	3.5
T1B75	2100	966	2100	336	21	0.7	3.5	5.25
T3B75	2100	966	2100	336	28	2.1	3.5	5.25
T5B75	2100	966	2100	336	31.5	3.5	3.5	5.25

Stable conductive electrodes were essential for self-heating test and copper mesh was recommended (Dong et al. 2021; Wang et al. 2023b). Two pieces of copper mesh, with a dimension of 25 × 45 mm, were embedded in each specimen as electrodes. A part of

electrode was inserted in fresh mortar cube with the depth of 35 mm that provided large contact area with mortar. The rest part allowed the connection with power supplier. A gap of 30 mm was kept between two electrodes. The electrode distribution was centrosymmetric and the parameters were shown in Figure 6.1. The whole mould and cube were covered by plastic film eliminating moisture evaporation for one day. Then demoulded samples were kept at curing chamber (24 ℃ and humidity of 95%) until 28th day.

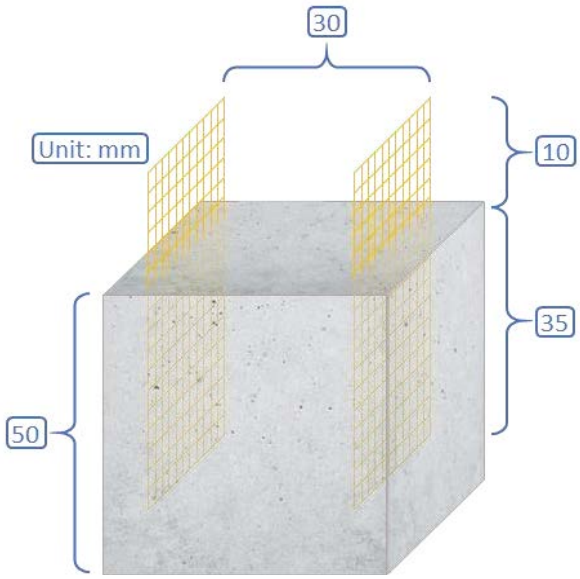

Figure 6.1 Setting of specimens with copper electrodes

6.2 Self-heating performance under DC

All prepared samples had two electrodes that were connected to the power supplier. The input standard Australian power, 240 V AC 50Hz was transferred to DC. The output voltage was set as 10 V. A handheld infrared thermometer was used to capture the temperature distribution and changes, which was manufactured by HIKMICRO Sensing Technology Co., Ltd. The testing distance was 0.5 m and the room temperature was ~23 ℃. A rough layer was placed under the sample to remove the infrared reflection

caused by the flat table. The recording started once the current was applied. The test was replicated on three parallel specimens, and the most representative specimen that governs the behaviours of two or three more specimens was presented. The test configuration is shown in Figure 6.2.

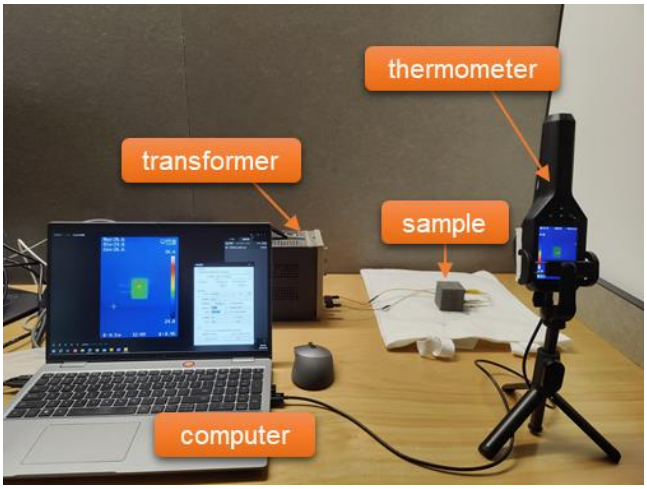

Figure 6.2 Configuration of helf-heating test

6.2.1 **Surface temperature distribution**

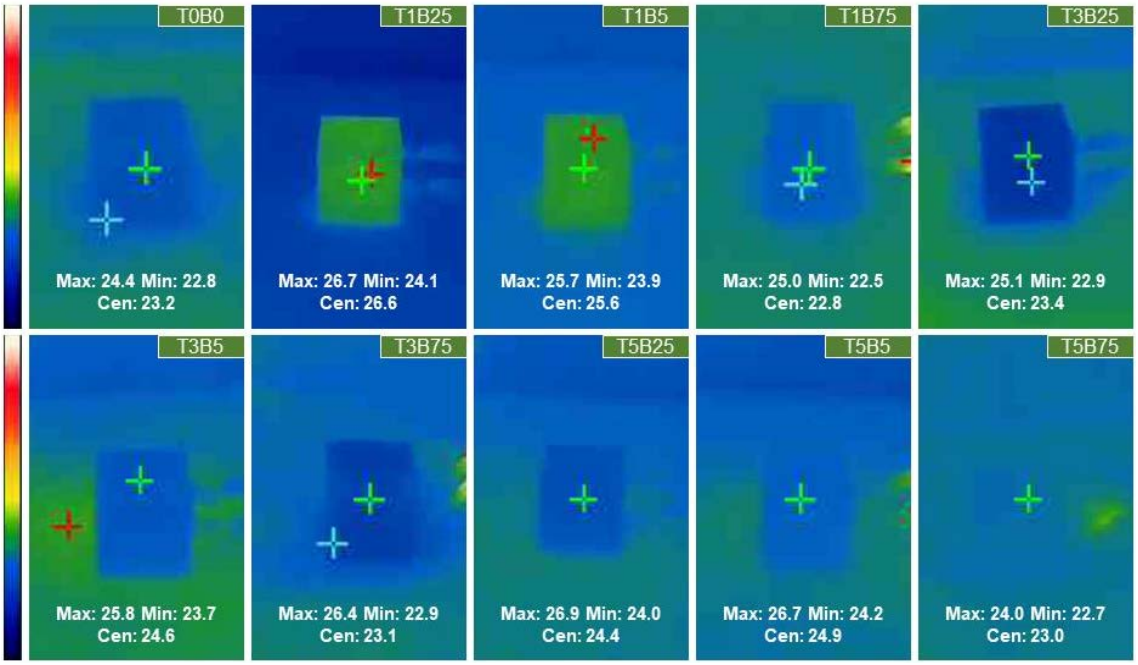

Figure 6.3 Temperature distribution field at 0 min

The original thermal mapping result was upside down because of the method to fix the thermometer as shown in Figure 6.2. All maps shown in this section were manually rotated 90°. The initial temperature distribution was shown in Figure 6.3. The same colour in different maps may presented different temperatures, where the legend with extremum value should be involved. All maps had the same temperature legend that was placed on the left. The two-end temperatures were marked in the map. The "cen" temperature was the central point temperature of the green "+". The maximum temperature point was observed on the insulating cover of electrodes caused by manual operation (e.g., T1B25), which did not affect the temperature distribution of samples. The surface temperature of the samples was close to the environmental temperature. The temperature may rise as shown in Figure 6.4.

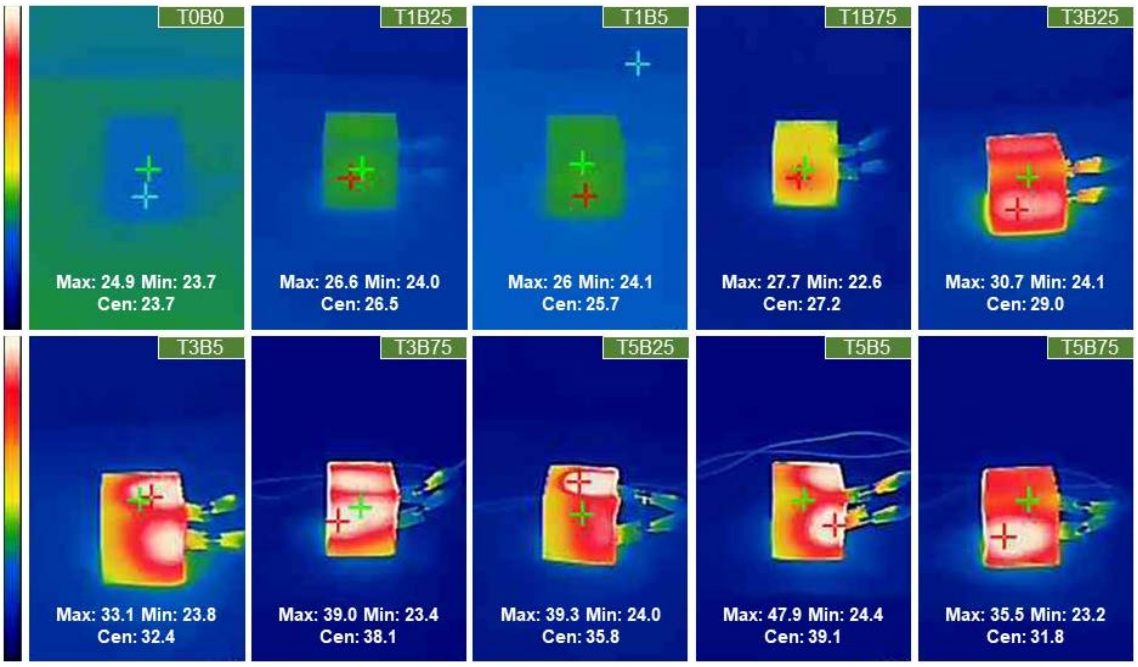

Figure 6.4 Temperature distribution field at 10 min

A temperature hike appeared in Figure 6.4 with different efficiency. Based on the difference with initial conditions, the improvement of T0B0, T1B25, and T1B5 was negligible. The content of additives failed to build a strong electrically conductive path.

The difference was found from T1B75, which can be defined as the threshold. The most area reached over 25 ℃. T3B25 showed similar results with moderately higher temperatures. The temperature distribution of T1B75 and T3B25 was generally uniform because the heating rate was not excellent. With the carbon addition, better heating efficiency was proved when the maximum value was observed in T5B5 (rocketed to 47.9 ℃). The evident temperature gradient occurred from T3B5 to T5B75 with the rough gaps of 5 ℃, 8 ℃, 8 ℃, 12 ℃, 6 ℃, respectively. This rank also agreed with a temperature rise, which both were caused by the various heating rates. The area close to the electrodes was hotter and showed an oval boundary. This was caused by the stronger current near electrodes.

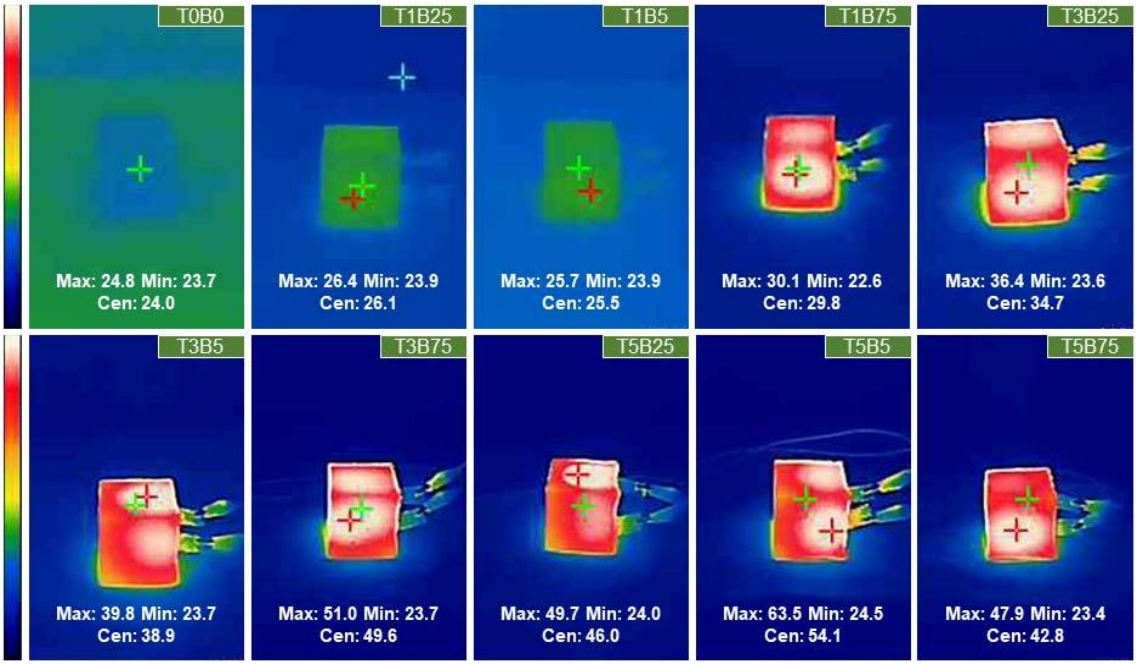

Figure 6.5 Temperature distribution field at 30 min

The temperature rose continuously with time in Figure 6.5. The non-conductive samples presented no change. The uneven temperature distribution appeared on T1B75 and T3B25 with the difference of ~2 ℃ and ~3 ℃, caused by the heat cumulation. The regulation was similar to other conductive samples. From T3B5 to T5B75, the temperature

distribution was maintained but the value was higher. T5B5 was still on the top of the list (maximum value up to 63.5 ℃ and central point reached to 54.1 ℃). In addition, the temperature gradients were relatively decreased compared to Figure 6.4, which declined to around 4 ℃, 7 ℃, 6.5 ℃, 10 ℃ and 6 ℃. Higher maximum temperature still synchronized with higher gradients that wan strongly attributed to heating generation rate. The temperature difference between samples and room became larger with time, according to Fourier's law, which contributed to the faster heat loss.

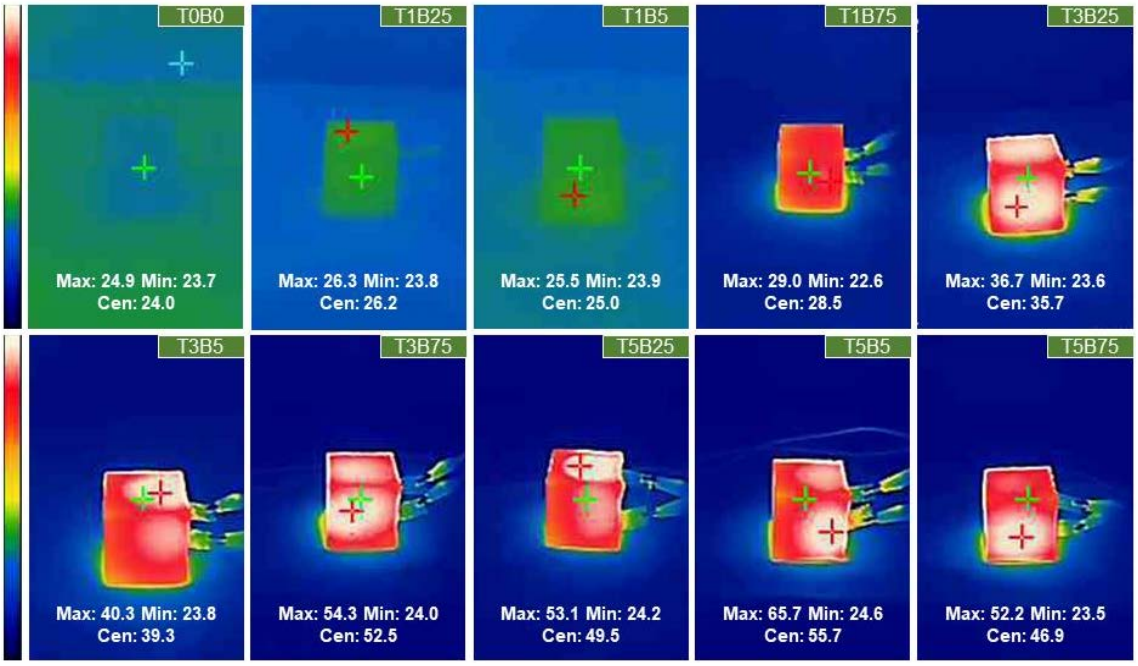

Figure 6.6 Temperature distribution field at 60 min

After one-hour current application, the temperature maps were recorded as shown in Figure 6.6. The current application can not change the conductivity and no self-heating was observed from T0B0 to T1B5. For conductive samples, the increase was weaker especially for T1B75 (even showed minor decrease) and T3B25. The main features of temperature distribution in Figure 6.5 were kept while the T1B75 changed to uniform. Higher temperature still concentrated near the electrodes, where the most heat was generated as explained for Figure 6.4, and the rest area tend to release heat. The similar

temperature distribution was caused by the balance of heat generation and loss. The stable states were approached after one-hour current application, while the temperature gradients were maintained at about 4 ℃, 7 ℃, 7 ℃, 10 ℃ and 6 ℃. The changes compared to Figure 6.5 were very limited. In this case, the results in Figure 6.6 were regarded as the finally stable state, which approached the highest temperature at this experiment.

6.2.2 **Temperature development of the central point in thermal maps**

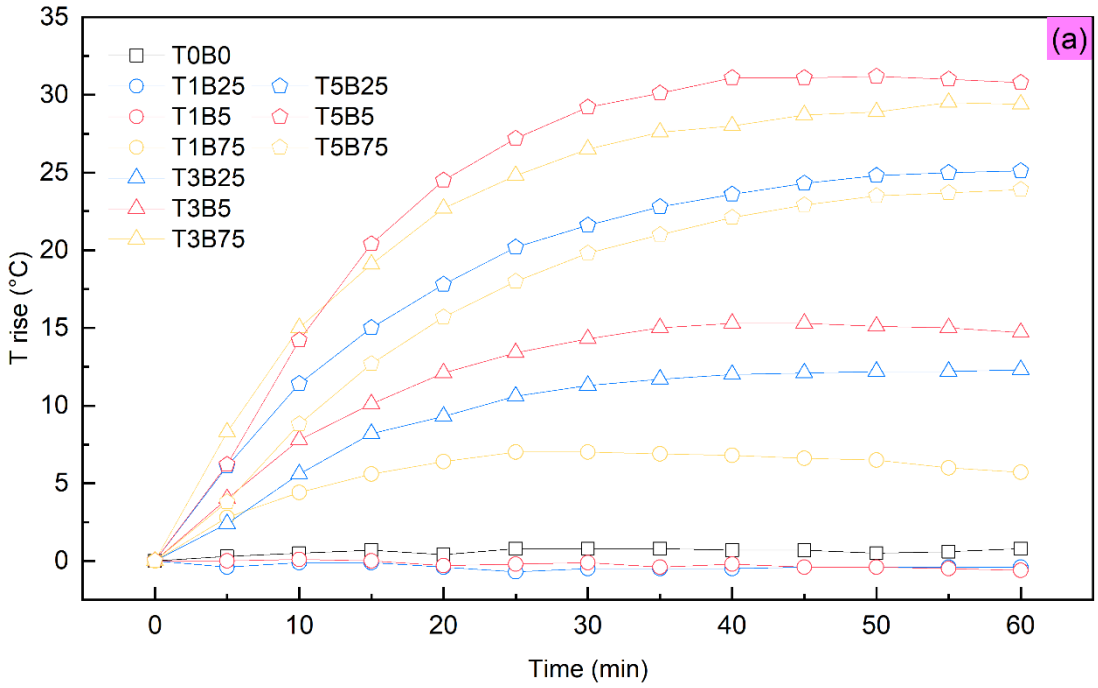

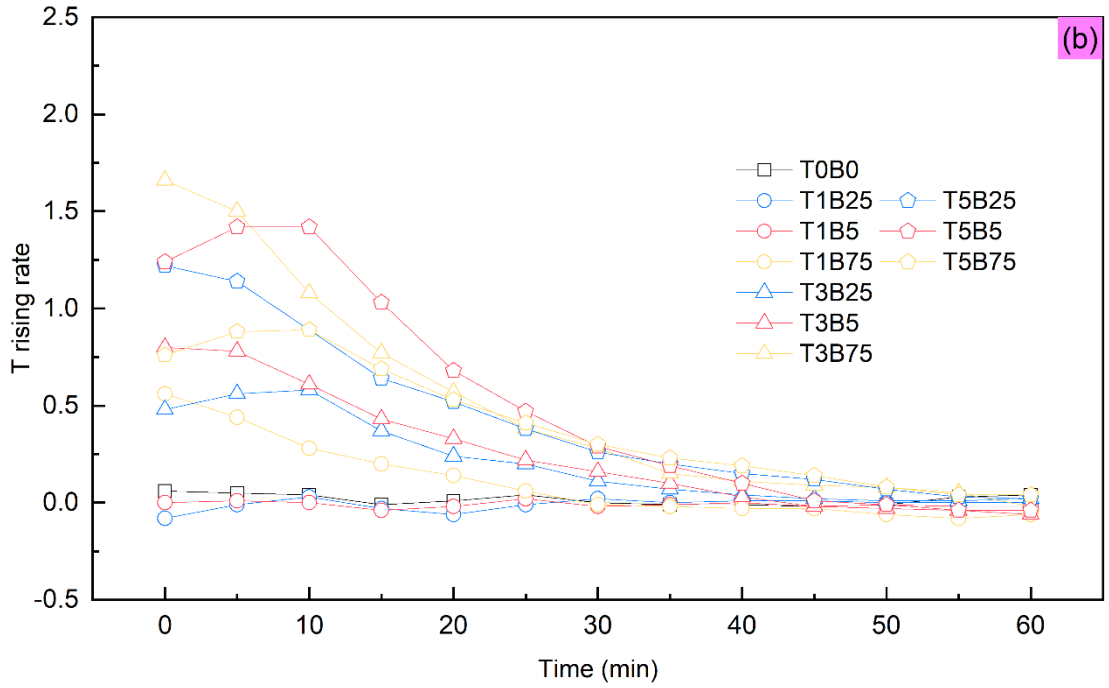

Figure 6.7 Temperature development of central point

To investigate the temperature rise associated with the self-heating function over time, the temperature variation at the central point and its first-order derivative were plotted in Figure 6.7. The difference to the initial temperature was the T increase to eliminate the slightly various room temperatures. According to the results, most samples showed obvious temperature climbing except T0B0, T1B25 and T1B5 where conductive path was not built as explained in Figure 6.4 (Kim et al. 2016). The increasing trend went minor with time but showed different heating results. All samples reached to stable after one hour. Generally, the higher content of carbon additives offered higher temperature. T5B5 presented the highest value and samples with T5 occupied 3 seats of the top 4 samples. T5B75 did not provided the best self-heating performance as expected that was even worse than T5B25. The superfluous nano-additives were prone to cause agglomeration that could hinder a uniform conductive path generation (Li et al. 2022).

The self-heating efficiency was shown in Figure 6.7 (b) by the first-order derivative. The heating rate moderately drop with time although a slight increment was observed in T3B25, T5B5, and T5B75. This exception can be explained by the ionic polarization at the first current application. The value rank at 10 min in Figure 6.7 (b) was in accord with the final value rank in Figure 6.7 (a). T1B75 presented zero increment firstly among conductive samples at 30 min. The rate of T5B5 fell to zero at 45 min that was similar to T3B25 and T3B5 even though the final temperature was much higher. T3B75, T5B25, and T5B75 showed better sustainable self-heating that was prolonged to 55 min.

6.2.3 **Assessment of conductive additives**

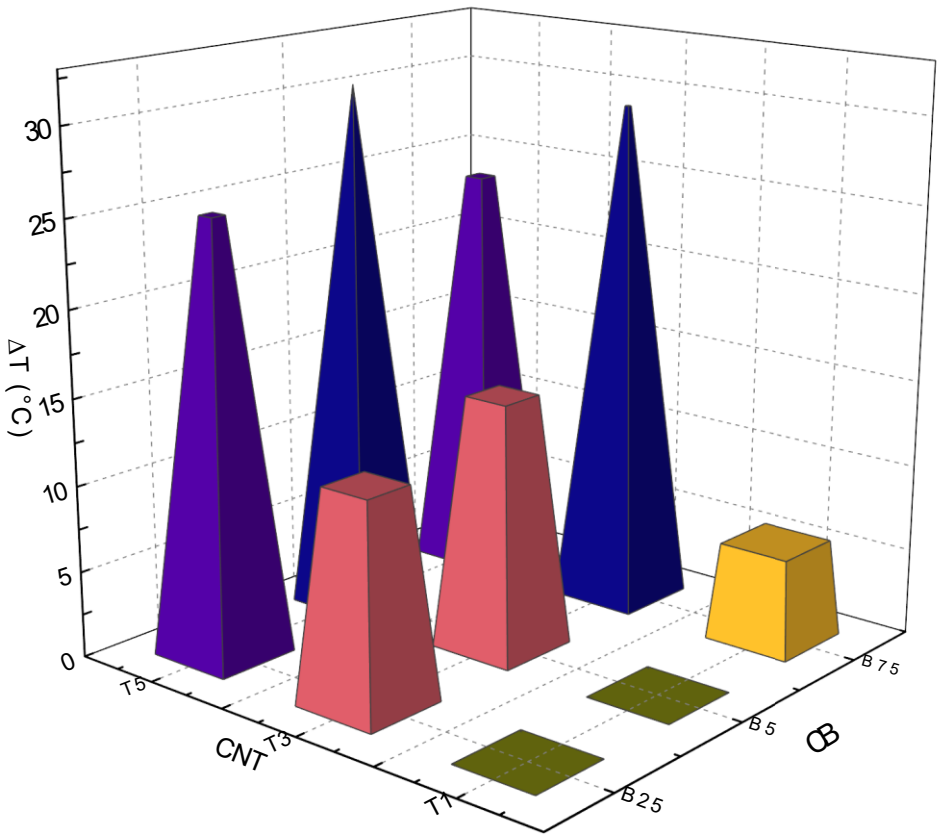

Figure 6.8 One-hour temperature increase amplitude

The expected critical assessment index, maximum temperature increment, was plotted in Figure 6.8. The gap between top 2 sample, T5B5 and T3B75, was negligible. T5B25 and

T5B75 followed the top 2 samples and the decrease was very limited. The advantages of top 4 was very remarkable, which doubled the performance of the rest samples. This work used varying CNT and CB with constant CF. The effectiveness of different additives can not be simply reflected by the maximum temperature increment.

The various material mixing plan influenced the improvement efficiency. To explore the efficiency of different carbon materials, it defined electrical sensitivity of CNT and CB as shown in Eq. (6.1) and Eq. (6.2).

$$S_{CNT} = \Delta T / M_{CNT} \tag{6.1}$$

$$S_{CB} = \Delta T / M_{CB} \tag{6.2}$$

where S_{CNT} and S_{CB} were the electrical sensitivity of CNT and CB, respectively; ΔT was the temperature difference between current and initial value; M_{CNT} and M_{CB} were the content of CNT and CB while this experiment used the 100× mass ratio to cement. For example, M_{CNT} and M_{CB} of T3B25 were 0.3 and 0.25.

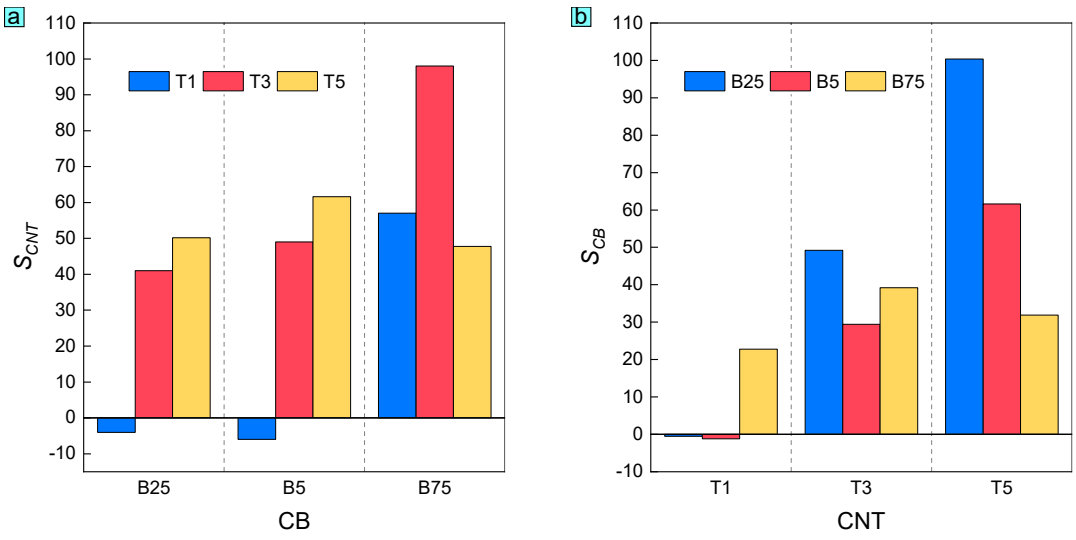

(a) electrical sensitivity of CNT (b) electrical sensitivity of CB

Figure 6.9 Electrical sensitivity of tested carbon materials

The calculated results for sensitivity are shown in Figure 6.9. Roughly, the extremely low content of additives can not reach the threshold to build a conductive path and this conclusion was valid for both CNT and CB. The effectiveness of CNT climbed up with the higher CB from B25 to B5. At the highest value of B75, the threshold of T1 was broken and jumped significantly over 50, but the benefit of T5 was impeded. T3 presented the optimal performance with B75 that reach to around 100. Most powers of CB was covered up with T1, but T3 enabled all samples to show attractive results. The values of B25 and B5 doubled cooperated with T5, while the sensitivity of B75 declined by ~ 25%. Increasing carbon additives raised the possibility of conductive path generation, while redundant nano materials disturbed particle distribution, leading to lower self-heating capability. T3B75 and T5B25 illustrated the optimal efficiency of CNT and CB, respectively.

A higher efficiency enabled less material consumption, less environmental burden, and lower cost. Combined with the result in Figure 6.8, T3B75 offered the second highest temperature, and the gap compared to the highest value was very slight. The performance of T3B75 can be proposed as optimal comprehensively among the groups in this experiment.

6.3 Electrical conductivity

The electrical resistance is a critical factor for the assessment of self-heating concrete. A multimeter with a maximum value of 200 kΩ was used to test the electrical resistance. Probes were connected to the electrodes of the samples. The tests were repeated five times and the average values were taken. Apart from the electrical resistance at room temperature (~23 °C), the samples were heated at 60 °C in an oven for 4 h for the electrical resistance at high temperature. An insulative table and a conductive layer were used to

eliminate interference. All samples were stored in sealed containers, except the experiment was ongoing.

According to Joule's Law, the higher electrical conductivity benefits higher power with the constant voltage. Concrete is typically non-conductor, so enhancing electrical conductivity is decisive, where lower electrical resistance helps better self-heating performance (Lee et al. 2020). The electrical resistance (R) is a crucial factor for the conductivity. The R values at room temperature and 60 ℃ were tested separately and the difference was analysed.

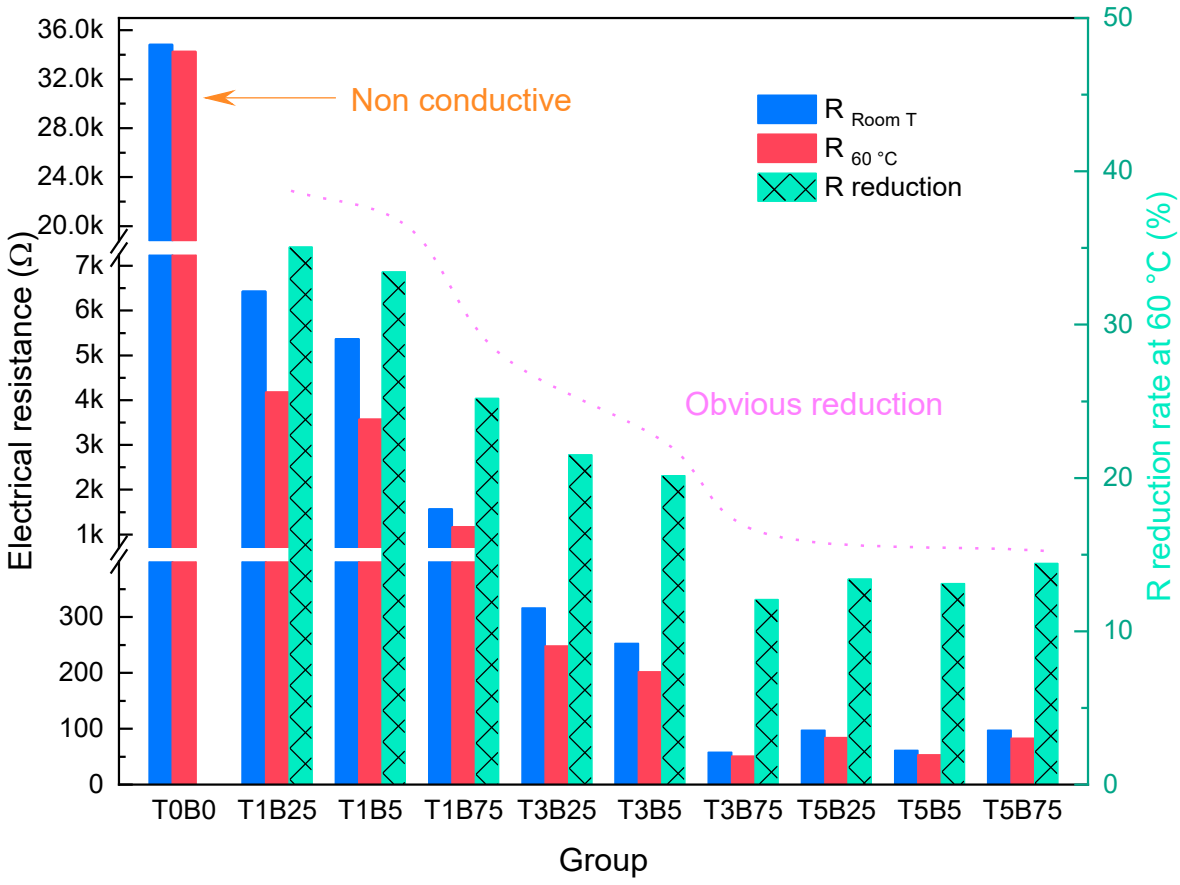

Figure 6.10 Electrical resistance at different temperatures and changes

Normally, the universal mortar was not conductive and temperature shows little effect like T0B0. As shown in Figure 6.10, the electrical resistance decreased obviously with

the help of carbon additives (Wang et al. 2023b). T1B25 and T1B5 became conductive but still did not break the threshold, although the R resistance loss was remarkable. T1B75 was the first sample showing self-heating ability with the R of ~ 1.5 kΩ, which could be regarded as the threshold in this experiment. Next, R of T3B25 and T3B5 dropped to around 250 Ω leading to the double temperature increment in Figure 6.8. With the further additive of T3B75, the R fell continuously. However, the R of T5 groups presented a relatively steady value. Compared with Figure 6.8, the temperature increment and R had similar regulation and a great relationship. The samples can be classified into 5 factions: non-conductive (T0B0), conductive but no self-heating (T1B25 and T1B5), threshold for self-heating (T1B75), self-heating with progress room (T3B25 and T3B5), and self-heating close to ceiling (T3B75, T5B25, T5B5 and T5B75).

It is noticeable that all samples (except non-conductive T0B0) illustrate R reduction from the room at a higher temperature, which is attributed to the PCM state change. The PCM changed from solid to liquid state with temperature increasing, where the inorganic hydrated salt was selected in this experiment. In the liquid state, the PCM composite contained free ions, and the ionic liquid improved the electrical conductivity. As shown in Figure 6.10, the R reduction of T1B25 was lower than 35% while it went down with more carbon additives. The benefit of PCM change on electrical conductivity was constant. Compared with significantly rising electrical conductivity caused by carbon additives, the advantage of PCM was relatively minor. With higher additive content, R reduction rate declined to 20% for T3B5. Then, it showed fluctuation with a slight amplitude that was similar to the fluctuation of electrical conductivity. In summary, the melted inorganic hydrated salt is able to enhance the electrical conductivity but the effectiveness is limited, especially for the samples with great self-heating performance. This result was contributed to the feature of selected PCM. In another case, the paraffin-

based PCM plays an adverse role in electrical conductivity improvement (Jang et al. 2023), which illustrates the compatibility of PCM deserves much attention in future research.

6.4 Electrical impedance

6.4.1 **Methodology**

Alternating current impedance spectroscopy is proposed to investigate the microstructure and conductive behaviours of cement-based materials, which is non-destructive and effective (Wang et al. 2023b). Two probe methods were adopted considering their reliability and accuracy. The tests were performed at room temperature (23 ℃) and temperature above the phase change point of PCM (60 ℃). For the test at 60 ℃, the specimens were placed in a 60 ℃ oven for 3 hours and then tested immediately. The data was tested via AMETEK 1260A Impedance/Gain-Phase Analyzer, which had a wide frequency range from 32 MHz to 10 μHz with 0.015 ppm resolution as shown in Figure 6.11. The obtained spectrum results were analysed according to the equivalent circuit method using ZView software.

Figure 6.11 AMETEK 1260A Impedance/Gain-Phase Analyzer

6.4.2 **Impedance spectroscopy**

Figure 6.12 presents the Nyquist plots of various groups. The plot of a plain PCM-filled sample (T0B0) contains a single high-frequency arc and low-frequency arc, while the plots of other samples with carbon additives contain two high-frequency arcs and one low-frequency cycle, which is consistent with the typical plot characteristics of conductive cement-based composites. A partial high-frequency arc is not visible since the testing frequency is limited to 10 MHz. The high-frequency arcs are influenced by the conductive phase and matrix structure of the composites, and the low-frequency arc is related to the electrochemical behaviour of the electrode-specimen interface. Meanwhile, the arc diameter, the intersection of the high-frequency arc and electrode arc (corresponding to DC resistance) are incrementally decreased with the increasing contents of CNT or CB, which partially validate the obtained impedance spectrum.

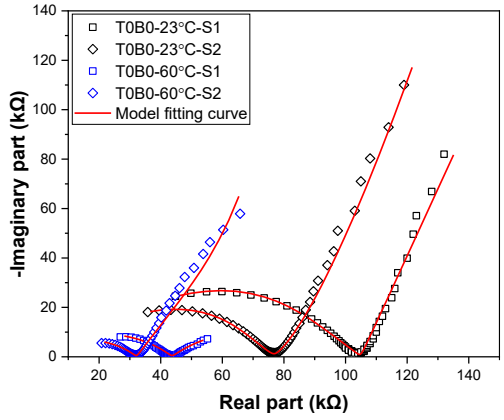

(a) T0B0

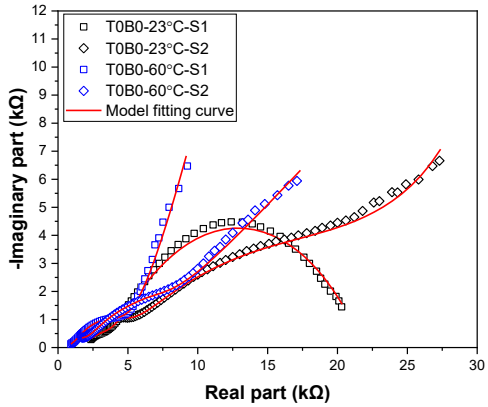

(b) T1B25

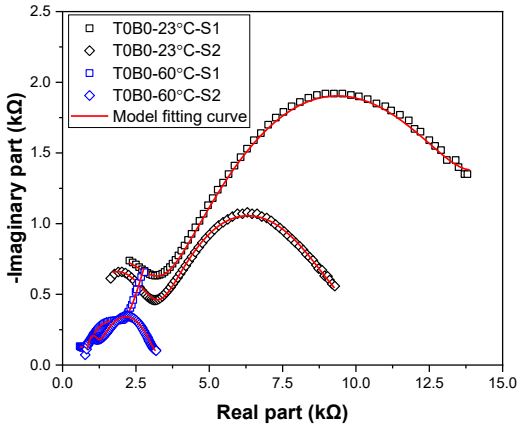

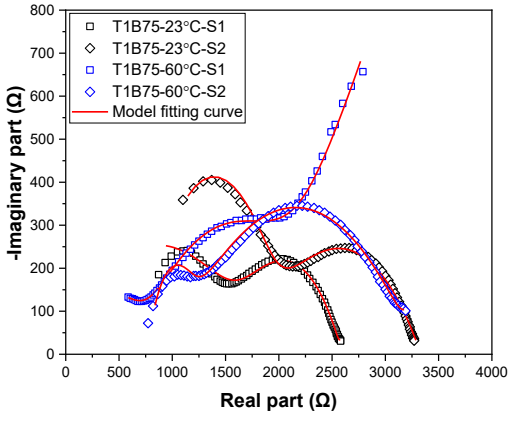

(c) T1B5

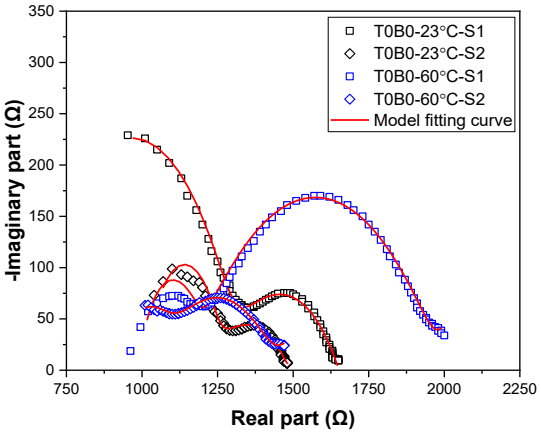

(d) T1B75

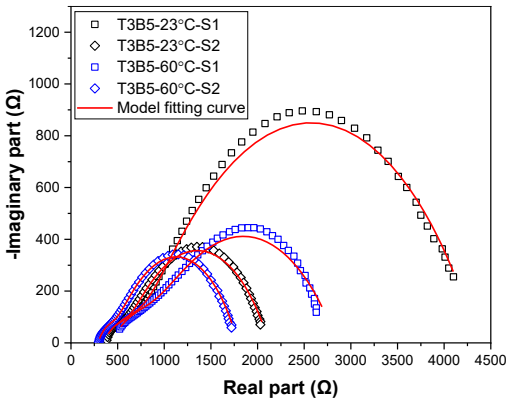

(e) T3B25

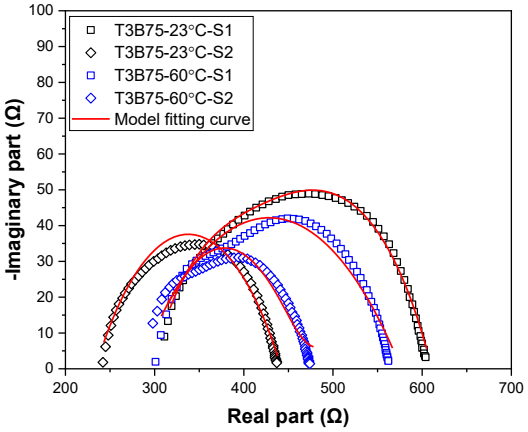

(f) T3B5

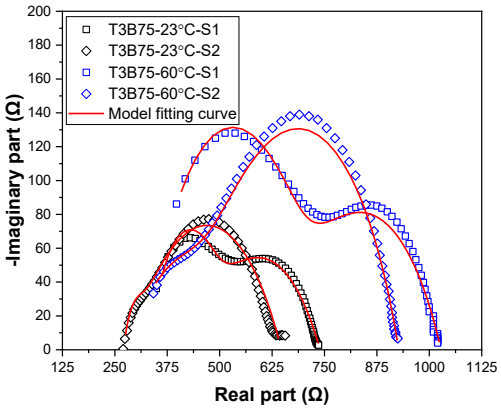

(g) T3B75

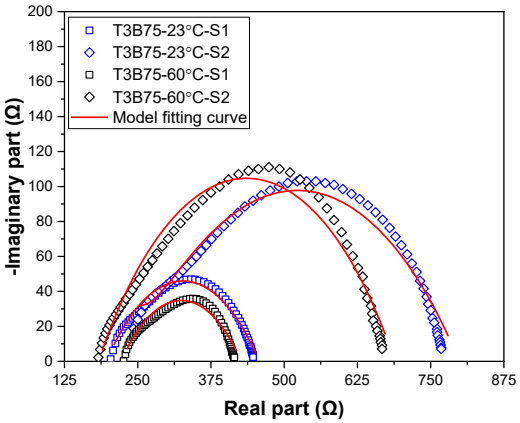

(h) T5B25

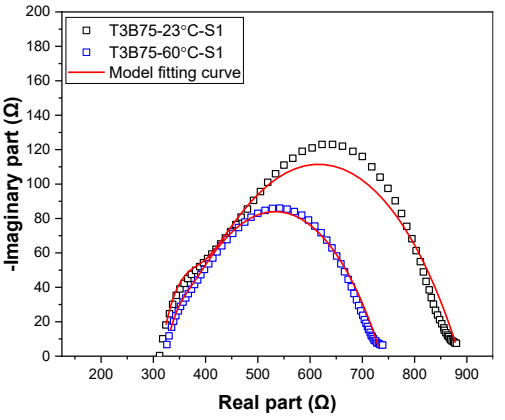

(i) T5B5

(j) T5B75

Figure 6.12 Nyquist plots of the specimens

It is seen that Nyquist plots are significantly influenced by the temperature. It has been proposed that the temperature has a complex influence on the electrical resistivity of the conductive cement-based composites through the charge carrier mobility, concentration,

and intrinsic resistivity of the conductive fillers (Qin et al. 2024). On the one hand, the increase in temperature leads to an enhancement in carrier transport current due to hole conduction (Wang et al. 2020). On the other hand, the electrical properties of a cement composite are altered as a consequence of the difference in the thermal expansion coefficients between the conductive filler and the cement matrix (Kim et al. 2017). It has been reported the thermal expansion coefficient of cement is ten times higher than that of CNT (Sellevold & Bjøntegaard 2006). It is noticeable that the impedance measurement was conducted on dried specimens to avoid the effect of free water; thus, the ionic conduction from pore solution contributed by free water is significantly eliminated. In this sense, the ionic conductivity contributed by the molten PCM under the temperature of 60 ℃ either above (60℃) or below (23℃) could be easily differentiated.

6.4.3 **Establishment of equivalent circuit**

Referring to previous studies, the plain and conductive cementitious composites can be modelled with equivalent circuits of Q(RW)(Q(RW)) and Q(RW)(QR)(Q(RW)), respectively. The corresponding equivalent circuit elements and their associated physical meanings are illustrated in Figure 6.13.

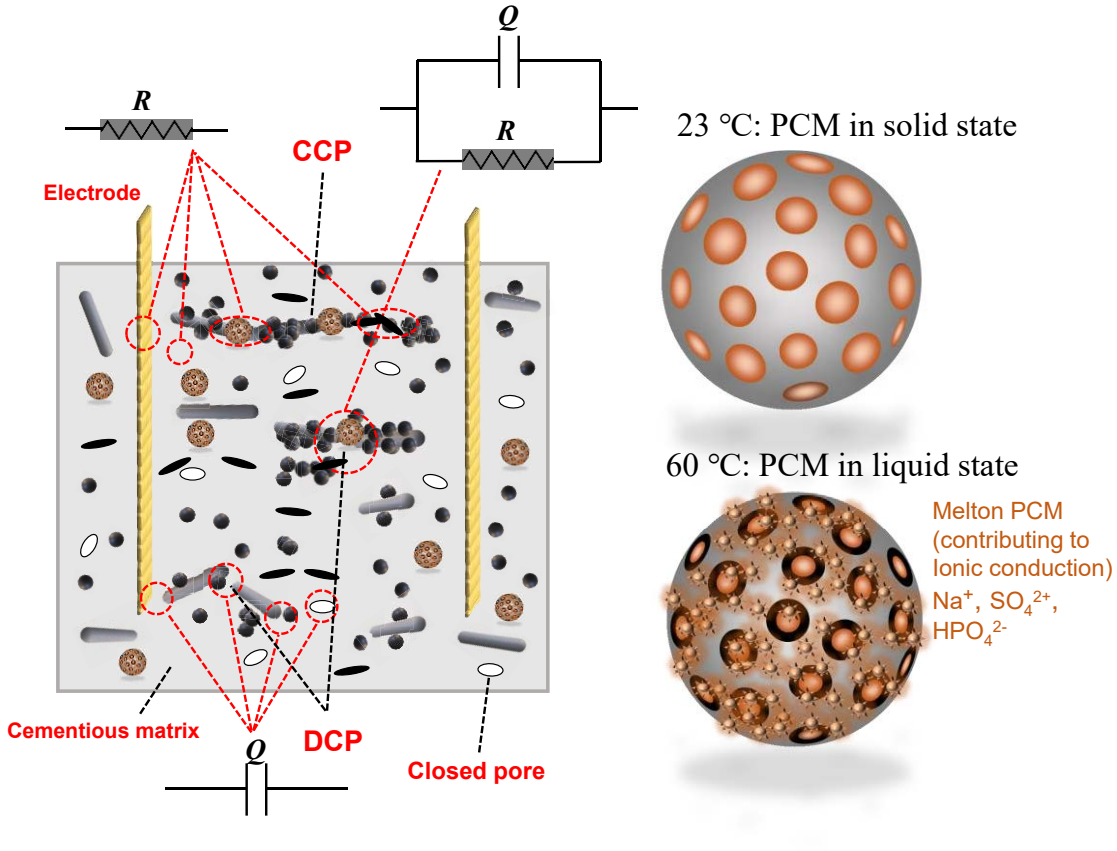

Figure 6.13 Equivalent circuit elements and physical meanings.

In general, the continuous conductive paths (CCP) are comprised of connected conductive elements, including connected conductive fillers and connected pores filled with pore solution, which act as resistance in the circuit. Differently, the discontinuous conductive paths (DCP) are comprised of disconnected conductive fillers, and closed pores can be regarded as capacitances. In addition, the clumps of conductive fillers can be represented by a RCR circuit element, the resistance and capacitance conducted in series and in parallel. As a consequence of the complex nature of pores, such as size, shape, moisture level, pore structure, etc, their time-constant response to various frequency ranges shows the discrepancy. Thus, pores cannot be regarded as a pure capacitor but instead as the constant phase elements (CPE, expressed by Q). The impedance of CPE is illustrated in Eq. (6-1)

$$Z_Q = \frac{1}{Y_0 \omega^n}(\cos\frac{n\pi}{2} - j\sin\frac{n\pi}{2}) \tag{6-1}$$

where Z_Q denotes the impedance (Ω); j is the imaginary unit; ω denotes the angular frequency (rad/s); Y_0 denotes the admittance; n is the parameter of CPE (CPE acts as a pure capacitor when n=1; CPE acts as a pure resistor when n=0).

The formula for the total impedance of circuit model Q(RW)(QR)(Q(RW)) is illustrated in Eq. (6-2).

$$\begin{aligned} Z &= \frac{1}{\frac{1}{Z_{Q_1}} + \frac{1}{Z_{R_{ct1}} + Z_{W_1}}} + \frac{1}{\frac{1}{Z_{Q_N}} + \frac{1}{Z_{R_N}}} + \frac{1}{\frac{1}{Z_{Q_2}} + \frac{1}{Z_{R_{ct2}} + Z_{W_2}}} \\ &= \frac{Z_{Q_1}(Z_{R_{ct1}} + Z_{W_1})}{Z_{R_{ct1}} + Z_{W_1} + Z_{Q_1}} + \frac{Z_{Q_N} \times Z_{R_N}}{Z_{Q_N} + Z_{R_N}} + \frac{Z_{Q_2}(Z_{R_{ct2}} + Z_{W_2})}{Z_{R_{ct2}} + Z_{W_2} + Z_{Q_2}} \end{aligned} \tag{6-2}$$

where Q_N represents the constant phase element of conductive fillers (CB, CNT, CF); R_N represents the resistance of the CCP comprised of connected conductive fillers; R_{ct1} and R_{ct2} denote the electron transfer resistance in the cement matrix (mainly contributed by DCP) and the surface of electrodes, respectively; Q_1 denotes the constant phase element in the cement matrix; Q_2 denotes the constant phase element between the cement/conductive fillers and the electrodes; W_1 and W_2 are the Warburg resistance triggered by the electron diffusion in the cement pastes and the electrodes, respectively. The impedance formulas of W_1 and W_2 are displayed in Eqs (6-3) and (6-4).

$$Z_{W_1} = \frac{\sigma_1}{\sqrt{\omega}} - j\frac{\sigma_2}{\sqrt{\omega}} \tag{6-3}$$

$$Z_{W_2} = \frac{\sigma_2}{\sqrt{\omega}} - j\frac{\sigma_2}{\sqrt{\omega}} \tag{6-4}$$

Specific to this study, the electrical role of SSPCM is temperature-dependent. The PCM adopted in this study is eutectic hydrated salt and possesses a melting point of approximately 28℃. With the temperature increasing from 23℃ to 60℃, the PCM transferred from solid to liquid state; there are free ions, including Na^{+}, SO_4^{2+}, and HPO_4^{2-} absorbed on the surface of open porosity. In addition, there is inevitably leakage of a minor quantity of PCM. The movement of these free ions surrounding the EP contributes to the ionic conduction, making it partially conductive. In other words, the inorganic hydrated salt PCM-impregnated EP alters to a 'semi-conductive aggregate' under 60 ℃. Plenty of 'semi-conductive aggregate' broadly distributed in the cement matrix may act as conductive components contributing to either CCP or DCP (Lu et al. 2023).

6.4.4 **Analysis of circuit parameters**

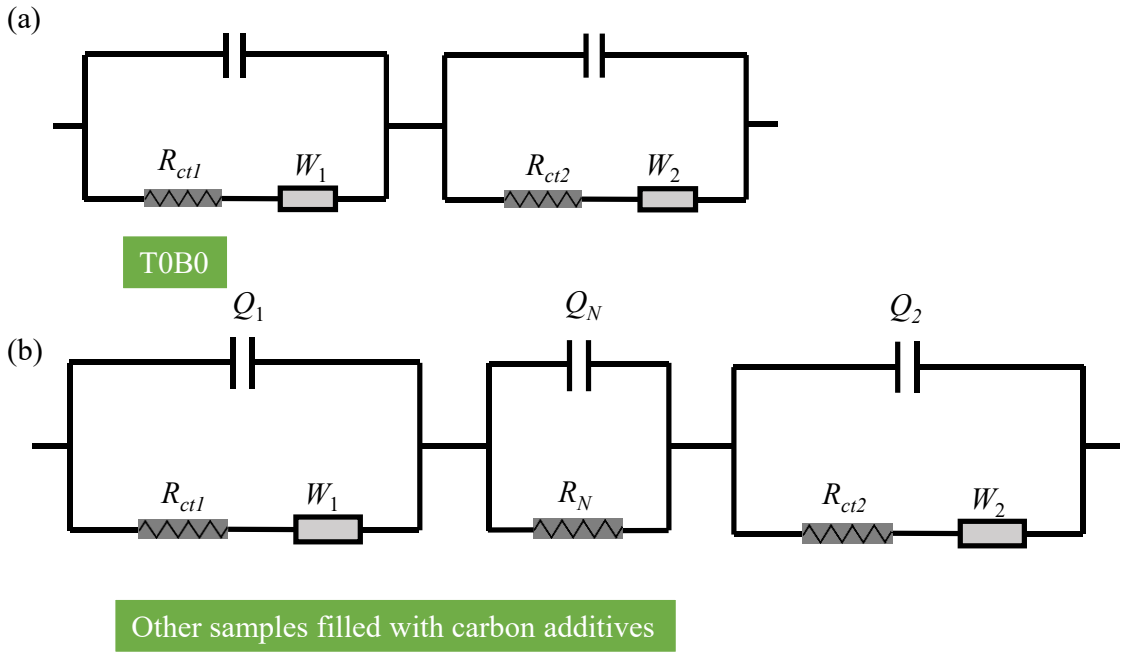

Figure 6.14 Equivalent circuit models for specimens

The fitting curves of the proposed equivalent model are illustrated in Figure 6.14. To analyse the influence mechanism of PCM on the electrical behaviour of multiple carbon additives filled mortar, the variations of two essential parameters R_N and R_{ct1}, which stand

for CCP and DCP, respectively. are illustrated Figure 6.15. With respect to plain group T0B0, there is a significant drop in R_1 by approximately 47.1% when ambient increasing from 23℃ to 60 ℃. Since free water is eliminated in the specimens, the drop in R_1 is deduced to be mainly contributed by the SSPCM as semi-conductive aggregates in liquid state, which should validate the positive role of PCM in the liquated state in enhancing the conductivity of SSPCM. This hypothesis is further supported by the obvious drops in both R_N and R_{ct1} for the groups T1B25 and T1B5 where the CNT and CB contents are relatively low. In these cases, the thermal expansion coefficient contributed to the limited effect on the electrical conductivity because of the less presence of conductive paths that are marginally distributed in the matrix. As a consequence, the role of 'conductive' SSPCM in enriching the conductive passages is pronounced, actively contributing to the increase of both DCP and CCP, which shows a good agreement with simultaneous drops in R_N and R_{ct1} for the groups T1B25 and T1B5. On the contrary, it is seen that R_N under 60 ℃ is higher than that under 23 ℃ as the increases of CB and CNT contents, which is detected in the groups of T1B75, T3B5, and T5B75.

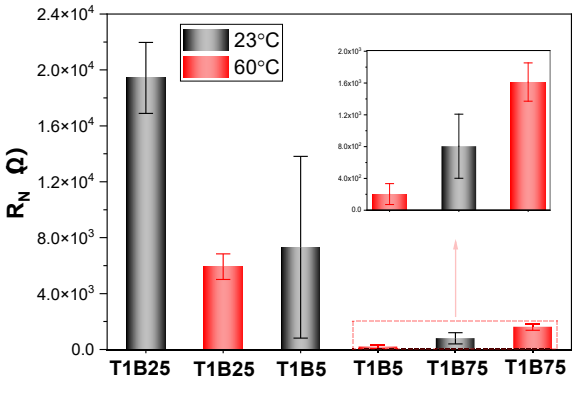

(a) R_N variation of T1 groups

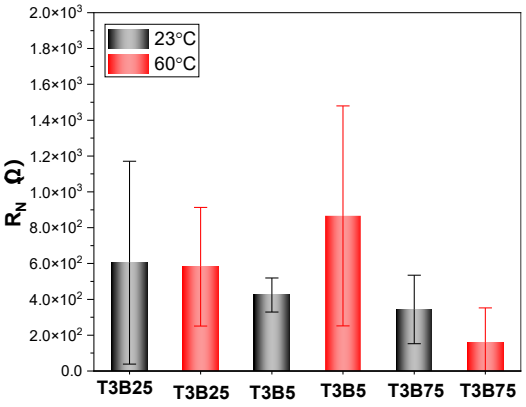

(a) R_N variation of T3 groups

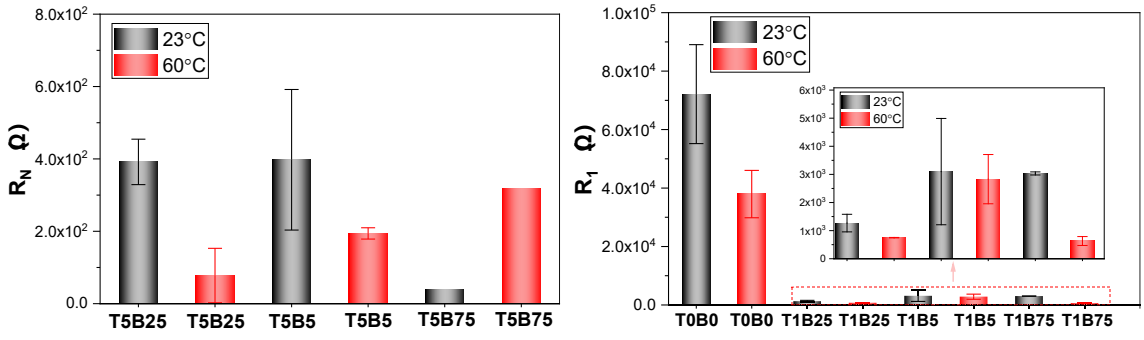

(c) R_N variation of T5 groups (e) R_{ct1} variation of T0B0 sample and T1 groups

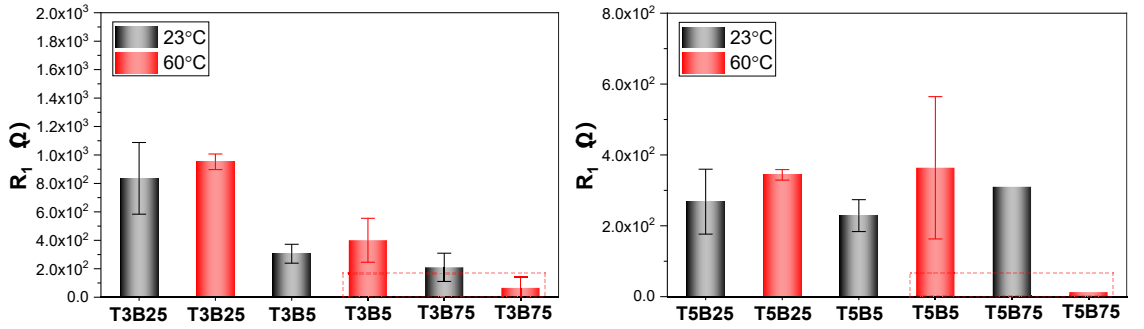

(a) R_{ct1} variation of T3 groups (a) R_{ct1} variation of T3 groups

Figure 6.15 Variations of R_N and R_{ct1}

In these cases, due to the presence of rich conductive paths, the thermal expansion effect enlarges the potential barrier between adjacent fillers, thus impairing the continuity of conductive paths and leading to a positive temperature coefficient effect (PTC, the resistivity increases with increasing temperature). There are several exceptions including T3B75, T5B5 and T5B75, wherein a significant drop in R_N was observed. Previous studies (Kim et al. 2017; Kim et al. 2016; Yoon et al. 2024) proposed that the occurrence of the PTC effect required the degree of thermal expansion to reach a certain level (Kim et al. 2017; Kim et al. 2016; Yoon et al. 2024), the thermal treatment of the present study (stored in 60 ℃ oven for 3hrs) should fulfil such thermal expansion degree. In comparison to R_N, R_{ct1} is less varied for these groups from 23℃ to 60℃. This suggests that thermal expansion mainly contributed to the reduction in length and continuity of CCP rather than the DCP. The value R_N under 60 ℃ is significantly higher than that under 23 ℃ for the composites with higher content of CNT or CB (T5 and B75 cluster groups), which is in

compliance with the fact that the thermal expansion poses a more pronounced impact on CCP when abundant conductive paths are presented. Interestingly, for all B75 cluster groups, accompanied by the fact that R_N is significantly increased, R_{ct1} is significantly reduced when temperature increases from 23℃ to 60 ℃, revealing the significant increase in length and continuity of DCP. Studies (Dong et al. 2020b; Gu et al. 2024; Li et al. 2024; Zhang et al. 2022) proposed that loose and porous CB particles and their agglomerations are prone to absorb part of the free water in the cementitious matrix, which hindered the hydration process, thus resulting in an increase in porosity and reduced compactness in the cementitious matrix. Consequently, it is induced that the porous matrix is more prone to thermal expansion.

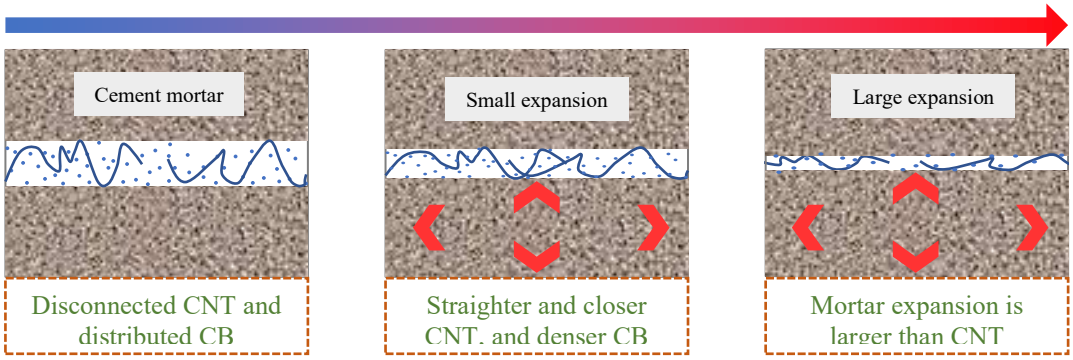

Figure 6.16 Effect of thermal expansion on conductive paths

Yoon et al. (2024) proposed that the physicochemical structure of the cement matrix, such as the generation of additional pores, expedited the PTC effect of conductive cementitious composite, as shown in Figure 6.16. The pronounced thermal expansion of cement not only increases the discontinuity of CCP but also contributes to the increase in the number and length of DCP. For other groups, the variation of R_{ct1} is milder, evidencing less interference of DCP from the thermal expansion effect due to a more compact matrix. The significant variations of R_N and R_{ct1} in B75 cluster groups imply substantial alterations of both CCP and DCP in the composite, showing the presence of a high content

of CB can lead to significant temperature-dependent electrical characteristics of the composite. The temperature-dependent electrical behaviour is not ideal for the multifunctional cementitious composite, and thus, limiting the CB content is important.

6.4.5 **Linkage to self-heating performance**

The foregoing analysis indicates that the substantial CCP has been disconnected and evolved to DCP when temperature increases from 23℃ to 60℃, and this effect initiates at the phase change point (28 ℃). This could interpret the fact that although the conductivity of T5B75 is comparable to T5B25, T5B5 and T3B75. T5B75 exhibits obviously inferior self-heating performance compared to them. Conversely, T3B75, T5B25 and T5B5 manifest a significant drop in R_N and a margin increase in R_{ct1} when temperature increases from 23℃ to 60℃, implying that the amelioration effect of the increase in CCP initiating at the phase change point (28 ℃), which is well aligned with the superior heating performance of T5B25 against T5B5 and T5B5 against T5B75. The good coincidence between the analytic results induced from the equivalent circuit model and macro self-heating performance should prove the validity of the proposed model.

6.5 Characterisation of mortar

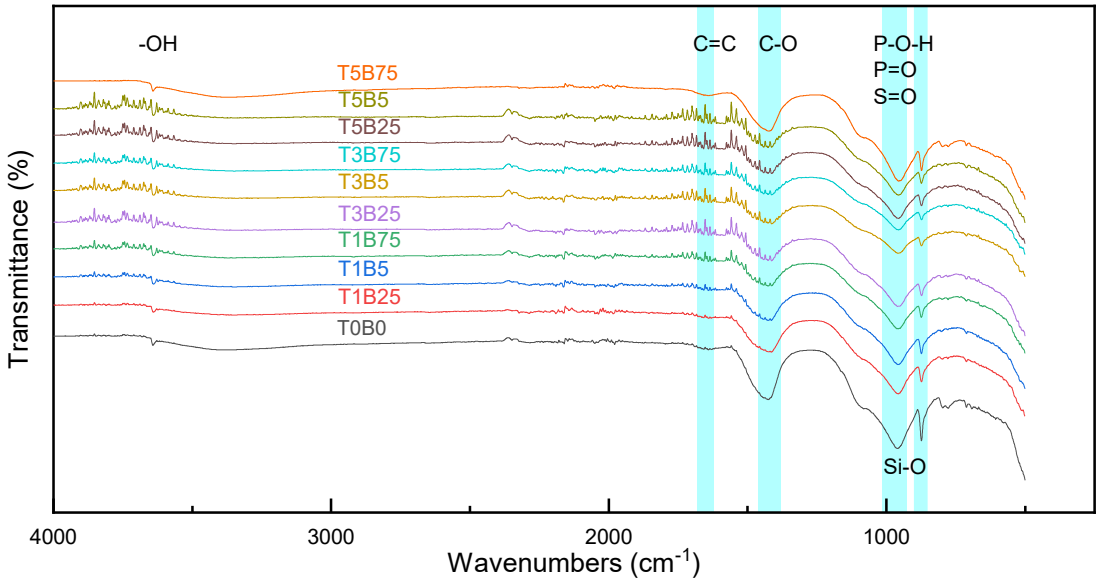

Figure 6.17 FTIR for samples after 28-day curing

The chemical component is illustrated in Figure 6.17. The expected peaks for cement hydration products are found such as Si-O. Compared with reference group T0B0, all samples have similar FTIR spectrum model. The small number of additives reduces the noise, but superfluous additives increase it again to a worse state. The main peaks are observed, and there is no new peak. It is generally concluded that the modification of PCM and carbon additives do not change the chemical components of the designed mortar.

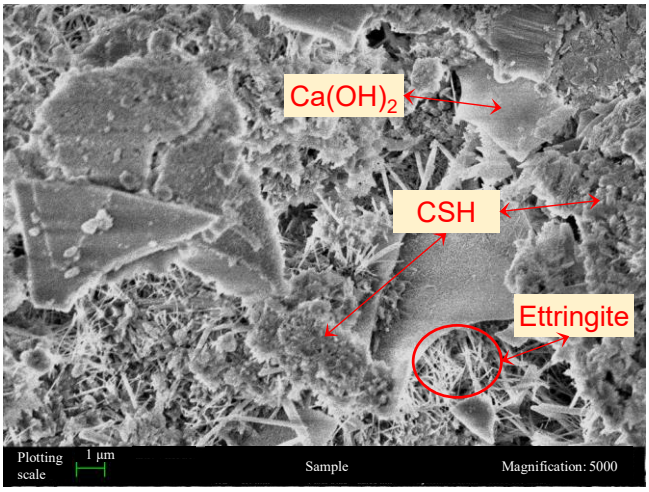

Figure 6.18 T0B0 without additives

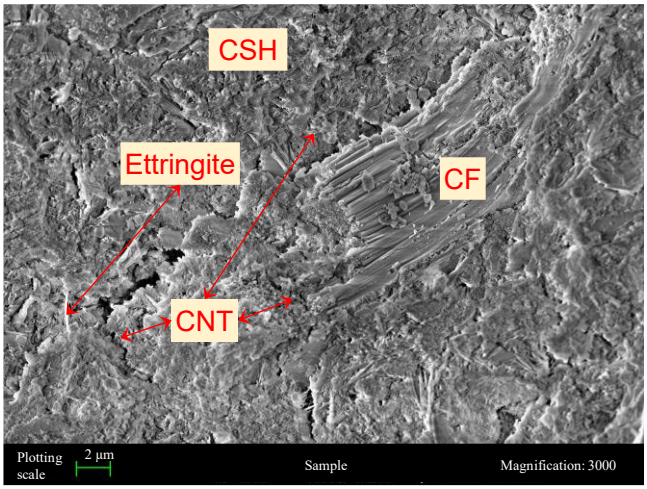

Figure 6.19 T1B5 with additives

Same with universal cement-based material, CSH, portlandite, and ettringite are found in Figure 6.18 that are stacked or connected. These materials have very high electrical resistance. A lot of pores and cracks are obvious that aggravate the bad electrical conduction. With the carbon additive, the conductive path is possible. As shown in Figure 6.19, CF is huge enough to bridge cracks to eliminate the adverse influence of pores and cracks. Nano scale additives are distributed in cement paste to enhance the electrical conductivity of cement paste. Cementitious products wrap CF, providing much contact area, which enables the establishment of whole conductive samples. The higher proportion of additives offers a higher possibility of a long conductive path, which is effective in electrical circuits and electrical networks.

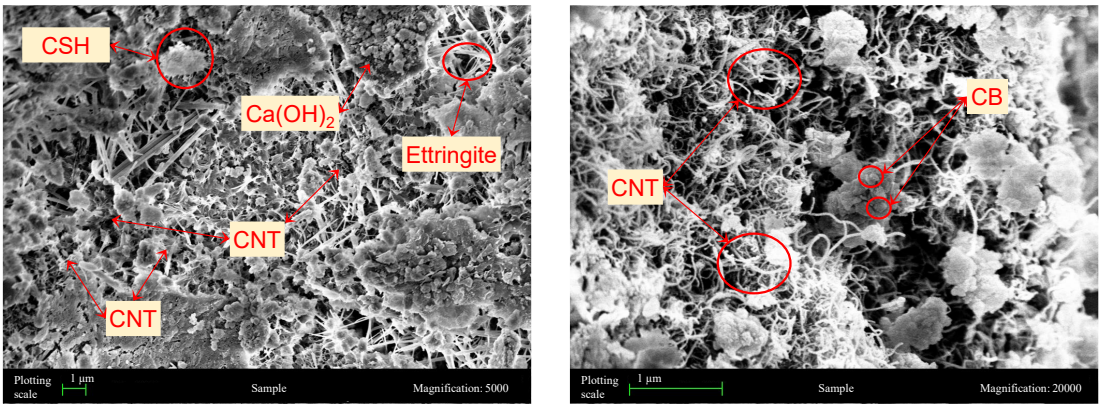

Figure 6.20 Microstructure of T3B75 with well-distributed additives

With the increasing content of conductive additives, stronger electrical conduction is achieved. As shown in Figure 6.20, CNT is integrated with various hydration products, including CSH, portlandite, and ettringite. The well-distributed CNT plays a significant role in changing the cement matrix from non-conductive to conductive. At a high magnification of 20k, a cluster of CNT is remarkable and CB is scattered. CB is found on the surface of small CSH, providing a large conductive surface connected with CNT, which benefits the building of an electrical network. At the same time, CB and CNT are engaged with CSH in different ways like wrapping, adhering and connecting. The mixed coexist formation allows conductive additives to improve the electrical properties of cement matrix from multi-scale. The cement matrix is the critical part of integrating all components like aggregate and fibre. Therefore, the enhancement of the cement matrix contributed by nano-additives is significant for the comprehensive performance, in addition to the millimetre additives like carbon fibre.

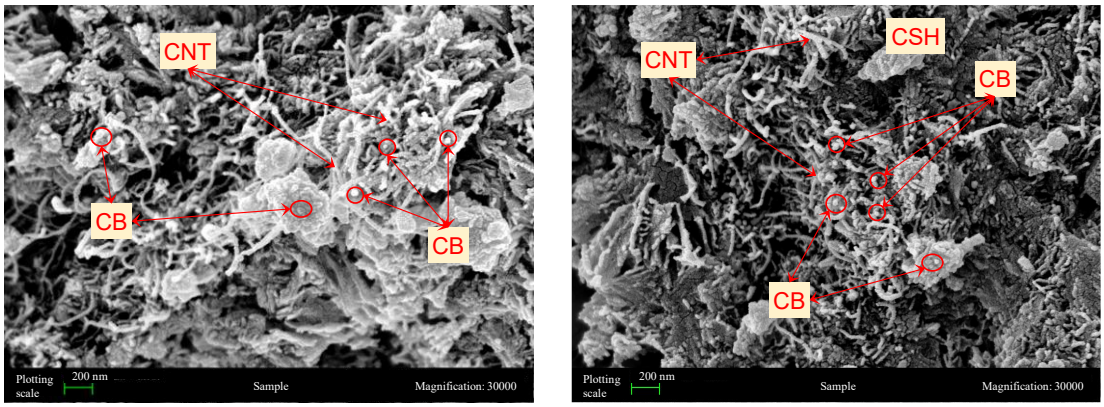

Figure 6.21 Microstructure of T5B5 showing additive agglomeration

The advantages of nano-additives have been proven, but it is hard to achieve optimal results because the operation and control are difficult. As shown in Figure 6.21, additives are obvious. At a large magnification of 30k, the uneven distribution is clear. CNT is prone to be agglomerated as a large group, and rich CB is scattered at every spot. The imperfect dispersion of raw materials is one reason. In addition, the electric charge and the interaction force of the large surface aggravated the agglomeration level. Hydration product, like CSH, still shows a stable connection with additives. Although the CSH with rich additives has excellent electrical conductivity, the whole electrical network is broken. The benefit of CNT length is restricted leading to less conductive connection. The self-heating ability relies on the whole electrical circuit that is restrained. On the other hand, agglomeration mainly affects CNT morphology, stretch, and distribution. This defect presents little influence on CB, but is still effective in enhancing the electrical properties of hydration products. CNT and CB should cooperate in optimal content.

6.6 Summary

This paper designs a self-heating mortar with PCM then investigating the influence and reasons. This multifunctional mortar has the heat generation and storage abilities in same time. Various carbon additives are incorporated to enhance the functions. This work

provides significant result to develop an energy-effective building material for near zero energy building. Many important conclusions are given as followings:

(a) Universal mortar is not electrically conductive while carbon additives can significantly enhance it to achieve self-heating performance. In this experiment, T3B75 and T5B5 have best electrical conductivity with the same content of CF, when the optimal result research to around 50 Ω. The drop of electrical resistance is remarkable over 80% even for the sample with lowest additives. The reduced electrical resistance is closely related with improved self-heating efficiency. T3B75 – T5B75 have the top four electrical conductivity and temperature increment.

(b) In this experiment, it is regarded as threshold. T1B25 and T1B5 do not show any increasing temperature although their electrical resistance declines significantly of ~ 80% than T0B0. The currency of them is not enough to generate thermal energy and captured by the mortar. T1B75 has an obvious self-heating performance with lowest additives that shows the temperature increment lower than 5 ℃. The increment keeps uptrend with additives for most samples but redundant additives pose adverse influence. T5B5 presents the best enhancement over 30 ℃ followed by T3B75 with minor gap. T3B75 is proposed as the optimal sample because the price and operation of CB is better.

(c) The sensitivity of CB and CNT is different and mutually affecting. In most samples, the higher content of one material will benefit the effectiveness of the other material. The optimal sensitivity of CB is incorporated with B75 and CNT counterpart occurs with T5. In proposed sample T3B75, full power of CNT is used and significant advantage of CB is used.

(d) Considering the electrical conductivity and SEM results, CF can bridge most cracks and porous while CB and CNT modify the micro properties. Although both nano additives improve the electrical conductivity, CNT has better connection performance

due to its larger asp ratio. CB is prone to incorporated (wrap and attach) with hydration product. CB contributes brilliant electrical conductivity to cement matrix and CNT has additional ability to build stable electrical network.

(e) At the temperature over the melting point of PCM, the electrical conductivity is increased with various rate. With higher content carbon additives, the improvement effectiveness caused by PCM is weaker. However, the lowest improving rate still access 10%. Melted PCM is rich ion solution in this experiment that provides free ion for electron transmission. This benefit improves the electrical properties of aggregates directly then leading to the enhancement on whole sample performance.

(f) A novel Q(RW)(QR)(Q(RW)) equivalent circuit model is proposed to understand the electrical behaviours during the self-heating process, which is validated based on the good fitting degree and analysis of variations model parameters. The analytic results deduced from latter shows an excellent coincidence with macro self-heating performance. Overall, the novel circuit model not only provide a new insight into the material design of multifunctional cement-based materials, but also highlight the importance of PCM in affecting the electrical paths during the self-heating process if the phase change point within such range.

CHAPTER 7. CONCLUSION AND RECOMMENDATION

7.1 Conclusions

In conclusion, while phase change material (PCM) concrete holds considerable potential for widespread application in practical engineering projects, it requires further development and refinement to become more viable. This study contributes significantly to advancing PCM concrete by addressing key aspects from composite fabrication to application, as well as potential function.

The use of porous aggregates as supporting materials for salt-structured phase change materials (SSPCM) in concrete has been shown to enhance material compatibility and enable satisfactory PCM loading rates. The internal structure of coarse aggregates significantly affects the behaviour of SSPCM composites, with structural modifications playing a critical role in their performance. Large pores within the aggregates allow for higher PCM loading, which is beneficial for thermal energy storage, but they also present challenges related to leakage prevention. Based on the experimental results, it is recommended that the aggregate pores be uniform in size, with a diameter not exceeding 0.3 mm, and located further from the concrete surface. This configuration optimises PCM loading while minimising the risk of leakage. Furthermore, the presence of interconnected tubules within the aggregate structure is crucial for ensuring complete PCM loading and preventing leakage by providing continuous pathways for the PCM to distribute evenly within the concrete matrix. It is also important to note that strength degradation in PCM composites is not always inevitable. With careful optimization, it is possible to mitigate strength loss and develop durable, high-performance PCM concrete.

Furthermore, the melting point of PCM is often aligned with typical room temperatures, which are lower than the peak temperatures required for optimal cement hydration. This presents a significant challenge in PCM concrete applications, as it affects both the hydration process and the resulting mechanical properties. The thermal characteristics of the PCM play a crucial role in this behaviour. For the specific PCM used in this study, hydration is initially accelerated, but the final hydration level remains lower than in conventional concrete due to the PCM's temperature-regulating properties. The constant temperature maintained during the phase change limits further hydration, preventing the typical rise in temperature that would otherwise promote continued hydration. These factors directly contribute to the reduced strength observed in the PCM mortar. Additionally, the small expansion observed during the shrinkage test is closely linked to the specific properties of the chosen PCM and should not be regarded as a universal issue for all PCM mortars. This work provides an interesting perspective to understand the mechanical loss of PCM mortar.

Incorporating carbon-based materials of varying sizes has demonstrated the potential for enhancing the mechanical performance of PCM concrete, providing promising results in improving strength and durability. Beyond mechanical properties, the study also addresses key thermal characteristics of PCM concrete. Modifications in thermal properties, such as enhanced thermal convection, can lead to improved efficiency, although the benefits are contingent on the careful selection of additives and an optimised mixing design. Excessive use of additives or improper formulation can diminish the positive effects, underlining the importance of precise design optimisation.

Finally, carbon-based materials were also explored for their multifunctional potential, particularly in the area of self-heating. The working condition of PCM concrete is passive but that of self-heating concrete is active. The results indicate that incorporating carbon-

based additives can significantly enhance the self-heating capabilities of PCM concrete, providing a synergistic effect with PCM's thermal energy storage. This dual-functionality—temperature regulation through self-heating and PCM energy storage—offers a promising approach to reducing energy consumption while improving overall thermal management in concrete structures.

In summary, this work highlights the multifaceted benefits and challenges associated with PCM concrete. While significant strides have been made, further research is needed to optimize the material's performance, particularly in terms of hydration control, mechanical enhancement, and multifunctional applications, to unlock its full potential in sustainable and energy-efficient construction.

7.2 Future research

The development of PCM concrete needs specific work to solve crucial issues, which can be classified into two problems: maintaining the stability of concrete and improving the thermal performance. The former mostly relies on compatible PCM composites. It requires both adequate strength and bond with cementitious material, which may be affected by leakage, surface roughness, corrosion resistance, etc. An enhancement method is required to maintain the great mechanical properties of conventional concrete. In addition, the basic properties of PCM, or selection of PCM, are more important than expected. The influence starts from concrete curing and keeps in concrete operation. This work also reveals the impact on the cement hydration process, which demands concern about cementitious materials like Portland cement, slag cement, geopolymer, etc. The latter requires not only raw PCM properties but also adaptive thermal properties of PCM concrete. The low thermal convection of universal concrete requests much attention and improving factors are various. Increasing thermal conductivity is a directly basic method

but not comprehensive. The ideal thermal convection should match the demanded heat flow direction, which must consider the properties of PCM concrete, desired circumstances, and ambient conditions. The future research asks for big data analyses to build the relation among them and propose optimal designing methods.

Energy storage and saving are the foundational purposes of PCM concrete. In the development as presented above, many potential functions can be incorporated. This work investigates the performance of self-heating and analyses the intrinsic effect. Moreover, the potential can be expanded, like anti-ice, energy harvest, self-sensing, etc. The compatibility and cooperation with PCM are noticeable, and these topics deserve continuous exploration.

REFERENCES

Acır, A. & Emin Canlı, M. 2018, 'Investigation of fin application effects on melting time in a latent thermal energy storage system with phase change material (PCM)', *Applied Thermal Engineering*, vol. 144, pp. 1071-80.

Adesina, A. 2019, 'Use of phase change materials in concrete: current challenges', *Renew. Energy Environ. Sustain.*, vol. 4.

Ahangari, M. & Maerefat, M. 2019, 'An innovative PCM system for thermal comfort improvement and energy demand reduction in building under different climate conditions', *Sustainable Cities and Society*, vol. 44, pp. 120-9.

Al-Absi, Z.A., Mohd Isa, M.H. & Ismail, M. 2020, 'Phase Change Materials (PCMs) and Their Optimum Position in Building Walls', *Sustainability*, vol. 12, no. 4, p. 1294.

Al-Rashed, A.A.A.A., Alnaqi, A.A. & Alsarraf, J. 2021, 'Energy-saving of building envelope using passive PCM technique: A case study of Kuwait City climate conditions', *Sustainable Energy Technologies and Assessments*, vol. 46, p. 101254.

Al-Yasiri, Q. & Szabó, M. 2021, 'Experimental evaluation of the optimal position of a macroencapsulated phase change material incorporated composite roof under hot climate conditions', *Sustainable Energy Technologies and Assessments*, vol. 45, p. 101121.

Arıcı, M., Bilgin, F., Nižetić, S. & Karabay, H. 2020a, 'PCM integrated to external building walls: An optimization study on maximum activation of latent heat', *Applied Thermal Engineering*, vol. 165, p. 114560.

Arıcı, M., Tütüncü, E., Yıldız, Ç. & Li, D. 2020b, 'Enhancement of PCM melting rate via internal fin and nanoparticles', *International Journal of Heat and Mass Transfer*, vol. 156, p. 119845.

Arkar, C. & Medved, S. 2007, 'Free cooling of a building using PCM heat storage integrated into the ventilation system', *Solar Energy*, vol. 81, no. 9, pp. 1078-87.

Arumugam, C. & Shaik, S. 2021, 'Air-conditioning cost saving and CO2 emission reduction prospective of buildings designed with PCM integrated blocks and roofs', *Sustainable Energy Technologies and Assessments*, vol. 48, p. 101657.

AS 2006, *2350.13-2006 Methods of testing portland, blended and masonry cements Determination of drying shrinkage of cement mortars*, Standards Australia.

ASTM 2017, *C157/C157M − 17 Standard Test Method for Length Change of Hardened Hydraulic-Cement Mortar and Concrete*, ASTM International, West Conshohocken, PA.

ASTM 2018, *C349 - 18 Standard Test Method for Compressive Strength of Hydraulic-Cement Mortars (Using Portions of Prisms Broken in Flexure)*, ASTM International, West Conshohocken, PA.

ASTM 2021a, *C109/C109M - 21 Standard Test Method for Compressive Strength of Hydraulic Cement Mortars (Using 2-in. or [50 mm] Cube Specimens)*, ASTM International, West Conshohocken, PA.

ASTM 2021b, *C348 - 21 Standard Test Method for Flexural Strength of Hydraulic-Cement Mortars*, ASTM International, West Conshohocken, PA.

Bauer, T., Laing, D. & Tamme, R. 2012, 'Characterization of sodium nitrate as phase change material', *International Journal of Thermophysics*, vol. 33, no. 1, pp. 91-104.

Beiranvand, M. & Mohaghegh, M.R. 2021, 'Energy analysis and simulation of PCM-enhanced building envelopes in commercial buildings: A case study', *Energy Storage*, vol. 3, no. 4, p. e246.

Bhamare, D.K., Rathod, M.K. & Banerjee, J. 2020, 'Selection of phase change material and establishment of thermophysical properties of phase change material integrated with roof of a building using Measure of Key Response index: Proposal of a new parameter', *Journal of Energy Storage*, vol. 32, p. 101812.

Bogatu, D.-I., Kazanci, O.B. & Olesen, B.W. 2021, 'An experimental study of the active cooling performance of a novel radiant ceiling panel containing phase change material (PCM)', *Energy and Buildings*, vol. 243, p. 110981.

Boobalakrishnan, P., Manoj Kumar, P., Balaji, G., Jenaris, D.S., Kaarthik, S., Jaya Prakash Babu, M. & Karthhik, K. 2021, 'Thermal management of metal roof building using phase change material (PCM)', *Materials Today: Proceedings*.

Boussaba, L., Foufa, A., Makhlouf, S., Lefebvre, G. & Royon, L. 2018, 'Elaboration and properties of a composite bio-based PCM for an application in building envelopes', *Construction and Building Materials*, vol. 185, pp. 156-65.

Brooks, A.L., Fang, Y., Shen, Z., Wang, J. & Zhou, H. 2021, 'Enabling high-strength cement-based materials for thermal energy storage via fly-ash cenosphere encapsulated phase change materials', *Cement and Concrete Composites*, vol. 120, p. 104033.

Cao, V.D., Bui, T.Q. & Kjøniksen, A.-L. 2019, 'Thermal analysis of multi-layer walls containing geopolymer concrete and phase change materials for building applications', *Energy*, vol. 186, p. 115792.

Cao, X., Yuan, Y., Xiang, B., Sun, L. & Xingxing, Z. 2018, 'Numerical investigation on optimal number of longitudinal fins in horizontal annular phase change unit at different wall temperatures', *Energy and Buildings*, vol. 158, pp. 384-92.

Cárdenas-Ramírez, C., Gómez, M.A., Jaramillo, F., Cardona, A.F., Fernández, A.G. & Cabeza, L.F. 2022, 'Experimental steady-state and transient thermal performance

of materials for thermal energy storage in building applications: From powder SS-PCMs to SS-PCM-based acrylic plaster', *Energy*, vol. 250, p. 123768.

Chen, M., Zheng, S., Wu, S. & Xu, G. 2010, 'Melting intercalation method to prepare lauric acid/organophilic montmorillonite shape-stabilized phase change material', *Journal of Wuhan University of Technology-Mater. Sci. Ed.*, vol. 25, no. 4, pp. 674-7.

Chen, S.-B., Saleem, S., Alghamdi, M.N., Nisar, K.S., Arsalanloo, A., Issakhov, A. & Xia, W.-F. 2021a, 'Combined effect of using porous media and nano-particle on melting performance of PCM filled enclosure with triangular double fins', *Case Studies in Thermal Engineering*, vol. 25, p. 100939.

Chen, W., Liang, X., Wang, S., Gao, X., Zhang, Z. & Fang, Y. 2021b, 'Polyurethane macro-encapsulation for CH3COONa·3H2O-Na2S2O3·5H2O/Melamine sponge to fabricate form-stable composite phase change material', *Chemical Engineering Journal*, vol. 410, p. 128308.

Chen, Y., Li, X., Gao, J., Yang, M., Liu, Y., Liu, Y. & Tang, X. 2021c, 'Carbon layer-modified mesoporous silica supporter for PEG to improve the thermal properties of composite phase change material', *Journal of Materials Science*, vol. 56, no. 9, pp. 5786-801.

Chi, B., Yao, Y., Cui, S. & Jin, X. 2021, 'Preparation of graphene oxide coated tetradecanol/expanded graphite composite phase change material for thermal energy storage', *Materials Letters*, vol. 282, p. 128666.

Choi, K., Kim, D., Chung, W., Cho, C. & Kang, S.-W. 2022, 'Nanostructured thermoelectric composites for efficient energy harvesting in infrastructure construction applications', *Cement and Concrete Composites*, vol. 128, p. 104452.

Chriaa, I., Karkri, M., Trigui, A., Jedidi, I., Abdelmouleh, M. & Boudaya, C. 2021, 'The performances of expanded graphite on the phase change materials composites for thermal energy storage', *Polymer*, vol. 212, p. 123128.

da Cunha, S.R.L. & de Aguiar, J.L.B. 2020, 'Phase change materials and energy efficiency of buildings: A review of knowledge', *Journal of Energy Storage*, vol. 27, p. 101083.

Deb, R., Shrestha, N., Phan, K., Cissao, M., Namakiaraghi, P., Alqenai, Y., Visvalingam, S., Mutua, A. & Farnam Yaghoob, A. 2024, 'Development of self-heating concrete using low-temperature Phase Change Materials: Multiscale and in situ real-time evaluation of snow-melting and freeze–thaw performance', *Journal of Materials in Civil Engineering*, vol. 36, no. 6, p. 04024102.

Dehmous, M.h., Franquet, E. & Lamrous, N. 2021, 'Mechanical and thermal characterizations of various thermal energy storage concretes including low-cost bio-sourced PCM', *Energy and Buildings*, vol. 241, p. 110878.

Desai, A.N., Shah, H. & Singh, V.K. 2021, 'Novel inverted fin configurations for enhancing the thermal performance of PCM based thermal control unit: A numerical study', *Applied Thermal Engineering*, vol. 195, p. 117155.

Djamai, Z.I., Le Nguyen, K., Si Larbi, A., Salvatore, F. & Cai, G. 2021, 'PCM-modified textile-reinforced concrete slab: A multiscale and multiphysics investigation', *Construction and Building Materials*, vol. 293, p. 123483.

Do, J.Y., Son, N., Shin, J., Chava, R.K., Joo, S.W. & Kang, M. 2021, 'n-Eicosane-Fe3O4@SiO2@Cu microcapsule phase change material and its improved thermal conductivity and heat transfer performance', *Materials & Design*, vol. 198, p. 109357.

Dong, T., Jiang, W., Liu, Y., Wu, Y., Qi, Y., Li, J., Ma, Y., Ben, H. & Han, G. 2020a, 'A phase change material embedded composite consisting of kapok and hollow PET fibers for dynamic thermal comfort regulation', *Industrial Crops and Products*, vol. 158, p. 112945.

Dong, W., Li, W., Guo, Y., He, X. & Sheng, D. 2020b, 'Effects of silica fume on physicochemical properties and piezoresistivity of intelligent carbon black-cementitious composites', *Construction and Building Materials*, vol. 259, p. 120399.

Dong, W., Li, W., Zhu, X., Sheng, D. & Shah, S.P. 2021, 'Multifunctional cementitious composites with integrated self-sensing and hydrophobic capacities toward smart structural health monitoring', *Cement and Concrete Composites*, vol. 118, p. 103962.

EN 2002, *12617-4: Products and systems for the protection and repair of concrete structures—Test methods—Part 4: Determination of shrinkage and expansion*, BSI.

Esmaeeli, H.S., Farnam, Y., Haddock, J.E., Zavattieri, P.D. & Weiss, W.J. 2018, 'Numerical analysis of the freeze-thaw performance of cementitious composites that contain phase change material (PCM)', *Materials & Design*, vol. 145, pp. 74-87.

Essid, N., Loulizi, A. & Neji, J. 2019, 'Compressive strength and hygric properties of concretes incorporating microencapsulated phase change material', *Construction and Building Materials*, vol. 222, pp. 254-62.

Fan, X., Pu, Z., Zhu, M., Jiang, Z. & Xu, J. 2021, 'Solvent-free synthesis of PEG modified polyurethane solid-solid phase change materials with different Mw for thermal energy storage', *Colloid and Polymer Science*.

Fang, Y., Ahmad, M.R., Lao, J.-C., Qian, L.-P. & Dai, J.-G. 2022, 'Development of artificial geopolymer aggregates with thermal energy storage capacity', *Cement and Concrete Composites*, vol. 135, p. 104834.

Fang, Y., Su, J., Tang, Y., Liang, X., Wang, S., Gao, X. & Zhang, Z. 2020, 'Form-stable Na2SO4·10H2O-Na2HPO4·12H2O eutectic/hydrophilic fumed silica composite phase change material with low supercooling and low thermal conductivity for indoor thermal comfort improvement', *International Journal of Energy Research*, vol. 44, no. 4, pp. 3171-82.

Fang, Y., Wang, K., Ding, Y., Liang, X., Wang, S., Gao, X. & Zhang, Z. 2021, 'Fabrication and thermal properties of CaCl2·6H2O–CO(NH2)2/SiO2 as room-temperature shape-stable composite PCM for building thermal insulation', *Solar Energy Materials and Solar Cells*, vol. 232, p. 111355.

Farcas, C., Galao, O., Navarro, R., Zornoza, E., Baeza, F.J., Del Moral, B., Pla, R. & Garcés, P. 2021, 'Heating and de-icing function in conductive concrete and cement paste with the hybrid addition of carbon nanotubes and graphite products', *Smart Materials and Structures*, vol. 30, no. 4, p. 045010.

Farnam, Y., Esmaeeli, H.S., Zavattieri, P.D., Haddock, J. & Weiss, J. 2017, 'Incorporating phase change materials in concrete pavement to melt snow and ice', *Cement and Concrete Composites*, vol. 84, pp. 134-45.

Farnam, Y., Wiese, A., Bentz, D., Davis, J. & Weiss, J. 2015, 'Damage development in cementitious materials exposed to magnesium chloride deicing salt', *Construction and Building Materials*, vol. 93, pp. 384-92.

Feng, D., Li, P., Feng, Y., Yan, Y. & Zhang, X. 2021, 'Using mesoporous carbon to pack polyethylene glycol as a shape-stabilized phase change material with excellent

energy storage capacity and thermal conductivity', *Microporous and Mesoporous Materials*, vol. 310, p. 110631.

GB/T 1981, *2842 Test method for lightweight aggregates*.

Gencel, O., Sarı, A., Kaplan, G., Ustaoglu, A., Hekimoğlu, G., Bayraktar, O.Y. & Ozbakkaloglu, T. 2022, 'Properties of eco-friendly foam concrete containing PCM impregnated rice husk ash for thermal management of buildings', *Journal of Building Engineering*, vol. 58, p. 104961.

Gil, A., Peiró, G., Oró, E. & Cabeza, L.F. 2018, 'Experimental analysis of the effective thermal conductivity enhancement of PCM using finned tubes in high temperature bulk tanks', *Applied Thermal Engineering*, vol. 142, pp. 736-44.

González, B. & Prieto, M.M. 2021, 'Radiant heating floors with PCM bands for thermal energy storage: A numerical analysis', *International Journal of Thermal Sciences*, vol. 162, p. 106803.

Grabo, M., Acar, E. & Kenig, E.Y. 2021, 'Modeling and improvement of a packed bed latent heat storage filled with non-spherical encapsulated PCM-Elements', *Renewable Energy*, vol. 173, pp. 1087-97.

Gu, G., Ma, T., Chen, F., Han, C., Li, H. & Xu, F. 2024, 'Co-modifying geopolymer composite by nano carbon black and carbon fibers to reduce CO2 emissions in airport pavement induction heating', *Composites Part A: Applied Science and Manufacturing*, vol. 177, p. 107951.

Guo, J. & Zhang, G. 2021, 'Investigating the performance of the PCM-integrated building envelope on a seasonal basis', *Journal of the Taiwan Institute of Chemical Engineers*.

Guo, Y., Li, W., Dong, W., Luo, Z., Qu, F., Yang, F. & Wang, K. 2022, 'Self-sensing performance of cement-based sensor with carbon black and polypropylene fibre

subjected to different loading conditions', *Journal of Building Engineering*, vol. 59, p. 105003.

Guthrie, F. 1884, 'On Eutexia', *Proceedings of the Physical Society of London*, vol. 6, no. 1, pp. 124-46.

Hamad, F.A., Egelle, E., Gooneratne, S. & Russell, P. 2021, 'The effect of aspect ratio on PCM melting behaviour in rectangular enclosure', *International Journal of Sustainable Engineering*, vol. 14, no. 5, pp. 1251-68.

Hekimoğlu, G., Nas, M., Ouikhalfan, M., Sarı, A., Kurbetci, Ş., Tyagi, V.V., Sharma, R.K. & Saleh, T.A. 2021a, 'Thermal management performance and mechanical properties of a novel cementitious composite containing fly ash/lauric acid-myristic acid as form-stable phase change material', *Construction and Building Materials*, vol. 274, p. 122105.

Hekimoğlu, G., Nas, M., Ouikhalfan, M., Sarı, A., Tyagi, V.V., Sharma, R.K., Kurbetci, Ş. & Saleh, T.A. 2021b, 'Silica fume/capric acid-stearic acid PCM included-cementitious composite for thermal controlling of buildings: Thermal energy storage and mechanical properties', *Energy*, vol. 219, p. 119588.

Hekimoğlu, G. & Sarı, A. 2022, 'Shape stabilized attapulgite/myristic-palmitic acid composite PCM for thermal energy storage implementations in buildings', *Materials Today: Proceedings*, vol. 58, pp. 1350-3.

Hekimoğlu, G., Sarı, A., Gencel, O. & Tyagi, V.V. 2022, 'Thermal conductivity enhancement of silica fume based composite thermal energy storage material using different carbon nanomaterials', *Energy and Buildings*, vol. 257, p. 111789.

Hirschey, J., Goswami, M., Akamo, D.O., Kumar, N., Li, Y., LaClair, T.J., Gluesenkamp, K.R. & Graham, S. 2022, 'Effect of expanded graphite on the thermal conductivity

of sodium sulfate decahydrate (Na2SO4·10H2O) phase change composites', *Journal of Energy Storage*, vol. 52, p. 104949.

Hosseinzadeh, K., Montazer, E., Shafii, M.B. & Ganji, A.R.D. 2021, 'Solidification enhancement in triplex thermal energy storage system via triplets fins configuration and hybrid nanoparticles', *Journal of Energy Storage*, vol. 34, p. 102177.

Hunger, M., Entrop, A.G., Mandilaras, I., Brouwers, H.J.H. & Founti, M. 2009, 'The behavior of self-compacting concrete containing micro-encapsulated Phase Change Materials', *Cement and Concrete Composites*, vol. 31, no. 10, pp. 731-43.

Ilyas, A., Ahad, M.Z., Durrani, M.A.Q.J. & Naveed, A. 2021, 'Synthesis and characterization of PCM based insulated concrete for thermal energy storage', *Materials Research Express*, vol. 8, no. 7, p. 075503.

Islam, M.N. & Ahmed, D.H. 2021, 'Delaying the temperature fluctuations through PCM integrated building walls—Room conditions, PCM placement, and temperature of the heat sources', *Energy Storage*, vol. 3, no. 5, p. e245.

Jang, D., Yoon, H.N., Yang, B. & Khalid, H.R. 2023, 'Cyclic heat-generation and storage capabilities of self-heating cementitious composite with an addition of phase change material', *Construction and Building Materials*, vol. 369, p. 130512.

Jeong, S.-G., Chang, S.J., Wi, S., Lee, J. & Kim, S. 2017, 'Energy performance evaluation of heat-storage gypsum board with hybrid SSPCM composite', *Journal of Industrial and Engineering Chemistry*, vol. 51, pp. 237-43.

Ji, C., Qin, Z., Dubey, S., Choo, F.H. & Duan, F. 2018, 'Simulation on PCM melting enhancement with double-fin length arrangements in a rectangular enclosure induced by natural convection', *International Journal of Heat and Mass Transfer*, vol. 127, pp. 255-65.

Jia, C., Geng, X., Liu, F. & Gao, Y. 2021a, 'Thermal Behavior Improvement of Hollow Sintered Bricks integrated with Both Thermal Insulation Material (TIM) and Phase-Change Material (PCM)', *Case Studies in Thermal Engineering*, vol. 25, p. 100938.

Jia, J., Liu, B., Ma, L., Wang, H., Li, D. & Wang, Y. 2021b, 'Energy saving performance optimization and regional adaptability of prefabricated buildings with PCM in different climates', *Case Studies in Thermal Engineering*, vol. 26, p. 101164.

Jiang, F., Wang, X. & Zhang, Y. 2011, 'A new method to estimate optimal phase change material characteristics in a passive solar room', *Energy Conversion and Management*, vol. 52, no. 6, pp. 2437-41.

Jin, X., Medina, M.A. & Zhang, X. 2016, 'Numerical analysis for the optimal location of a thin PCM layer in frame walls', *Applied Thermal Engineering*, vol. 103, pp. 1057-63.

Jin, X., Zhang, S., Xu, X. & Zhang, X. 2014, 'Effects of PCM state on its phase change performance and the thermal performance of building walls', *Building and Environment*, vol. 81, pp. 334-9.

Joneidi, M.H., Rahimi, M., Pakrouh, R. & Bahrampoury, R. 2020, 'Experimental analysis of Transient melting process in a horizontal cavity with different configurations of fins', *Renewable Energy*, vol. 145, pp. 2451-62.

Joulin, A., Zalewski, L., Lassue, S. & Naji, H. 2014, 'Experimental investigation of thermal characteristics of a mortar with or without a micro-encapsulated phase change material', *Applied Thermal Engineering*, vol. 66, no. 1, pp. 171-80.

Kao, H., Li, M., Lv, X. & Tan, J. 2012, 'Preparation and thermal properties of expanded graphite/paraffin/organic montmorillonite composite phase change material', *Journal of Thermal Analysis and Calorimetry*, vol. 107, no. 1, pp. 299-303.

Karaman, S., Karaipekli, A., Sarı, A. & Biçer, A. 2011, 'Polyethylene glycol (PEG)/diatomite composite as a novel form-stable phase change material for thermal energy storage', *Solar Energy Materials and Solar Cells*, vol. 95, no. 7, pp. 1647-53.

Kastiukas, G., Zhou, X. & Castro-Gomes, J. 2016, 'Development and optimisation of phase change material-impregnated lightweight aggregates for geopolymer composites made from aluminosilicate rich mud and milled glass powder', *Construction and Building Materials*, vol. 110, pp. 201-10.

Kawaguchi, T., Sakai, H., Sheng, N., Kurniawan, A. & Nomura, T. 2020, 'Microencapsulation of Zn-Al alloy as a new phase change material for middle-high-temperature thermal energy storage applications', *Applied Energy*, vol. 276, p. 115487.

Khan, R.J., Bhuiyan, M.Z.H. & Ahmed, D.H. 2020, 'Investigation of heat transfer of a building wall in the presence of phase change material (PCM)', *Energy and Built Environment*, vol. 1, no. 2, pp. 199-206.

Kim, G., Park, S., Ryu, G. & Lee, H.-K. 2017, 'Electrical characteristics of hierarchical conductive pathways in cementitious composites incorporating CNT and carbon fiber', *Cement and Concrete Composites*, vol. 82, pp. 165-75.

Kim, G.M., Naeem, F., Kim, H.K. & Lee, H.K. 2016, 'Heating and heat-dependent mechanical characteristics of CNT-embedded cementitious composites', *Composite Structures*, vol. 136, pp. 162-70.

Konuklu, Y., Ersoy, O., Akar, H.B. & Erzin, F. 2020, 'Effect of pre-treatment methods on natural raw materials-based phase change material composites for building applications', *Construction and Building Materials*, vol. 263, p. 120114.

Kuzmenko, K., Ducoulombier, N., Feraille, A. & Roussel, N. 2022, 'Environmental impact of extrusion-based additive manufacturing: generic model, power measurements and influence of printing resolution', *Cement and Concrete Research*, vol. 157, p. 106807.

Lagou, A., Kylili, A., Šadauskienė, J. & Fokaides, P.A. 2019, 'Numerical investigation of phase change materials (PCM) optimal melting properties and position in building elements under diverse conditions', *Construction and Building Materials*, vol. 225, pp. 452-64.

Laing, D., Bauer, T., Lehmann, D. & Bahl, C. 2009, 'Development of a thermal energy storage system for parabolic trough power plants with direct steam generation', vol. ASME 2009 3rd International Conference on Energy Sustainability, Volume 2, pp. 551-9.

Lakhdari, Y.A., Chikh, S. & Campo, A. 2020, 'Analysis of the thermal response of a dual phase change material embedded in a multi-layered building envelope', *Applied Thermal Engineering*, vol. 179, p. 115502.

Larwa, B., Cesari, S. & Bottarelli, M. 2021, 'Study on thermal performance of a PCM enhanced hydronic radiant floor heating system', *Energy*, vol. 225, p. 120245.

Lee, H., Yu, W., Loh, K.J. & Chung, W. 2020, 'Self-heating and electrical performance of carbon nanotube-enhanced cement composites', *Construction and Building Materials*, vol. 250, p. 118838.

Lee, K.O., Medina, M.A., Raith, E. & Sun, X. 2015, 'Assessing the integration of a thin phase change material (PCM) layer in a residential building wall for heat transfer reduction and management', *Applied Energy*, vol. 137, pp. 699-706.

Li, C., Wen, X., Cai, W., Yu, H. & Liu, D. 2023, 'Phase change material for passive cooling in building envelopes: A comprehensive review', *Journal of Building Engineering*, vol. 65, p. 105763.

Li, H., Fang, G. & Liu, X. 2010, 'Synthesis of shape-stabilized paraffin/silicon dioxide composites as phase change material for thermal energy storage', *Journal of Materials Science*, vol. 45, no. 6, pp. 1672-6.

Li, H., Hu, C., He, Y., Tang, D., Wang, K. & Hu, X. 2021a, 'Visualized-experimental investigation on the energy storage performance of PCM infiltrated in the metal foam with varying pore densities', *Energy*, vol. 237, p. 121540.

Li, M.-J., Jin, B., Ma, Z. & Yuan, F. 2018, 'Experimental and numerical study on the performance of a new high-temperature packed-bed thermal energy storage system with macroencapsulation of molten salt phase change material', *Applied Energy*, vol. 221, pp. 1-15.

Li, Q., Wang, Y., Ma, L., Arıcı, M., Li, D., Yıldız, Ç. & Zhu, Y. 2021b, 'Effect of sunspace and PCM louver combination on the energy saving of rural residences: Case study in a severe cold region of China', *Sustainable Energy Technologies and Assessments*, vol. 45, p. 101126.

Li, W., Dong, W., Guo, Y., Wang, K. & Shah, S.P. 2022, 'Advances in multifunctional cementitious composites with conductive carbon nanomaterials for smart infrastructure', *Cement and Concrete Composites*, vol. 128, p. 104454.

Li, W., Guo, Y., Zhang, X., Dong, W., Li, X., Yu, T. & Wang, K. 2024, 'Development of self-sensing ultra-high-performance concrete using hybrid carbon black and carbon nanofibers', *Cement and Concrete Composites*, p. 105466.

Li, Y., Guo, B., Huang, G., Shu, P., Kiriki, H., Kubo, S., Ohno, K. & Kawai, T. 2015, 'Eutectic compound (KNO3/NaNO3 : PCM) quasi-encapsulated into SiC-

honeycomb for suppressing natural convection of melted PCM', *International Journal of Energy Research*, vol. 39, no. 6, pp. 789-804.

Li, Z.X., Al-Rashed, A.A.A.A., Rostamzadeh, M., Kalbasi, R., Shahsavar, A. & Afrand, M. 2019, 'Heat transfer reduction in buildings by embedding phase change material in multi-layer walls: Effects of repositioning, thermophysical properties and thickness of PCM', *Energy Conversion and Management*, vol. 195, pp. 43-56.

Liu, C., Wu, Y., Zhu, Y., Li, D. & Ma, L. 2018, 'Experimental investigation of optical and thermal performance of a PCM-glazed unit for building applications', *Energy and Buildings*, vol. 158, pp. 794-800.

Liu, K. & Tovar, A. 2014, 'An efficient 3D topology optimization code written in Matlab', *Structural and Multidisciplinary Optimization*, vol. 50, no. 6, pp. 1175-96.

Liu, Y., Yu, K., Lu, S., Wang, C., Li, X. & Yang, Y. 2020, 'Experimental research on an environment-friendly form-stable phase change material incorporating modified rice husk ash for thermal energy storage', *Journal of Energy Storage*, vol. 31, p. 101599.

Lu, D., Huo, Y., Jiang, Z. & Zhong, J. 2023, 'Carbon nanotube polymer nanocomposites coated aggregate enabled highly conductive concrete for structural health monitoring', *Carbon*, vol. 206, pp. 340-50.

Lu, D., Wang, D. & Zhong, J. 2022, 'Highly conductive and sensitive piezoresistive cement mortar with graphene coated aggregates and carbon fiber', *Cement and Concrete Composites*, vol. 134, p. 104731.

Medved', I. & Trník, A. 2018, 'Behavior of a PCM at Varying Heating Rates: Experimental and Theoretical Study with an Aim at Temperature Moderation in Radionuclide Concrete Encasements', *International Journal of Thermophysics*, vol. 39, no. 7, p. 83.

Meng, D. & Wang, A. 2020, 'Preparation and characterization of fatty acid eutectic/diatomite filter aid form-stable phase change material for thermal energy storage', *IOP Conference Series: Earth and Environmental Science*, vol. 467, p. 012002.

Meng, D., Zhao, K., Wang, A. & Wang, B. 2020a, 'Preparation and properties of Paraffin/PMMA xhape-stabilized Phase Change material for building thermal energy storage', *Journal of Wuhan University of Technology-Mater. Sci. Ed.*, vol. 35, no. 1, pp. 231-9.

Meng, X., Yan, L., Xu, J., He, F., Yu, H. & Zhang, M. 2020b, 'Effect of porosity and pore density of copper foam on thermal performance of the paraffin-copper foam composite Phase-Change Material', *Case Studies in Thermal Engineering*, vol. 22, p. 100742.

Mi, X., Liu, R., Cui, H., Memon, S.A., Xing, F. & Lo, Y. 2016, 'Energy and economic analysis of building integrated with PCM in different cities of China', *Applied Energy*, vol. 175, pp. 324-36.

Miliozzi, A., Chieruzzi, M. & Torre, L. 2019, 'Experimental investigation of a cementitious heat storage medium incorporating a solar salt/diatomite composite phase change material', *Applied Energy*, vol. 250, pp. 1023-35.

Moman, A.A., Butt, A.A. & Nassiri, S. 2023, 'Feasibility assessment of self-deicing concrete pavements with recycled CFRP reinforcement: Environmental and mechanical performance', *Resources, Conservation and Recycling*, vol. 198, p. 107213.

Nitsas, M. & Koronaki, I.P. 2021, 'Performance analysis of nanoparticles-enhanced PCM: An experimental approach', *Thermal Science and Engineering Progress*, vol. 25, p. 100963.

Niu, D., Zhang, T., Zhang, X., Tan, Y. & Zhang, W. 2023, 'Experimental and numerical investigation of the thermal performance of phase-change module using built-in electrical heating', *Energy and Buildings*, vol. 299, p. 113597.

Park, J.H., Jeon, J., Lee, J., Wi, S., Yun, B.Y. & Kim, S. 2019, 'Comparative analysis of the PCM application according to the building type as retrofit system', *Building and Environment*, vol. 151, pp. 291-302.

Peng, W. & Sadaghiani, O.K. 2021, 'Thermal function improvement of phase-change material (PCM) using alumina nanoparticles in a circular-rectangular cavity using Lattice Boltzmann method', *Journal of Energy Storage*, vol. 37, p. 102493.

Pilehvar, S., Cao, V.D., Szczotok, A.M., Valentini, L., Salvioni, D., Magistri, M., Pamies, R. & Kjøniksen, A.-L. 2017, 'Mechanical properties and microscale changes of geopolymer concrete and Portland cement concrete containing micro-encapsulated phase change materials', *Cement and Concrete Research*, vol. 100, pp. 341-9.

Pilehvar, S., Szczotok, A.M., Rodríguez, J.F., Valentini, L., Lanzón, M., Pamies, R. & Kjøniksen, A.-L. 2019, 'Effect of freeze-thaw cycles on the mechanical behavior of geopolymer concrete and Portland cement concrete containing micro-encapsulated phase change materials', *Construction and Building Materials*, vol. 200, pp. 94-103.

Pizzolato, A., Sharma, A., Maute, K., Sciacovelli, A. & Verda, V. 2017, 'Design of effective fins for fast PCM melting and solidification in shell-and-tube latent heat thermal energy storage through topology optimization', *Applied Energy*, vol. 208, pp. 210-27.

Qin, H., Ding, S., Ashour, A., Zheng, Q. & Han, B. 2024, 'Revolutionizing infrastructure: The evolving landscape of electricity-based multifunctional concrete from concept to practice', *Progress in Materials Science*, p. 101310.

Qin, Y., Ghalambaz, M., Sheremet, M., Fteiti, M. & Alresheedi, F. 2023, 'A bibliometrics study of phase change materials (PCMs)', *Journal of Energy Storage*, vol. 73, p. 108987.

Qu, Y., Chen, J., Liu, L., Xu, T., Wu, H. & Zhou, X. 2020, 'Study on properties of phase change foam concrete block mixed with paraffin / fumed silica composite phase change material', *Renewable Energy*, vol. 150, pp. 1127-35.

Qu, Y., Zhou, D., Xue, F. & Cui, L. 2021, 'Multi-factor analysis on thermal comfort and energy saving potential for PCM-integrated buildings in summer', *Energy and Buildings*, vol. 241, p. 110966.

Rabienataj Darzi, A.A., Jourabian, M. & Farhadi, M. 2016, 'Melting and solidification of PCM enhanced by radial conductive fins and nanoparticles in cylindrical annulus', *Energy Conversion and Management*, vol. 118, pp. 253-63.

Rahman, M.L., Malakooti, A., Ceylan, H., Kim, S. & Taylor, P.C. 2022, 'A review of electrically conductive concrete heated pavement system technology: From the laboratory to the full-scale implementation', *Construction and Building Materials*, vol. 329, p. 127139.

Ramakrishnan, S., Sanjayan, J., Wang, X., Alam, M. & Wilson, J. 2015, 'A novel paraffin/expanded perlite composite phase change material for prevention of PCM leakage in cementitious composites', *Applied Energy*, vol. 157, pp. 85-94.

Ramakrishnan, S., Wang, X., Sanjayan, J., Petinakis, E. & Wilson, J. 2017, 'Development of thermal energy storage cementitious composites (TESC) containing a novel

paraffin/hydrophobic expanded perlite composite phase change material', *Solar Energy*, vol. 158, pp. 626-35.

Ramezani, M., Dehghani, A. & Sherif, M.M. 2022, 'Carbon nanotube reinforced cementitious composites: A comprehensive review', *Construction and Building Materials*, vol. 315, p. 125100.

Rao, Z., Xu, T., Liu, C., Zheng, Z., Liang, L. & Hong, K. 2018, 'Experimental study on thermal properties and thermal performance of eutectic hydrated salts/expanded perlite form-stable phase change materials for passive solar energy utilization', *Solar Energy Materials and Solar Cells*, vol. 188, pp. 6-17.

Rathore, P.K.S., Gupta, N.K., Yadav, D., Shukla, S.K. & Kaul, S. 2022, 'Thermal performance of the building envelope integrated with phase change material for thermal energy storage: an updated review', *Sustainable Cities and Society*, vol. 79, p. 103690.

Rathore, P.K.S. & Shukla, S.K. 2020, 'An experimental evaluation of thermal behavior of the building envelope using macroencapsulated PCM for energy savings', *Renewable Energy*, vol. 149, pp. 1300-13.

Rathore, P.K.S. & Shukla, S.k. 2021, 'Improvement in thermal properties of PCM/Expanded vermiculite/expanded graphite shape stabilized composite PCM for building energy applications', *Renewable Energy*, vol. 176, pp. 295-304.

Razak, R.A., Zhe, A.C.K., Abdullah, M.M.A.B., Yahya, Z. & Mortar, N.A.M. 2020, 'Paraffin as a phase change material in concrete for enhancing thermal energy storage', *IOP Conference Series Materials ence and Engineering*, vol. 743, p. 012012.

Ren, M., Liu, Y. & Gao, X. 2020, 'Incorporation of phase change material and carbon nanofibers into lightweight aggregate concrete for thermal energy regulation in buildings', *Energy*, vol. 197, p. 117262.

Ren, M., Wen, X., Gao, X. & Liu, Y. 2020, 'Thermal and mechanical properties of ultra-high performance concrete incorporated with microencapsulated phase change material', *Construction and Building Materials*, p. 121714.

Ren, Q., Xu, H. & Luo, Z. 2019, 'PCM charging process accelerated with combination of optimized triangle fins and nanoparticles', *International Journal of Thermal Sciences*, vol. 140, pp. 466-79.

Richardson, A., Heniegal, A. & Tindall, J. 2017, 'Optimal performance characteristics of mortar incorporating phase change materials and silica fume', *Journal of Green Building*, vol. 12, no. 2, pp. 59-78.

Rodriguez-Ubinas, E., Ruiz-Valero, L., Vega, S. & Neila, J. 2012, 'Applications of Phase Change Material in highly energy-efficient houses', *Energy and Buildings*, vol. 50, pp. 49-62.

Rolka, P., Przybylinski, T., Kwidzinski, R. & Lackowski, M. 2021, 'The heat capacity of low-temperature phase change materials (PCM) applied in thermal energy storage systems', *Renewable Energy*, vol. 172, pp. 541-50.

Sarani, I., Payan, S., Payan, A. & Nada, S.A. 2020, 'Enhancement of energy storage capability in RT82 phase change material using strips fins and metal-oxide based nanoparticles', *Journal of Energy Storage*, vol. 32, p. 102009.

Šavija, B. 2018, 'Smart crack control in concrete through use of phase change materials (PCMs): A review', *Materials*, vol. 11, no. 5, p. 654.

Šavija, B. & Schlangen, E. 2016, 'Use of phase change materials (PCMs) to mitigate early age thermal cracking in concrete: Theoretical considerations', *Construction and Building Materials*, vol. 126, pp. 332-44.

Sellevold, E. & Bjøntegaard, Ø. 2006, 'Coefficient of thermal expansion of cement paste and concrete: Mechanisms of moisture interaction', *Materials and structures*, vol. 39, pp. 809-15.

Sheikholeslami, M. 2018a, 'Finite element method for PCM solidification in existence of CuO nanoparticles', *Journal of Molecular Liquids*, vol. 265, pp. 347-55.

Sheikholeslami, M. 2018b, 'Numerical simulation for solidification in a LHTESS by means of nano-enhanced PCM', *Journal of the Taiwan Institute of Chemical Engineers*, vol. 86, pp. 25-41.

Sheikholeslami, M. & Mahian, O. 2019, 'Enhancement of PCM solidification using inorganic nanoparticles and an external magnetic field with application in energy storage systems', *Journal of Cleaner Production*, vol. 215, pp. 963-77.

Shen, Y., Liu, S., Zeng, C., Zhang, Y., Li, Y., Han, X., Yang, L. & Yang, X.e. 2021, 'Experimental thermal study of a new PCM-concrete thermal storage block (PCM-CTSB)', *Construction and Building Materials*, vol. 293, p. 123540.

Shi, J., Tan, J., Liu, B., Liu, Y., Xu, H., Wang, Z., Xiong, T. & Shi, J. 2020, 'Thermal and mechanical properties of thermal energy storage lightweight aggregate mortar incorporated with phase change material', *Journal of Energy Storage*, vol. 32, p. 101719.

Shi, T., Zhang, X., Qiao, J., Wu, X., Chen, G., Leng, G., Lin, F., Min, X. & Huang, Z. 2021a, 'Preparation and characterization of composite phase change materials based on paraffin and carbon foams derived from starch', *Polymer*, vol. 212, p. 123143.

Shi, X., Yazdani, M.R., Ajdary, R. & Rojas, O.J. 2021b, 'Leakage-proof microencapsulation of phase change materials by emulsification with acetylated cellulose nanofibrils', *Carbohydrate Polymers*, vol. 254, p. 117279.

Shukla, N., Fallahi, A. & Kosny, J. 2012, 'Performance characterization of PCM impregnated gypsum board for building applications', *Energy Procedia*, vol. 30, pp. 370-9.

Snoeck, D., Priem, B., Dubruel, P. & De Belie, N. 2016, 'Encapsulated Phase-Change Materials as additives in cementitious materials to promote thermal comfort in concrete constructions', *Materials and Structures*, vol. 49, no. 1, pp. 225-39.

Struhala, K. & Ostrý, M. 2022, 'Life-Cycle Assessment of phase-change materials in buildings: A review', *Journal of Cleaner Production*, vol. 336, p. 130359.

Sun, J., Zhao, J., Zhang, W., Xu, J., Wang, B., Wang, X., Zhou, J., Guo, H. & Liu, Y. 2023, 'Composites with a novel core–shell structural expanded perlite/polyethylene glycol composite PCM as novel green energy storage composites for building energy conservation', *Applied Energy*, vol. 330, p. 120363.

Sun, X., Liu, L., Mo, Y., Li, J. & Li, C. 2020, 'Enhanced thermal energy storage of a paraffin-based phase change material (PCM) using nano carbons', *Applied Thermal Engineering*, vol. 181, p. 115992.

Talebizadehsardari, P., Mahdi, J.M., Mohammed, H.I., Moghimi, M.A., Hossein Eisapour, A. & Ghalambaz, M. 2021, 'Consecutive charging and discharging of a PCM-based plate heat exchanger with zigzag configuration', *Applied Thermal Engineering*, vol. 193, p. 116970.

Tang, B., Wang, L., Xu, Y., Xiu, J. & Zhang, S. 2016, 'Hexadecanol/phase change polyurethane composite as form-stable phase change material for thermal energy storage', *Solar Energy Materials and Solar Cells*, vol. 144, pp. 1-6.

Thonon, M., Fraisse, G., Zalewski, L. & Pailha, M. 2021, 'Analytical modelling of PCM supercooling including recalescence for complete and partial heating/cooling cycles', *Applied Thermal Engineering*, vol. 190, p. 116751.

Tyagi, V.V., Chopra, K., Sharma, R.K., Pandey, A.K., Tyagi, S.K., Ahmad, M.S., Sarı, A. & Kothari, R. 2022, 'A comprehensive review on phase change materials for heat storage applications: Development, characterization, thermal and chemical stability', *Solar Energy Materials and Solar Cells*, vol. 234, p. 111392.

ul Hasnain, F., Irfan, M., Khan, M.M., Khan, L.A. & Ahmed, H.F. 2021, 'Melting performance enhancement of a phase change material using branched fins and nanoparticles for energy storage applications', *Journal of Energy Storage*, vol. 38, p. 102513.

Urgessa, G., Yun, K.-K., Yeon, J. & Yeon, J.H. 2019, 'Thermal responses of concrete slabs containing microencapsulated low-transition temperature phase change materials exposed to realistic climate conditions', *Cement and Concrete Composites*, vol. 104, p. 103391.

Uthaichotirat, P., Sukontasukkul, P., Jitsangiam, P., Suksiripattanapong, C., Sata, V. & Chindaprasirt, P. 2020, 'Thermal and sound properties of concrete mixed with high porous aggregates from manufacturing waste impregnated with phase change material', *Journal of Building Engineering*, vol. 29, p. 101111.

Wang, H., Zhang, A., Zhang, L., Wang, Q., Yang, X.-h., Gao, X. & Shi, F. 2020, 'Electrical and piezoresistive properties of carbon nanofiber cement mortar under different temperatures and water contents', *Construction and Building Materials*, vol. 265, p. 120740.

Wang, X., Li, W., Guo, Y., Kashani, A., Wang, K., Ferrara, L. & Agudelo, I. 2024, 'Concrete 3D printing technology for sustainable construction: A review on raw

material, concrete type and performance', *Developments in the Built Environment*, vol. 17, p. 100378.

Wang, X., Li, W., Huang, Y., Zhang, S. & Wang, K. 2023a, 'Study on shape-stabilised paraffin-ceramsite composites with stable strength as phase change material (PCM) for energy storage', *Construction and Building Materials*, vol. 388, p. 131678.

Wang, X., Li, W., Luo, Z., Wang, K. & Shah, S.P. 2022, 'A critical review on phase change materials (PCM) for sustainable and energy efficient building: Design, characteristic, performance and application', *Energy and Buildings*, vol. 260, p. 111923.

Wang, Z., Shao, T., Zhang, H., Huo, J., Liu, J., Zhang, T., Ji, X., Zhang, H., Wang, J., Guo, H. & Yu, P. 2023b, 'Principles, properties and applications of smart conductive cement-based composites: A state-of-the-art review', *Construction and Building Materials*, vol. 408, p. 133569.

Wu, D., Rahim, M., El Ganaoui, M., Djedjig, R., Bennacer, R. & Liu, B. 2021, 'Experimental investigation on the hygrothermal behavior of a new multilayer building envelope integrating PCM with bio-based material', *Building and Environment*, vol. 201, p. 107995.

Xiao, L.X., He, Y.T. & Wang, J.Q. 2021, 'Experimental study on the effect of Phase Change Material melting Point on TG/PCM Thermal control properties', *IOP Conference Series: Earth and Environmental Science*, vol. 701, no. 1, p. 012021.

Xiao, Z., Mishra, P., Mahdavi Nejad, A., Tao, M., Granados-Focil, S. & Van Dessel, S. 2021, 'Thermal optimization of a novel thermo-optically responsive SS-PCM coatings for building enclosures', *Energy and Buildings*, vol. 247, p. 111129.

Xie, J., Lee, H.M. & Xiang, J. 2019, 'Numerical study of thermally optimized metal structures in a Phase Change Material (PCM) enclosure', *Applied Thermal Engineering*, vol. 148, pp. 825-37.

Xie, J., Wang, W., Liu, J. & Pan, S. 2018, 'Thermal performance analysis of PCM wallboards for building application based on numerical simulation', *Solar Energy*, vol. 162, pp. 533-40.

Yan, T., Li, J., Gao, J., Xu, X. & Yu, J. 2021, 'Model validation and application of the coupled system of pipe-encapsulated PCM wall and nocturnal sky radiator', *Applied Thermal Engineering*, vol. 194, p. 117057.

Yang, H., Xu, Z., Cui, H., Bao, X., Tang, W., Sang, G. & Chen, X. 2022, 'Cementitious composites integrated phase change materials for passive buildings: An overview', *Construction and Building Materials*, vol. 361, p. 129635.

Yang, J., Yang, L., Xu, C. & Du, X. 2016, 'Experimental study on enhancement of thermal energy storage with phase-change material', *Applied Energy*, vol. 169, pp. 164-76.

Yang, Y., Wu, W., Fu, S. & Zhang, H. 2020, 'Study of a novel ceramsite-based shape-stabilized composite phase change material (PCM) for energy conservation in buildings', *Construction and Building Materials*, vol. 246, p. 118479.

Yao, S. & Huang, X. 2021, 'Study on solidification performance of PCM by longitudinal triangular fins in a triplex-tube thermal energy storage system', *Energy*, p. 120527.

Yoon, H., Bang, J., Jang, D. & Yang, B. 2024, 'Investigation on NTC/PTC effects of cement-based self-heating composites with varied conductive filler contents', *Developments in the Built Environment*, p. 100416.

Yousefi, A., Tang, W., Khavarian, M. & Fang, C. 2021, 'Development of novel form-stable phase change material (PCM) composite using recycled expanded glass for

thermal energy storage in cementitious composite', *Renewable Energy*, vol. 175, pp. 14-28.

Yu, K., Jia, M., Yang, Y. & Liu, Y. 2023, 'A clean strategy of concrete curing in cold climate: Solar thermal energy storage based on phase change material', *Applied Energy*, vol. 331, p. 120375.

Yu, K., Liu, Y., Jia, M., Wang, C. & Yang, Y. 2022, 'Thermal energy storage cement mortar containing encapsulated hydrated salt/fly ash cenosphere phase change material: Thermo-mechanical properties and energy saving analysis', *Journal of Energy Storage*, vol. 51, p. 104388.

Yu, X., Luan, J., Chen, W. & Tao, J. 2020, 'Preparation and characterization of paraffin microencapsulated phase change material with double shell for thermal energy storage', *Thermochimica Acta*, vol. 689, p. 178652.

Zhang, C., Li, J. & Chen, Y. 2020, 'Improving the energy discharging performance of a latent heat storage (LHS) unit using fractal-tree-shaped fins', *Applied Energy*, vol. 259, p. 114102.

Zhang, C., Yu, M., Fan, Y., Zhang, X., Zhao, Y. & Qiu, L. 2020, 'Numerical study on heat transfer enhancement of PCM using three combined methods based on heat pipe', *Energy*, vol. 195, p. 116809.

Zhang, N., Song, Y., Du, Y., Yuan, Y., Xiao, G. & Gui, Y. 2018, 'A novel solid–solid Phase Change Material: pentaglycerine/expanded graphite composite PCMs', *Advanced Engineering Materials*, vol. 20, no. 10, p. 1800237.

Zhang, Q., Luan, C., Yu, C., Huang, Y. & Zhou, Z. 2022, 'Mechanisms of carbon black in multifunctional cement matrix: Hydration and microstructure perspectives', *Construction and Building Materials*, vol. 346, p. 128455.

Zhang, T., Zhang, T., Zhang, J., Zhang, D., Guo, P., Li, H., Li, C. & Wang, Y. 2021, 'Design of stearic acid/graphene oxide-attapulgite aerogel shape-stabilized phase change materials with excellent thermophysical properties', *Renewable Energy*, vol. 165, pp. 504-13.

Zhang, X., Wen, R., Tang, C., Wu, B., Huang, Z., Min, X., Huang, Y., Liu, Y., Fang, M. & Wu, X. 2016, 'Thermal conductivity enhancement of polyethylene glycol/expanded perlite with carbon layer for heat storage application', *Energy and Buildings*, vol. 130, pp. 113-21.

Zhao, C., Opolot, M., Liu, M., Bruno, F., Mancin, S., Flewell-Smith, R. & Hooman, K. 2021, 'Simulations of melting performance enhancement for a PCM embedded in metal periodic structures', *International Journal of Heat and Mass Transfer*, vol. 168, p. 120853.

Zhou, D., Shire, G.S.F. & Tian, Y. 2014, 'Parametric analysis of influencing factors in Phase Change Material Wallboard (PCMW)', *Applied Energy*, vol. 119, pp. 33-42.

Zhou, S.-S., Almarashi, A., Talabany, Z.J., Selim, M.M., Issakhov, A., Li, Y.-M., Yao, S.-W. & Li, Z. 2021, 'Augmentation of performance of system with dispersion of nanoparticles inside PCM', *Journal of Molecular Liquids*, vol. 333, p. 115921.

Zhou, T., Darkwa, J. & Kokogiannakis, G. 2015, 'Thermal evaluation of laminated composite phase change material gypsum board under dynamic conditions', *Renewable Energy*, vol. 78, pp. 448-56.

Zhu, N., Deng, R., Hu, P., Lei, F., Xu, L. & Jiang, Z. 2021, 'Coupling optimization study of key influencing factors on PCM Trombe wall for year thermal management', *Energy*, p. 121470.